12-8-2017

Genome Maintenance by Selenoprotein H in the Nucleolus

Li Zhang

Genome maintenance by Selenoprotein H in the nucleolus

By

Li Zhang

A Dissertation
Submitted to the Faculty of
Mississippi State University
in Partial Fulfillment of the Requirements
for the Degree of Doctor of Philosophy
in Nutrition
in the Department of Food Science, Nutrition and Health Promotion

Mississippi State, Mississippi

December 2017

Genome maintenance by Selenoprotein H in the nucleolus

By

Li Zhang

Approved:

_____

Wen-Hsing Cheng
(Major Professor)

_____

Din-Pow Ma
(Committee Member)

_____

Ramakrishna Nannapaneni
(Committee Member)

_____

M. Wes Schilling
(Committee Member)

_____

Marion W. Evans, Jr.
(Graduate Coordinator)

_____

George M. Hopper
Dean
College of Agriculture and Life Sciences

Name: Li Zhang

Date of Degree: December 8, 2017

Institution: Mississippi State University

Major Field: Nutrition

Major Professor: Wen-Hsing Cheng

Title of Study: Genome maintenance by Selenoprotein H in the nucleolus

Pages in Study 127

Candidate for Degree of Doctor of Philosophy

Selenoprotein H (SELENOH) is a nucleolar oxidoreductase with DNA binding properties whose function is not well understood. To determine the functional and physiological roles of SELENOH, a knockout of *SELENOH* was generated in cell lines using CRISPR/Cas9-mediated genomic deletion and in mice by targeted disruption. Based on the sequenced genome, the results of deduced protein sequences indicated various forms of mutants in the CRISPR/Cas9-mediated knockout, including a frame-shift by aberrant splicing and truncated SELENOH by early termination of the translation process. Loss of SELENOH in HeLa cells induced slow cell proliferation, the formation of giant multinucleated cells, accumulation of unrepaired DNA damage and oxidative stress, and cellular senescence. *SELENOH* cells were enlarged and possessed a single large nucleolus. Atomic force microscope showed increased stiffness in the nucleoli of *SELENOH* knockout cells, which suggests that SELENOH maintains the flexible structure of the nucleolus. Furthermore, the knockout of SELENOH led to a large-scale reorganization of the nucleolar architecture with the movement of nucleolar protein into nucleolar cap regions in response to oxidative stress. The nucleolar reorganization is dependent on ATM signaling. Altogether, results suggest that SELENOH appears to be a

sensor of oxidative stress that plays critical roles in redox regulation and genome maintenance within the nucleolus.

To determine the physiological role of SELENOH *in vivo*, *Selenoh* knockout mice were generated by targeted deletion through homologous recombination. *Selenoh*$^{+/-}$ mice were fertile and phenotypically indistinguishable from wild-type littermates. Results from matings of *Selenoh*$^{+/-}$ mice showed a significantly reduced fraction of *Selenoh*$^{-/-}$ offspring on the basis of Mendelian segregation. Since some *Selenoh*$^{-/-}$ were born, it is likely that *Selenoh* is a partially essential gene in mice. Live-born *Selenoh*$^{-/-}$ mice were viable and born without apparent phenotypes. *Selenoh*$^{-/-}$ mice at 2-month of age showed increased GPX activity in the lung but not in the brain and liver. Furthermore, loss of *Selenoh* resulted in the aggravated formation of aberrant crypt foci in the colon of *Selenoh*$^{+/-}$ mice that were injected with azoxymethane. Altogether, SELENOH has critical roles in embryogenesis and colorectal carcinogenesis.

DEDICATION

I would like to dedicate this dissertation to my lovely family: my parents, Qingyu Zhang and Xiuyun Fu, my parents-in-law, Lianrong Zhang and Xiuyun Duan, my wife, Xue Zhang, and my daughters, Jiatong Zhang and Anna Zhang. They were always there cheering me up and stood by me through the good times and bad. I love you all.

ACKNOWLEDGEMENTS

I would like to express my deepest gratitude to my major advisor, Dr. Wen-Hsing Cheng, for his understanding, patience, enthusiasm, and encouragement and for pushing me farther than I thought I could go. I am thankful to Dr. Din-Pow Ma, Dr. Ramakrishna Nannapaneni and Dr. Wes Schilling for your assistance and suggestions throughout my project.

I would like to express my sincere appreciation to Dr. Chun-Yu Hsu at IGBB. Thank you for your willingness to help and provide suggestions. To Ms. Amanda Lawrence and Dr. I-Wei Chu at I^2AT, I am grateful for your help on Confocal Microscopy and AFM research. To Dr. Stephen Pruett and Dr. Wei Tan at CVM, I am thankful for your support on the cell cycle and microscopic observations. To Dr. Bridget Willeford, I am thankful for your help on taking care of mice. I am thankful to Dr. Alicia Olivier for helping me identify aberrant crypt foci in mice. I am thankful to my lab mates, Dr. Hsin-Yi Lu and Dr. Lei Cao for always listening and encouraging me. I am thankful to all my friends and family for their care, support, encouragement to help me go through all the frustrations and difficulties. Special thanks to my best friend, Lei Zheng, for his encouragement and support.

TABLE OF CONTENTS

LIST OF TABLES

LIST OF FIGURES

CHAPTER I

INTRODUCTION

1.1 Selenium

1.1.1 Nutritional essentiality

Selenium (Se) was identified as an element in 1817 by the Swedish chemist Jöns Jacob Berzelius (Berzelius 1818). Since the discovery of Se, this element was best known as a toxicant until 1957 when liver necrosis was found in rats that were fed a Se-deficient diet (Patterson *et al.* 1957; Schwarz *et al.* 1957; Schwarz & Foltz 1957). Other syndromes of dietary Se deficiency were subsequently found in other animal species, including exudative diathesis with pendulous appearance of the neck in chicks (Patterson *et al.* 1957; Schwarz *et al.* 1957), muscular dystrophy or white muscle disease in lambs (Hogue 1958; Muth *et al.* 1958), and mulberry heart disease in pigs (Van Vleet *et al.* 1970). Human Se deficiency syndromes include Keshan disease, which is characterized by cardiomyopathy, Kashin-Beck disease, which is characterized byosteochondropathy, and myxoedematous cretinism, which is characterized as a waxy or coarsened skin appearance (Yang *et al.* 1988; Vanderpas *et al.* 1990; Moreno-Reyes *et al.* 1998). These deficiency syndromes animal species and human led to the establishment of Se as a nutrient.

Nutrient regulation of gene expression is common, but Se is the only nutrient that is directly involved in the translation process. Se exerts its physiological function mainly

through selenoproteins, which are widespread in all three domains of life. However, the number of selenoprotein genes varies by species, ranging from 0 in fungi and some animal species such as beetles and silkworms, 1 in *C. elegans*, and as many as 59 in the pelagophyte *Aureococcus anophagefferens* (Labunskyy *et al.* 2014). In rodents and humans, the numbers are 24 and 25, respectively. Selenoprotein mRNAs contain the in-frame UGA codon, a stop codon elsewhere, which decodes for selenocysteine at the active site of all selenoproteins. The Se transporter selenoprotein P (SELENOP) contains ten selenocysteine residues, but all other selenoproteins in mammals contain only one selenocysteine. It has been widely accepted that selenocysteine is the "21st" amino acid, whose three and one letter abbreviations are assigned as Sec and U, respectively. Selenoprotein mRNAs are translated when selenocysteine-tRNAs carrying the anti-codon in complimentary to UGA and the selenocysteine moiety is added to a nascent polypeptide (Labunskyy *et al.* 2014).

Before the complete sequencing of the human genome in 2003 and the characterization of the selenoproteome by the Gladushev Lab (Kryukov *et al.* 2003), it was known that dietary Se fluctuations affect the regulation of selenoprotein expression at mRNA and protein levels. This was determined by evaluating individual selenoproteins such as glutathione peroxidase-1 (GPX1), thioredoxin reductase-1 (TXNRD1), and iodothyronine deiodinase-1 (DIO1), and SELENOP (Meinhold *et al.* 1993; Cheng *et al.* 1998a; Holmgren 2000). When dietary Se supply is low, Se delivery to selenoproteins through selenocysteine-tRNA is hampered, which stops the and thus translation of selenoprotein mRNAs at the UGA codon. These results in the degradation of selenoprotein mRNAs by nonsense-mediated mRNA decay and the incomplete

translation of selenoprotein by the ubiquitin ligase-mediated pathway (Seyedali & Berry 2014; Lin *et al.* 2015).

The "hierarchy concept" of Se distribution to tissues and selenoproteins was first proposed and developed by Dietrich Behne based on studies of ^{75}Se distribution in tissues and proteins of Se-deficient rats (Behne *et al.* 1988). These hierarchies of Se indicate that Se is prioritized to essential selenoproteins and tissues at the expense of other tissues and selenoproteins that do not have an immediate need to allocate Se for survival. In rodents, dietary Se deficiency prioritizes depletion of this nutrient in the liver and kidney but retention in the brain and testis. More recent studies demonstrate Se retention in the brain and testis is made possible through SELENOP and the tissue-specific expression of a SELENOP receptor apolipoprotein E receptor-2 in these two organs (Burk *et al.* 2007; Olson *et al.* 2007; Olson *et al.* 2008; Hill *et al.* 2012). SELENOP delivers Se from liver to brain and testis through binding to the apolipoprotein E receptor-2 and the subsequent endocytosis. Once inside the cells of these organs, selenocysteine residues on SELENOP are excised by selenocysteine lyase to release selenide for tissue usage. SELENOP mainly transfers Se from the liver to the brain and testis through the nine selenocysteine residues in its C-terminal domain (Schomburg *et al.* 2003; Hill *et al.* 2007). While the expression of apolipoprotein E receptor-2 is extremely low in tissues that are low in Se hierarchy such as the kidney and liver, it is highly expressed in the testis and brain. This observation is consistent with the pivotal roles of Se in male reproduction and optimal brain functions. Strikingly, Se concentrations are increased by 3.3-fold and 80%, respectively, in the brain and testis but decreased by 80% in the liver of mice that were fed a Se-deficient diet for 18 weeks (Burk & Hill 2009). Among those tissues that are

ranked high in tissue Se hierarchy, competition for the available Se is observed since castration is known to increase the Se concentration in the brain of *Scly*$^{-/-}$*Sepp1*$^{-/-}$ mice that have compromised Se transport and unitization (Pitts *et al.* 2015). Similarly, when body Se status is low, the depletion of GPX1, SELENOH, and SELENOW is faster than other selenoproteins such that these three selenoproteins are ranked at the bottom of selenoprotein hierarchy (Behne *et al.* 1988; Sunde & Raines 2011). Over the last 20 years, the mechanism by which selenoprotein hierarchy is regulated is becoming clear. In Se deficiency, selenoprotein hierarchy is partially attributed to nonsense-mediated decay or SECIS-binding mediators such as the stimulatory nucleolin and the inhibitory eukaryotic initiation factor 4a3 at the mRNA level, CRL2 ubiquitin ligase-mediated degradation of mis-incorporated or mis-folded selenoproteins, and choices of isoforms of selenocysteinyl-tRNA (Moustafa *et al.* 2001; Budiman *et al.* 2009; Miniard *et al.* 2010; Seyedali & Berry 2014; Lin *et al.* 2015). Such Se homeostasis and selenoprotein regulation are consistent with the observation of selenoprotein hierarchy in testis, as requirements for *Gpx1* mRNA levels are high but *Selenop* mRNA levels are low in this organ with priority to the acquisition of Se (Sunde & Raines, 2011).

In addition to selenoproteins, Se can be found in two other classes of Se-containing proteins that uphold Se non-specifically or independent of the UGA codon. First, as a result of sharing a chemical similarity in the chalcogen family of elements, Se may no-specific replace sulfur in methionine and cysteine residues of any protein. Second, as a result of structural configuration that is compatible with Se binding, there are two non-selenoproteins, Se-binding protein-1 and 14-kDa fatty acid binding protein, which specifically bind Se, despite the lack of selenocysteine. Besides, Se at

supranutritional levels may form Se metabolites that induce oxidative stress to modulate biological processes such as activation of earlier barriers of tumorigenesis at relatively lower doses in non-cancerous cells through senescence induction (Wu *et al.* 2010) or high doses in cancer cells through apoptosis (Jackson & Combs 2008). Thus, body Se status can influence physiological and pathophysiological conditions at nutritionally adequate, supranutritional, and toxic levels, primarily through selenoproteins and to a less extent through Se metabolites.

The essential nature of selenoproteins is evidenced by a model that deletes all 24 selenoproteins in mice. Noticeably, although it is technically feasible to use an amino acid-basal diet to dramatically reduce Se content in a purified diet, the residual Se that remains in the diet is sufficient to enable the expression of certain "high hierarchy" selenoproteins such as glutathione peroxidase-4 (Lei *et al.* 1995). Thus, it remains the only approach to assess the essentiality of total selenoproteins by the knockout of *Trsp*, the gene that encodes selenocysteine tRNA, in mice (Bosl *et al.* 1997). Since $Trsp^{-/-}$ mice are embryonic lethal, it is clear that at least some selenoproteins are essential to development and survival. So far, it is known that knockouts of glutathione peroxidase-4, thioredoxin reductase-1 and thioredoxin reductase-2 render mice embryonic lethal (Zhang *et al.* 2016) whereas some selenoproteins are not essential for life, including glutathione peroxidase 1-3 and SELENOP (Lei *et al.* 2016). However, these "non-essential" selenoproteins play important roles during stressed or diseased conditions. These includes the critical role of glutathione peroxidase-1 in response to acute oxidative stress (Cheng *et al.* 1998b), glutathione peroxidase-2 in tumorigenesis (Florian *et al.* 2010), and SELENOP in Se delivery (Florian *et al.* 2010).

The 25 selenoproteins in humans are grouped into families of glutathione peroxidase, thioredoxin reductase, iodothyronine deiodinase, Se storage and transport regulation, and those involving protein quality control. Selenoproteins are differentially expressed in various tissues and sub-cellular compartments under various physiological and pathophysiological conditions (Squires & Berry 2008; Zhang *et al.* 2010; Labunskyy *et al.* 2014). Based on the triage theory of aging proposed by Bruce Ames, 11 selenoproteins are sensitive to body Se fluctuations and are predicted to play important roles during the aging process (McCann & Ames 2011). Although *Trsp*$^{-/-}$mice are embryonic lethal, conditional knockout of *Trsp* in mice is viable, and they show such aging phenotypes such as alopecia in epidermal cells of *Trsp*$^{-/-}$ mice (Sengupta *et al.* 2010) and bone abnormality in osteo-chondroprogenitor cells of *Trsp*$^{-/-}$ mice (Downey *et al.* 2009). Our Lab has a special interest in genome maintenance and nuclear selenoproteins. Indeed, selenoprotein H (SELENOH) is the only selenoprotein that is predicted to be localized only in the nucleolus (Zhang *et al.* 2016), which has been experimentally verified when SELENOH is expressed together with a Green fluorescent protein (GFP) tag (Novoselov *et al.* 2007). It is well established that genome instability is one of the major factors that regulate aging, cancer, and other chronic diseases (Campisi 2005). Thus, it is of great interest to understand interactions between selenoproteins and Se metabolites in genome maintenance, aging, and age-related degeneration.

1.1.2 Selenium metabolism

The chemical forms of Se influence its bioavailability, retention, and metabolism (Van Dael *et al.* 2002; Wastney *et al.* 2011). Selenomethionine is the major dietary

source of Se from foods and foodstuffs in humans and animals. Although the exact mechanisms are unclear, selenomethionine is released in the enzymatic digestion of proteins and absorbed in the small intestine via simple or carrier-mediated diffusion and/(or) active transporters such as those for methionine transport. Similarly, it has been reported that selenomethionine competes with methionine for intracellular transport in Caco-2 colorectal cells (Thiry *et al.* 2013). Analyses of plasma Se concentrations in subjects over a wide range of Se status indicates that bioavailability is greater when it is originated from selenomethionine than inorganic forms (Xia *et al.* 2005; Burk *et al.* 2006). In the body, the majority of Se at nutritional levels of intake is retained in the body through co-translational incorporation by selenocysteine-tRNAs into selenoproteins and non-specific integration in sulfur-containing amino acids, this is because these two chalcagon elements share chemical similarities. At levels above the nutritional requirement, a significant amount of absorbed Se can be excreted through feces and urine with urine loss as the major excretory route (Pedrosa *et al.* 2012). While methylated Se compounds are the major form of urinary Se (Zeng & Combs 2008), they vary among species. The trimethylselenonium ion ($[CH_3]_3Se^+$) and the selenosugar (1β-methylseleno-*N*-acetyl-$_D$-galactosamine) are prominent forms of urinary Se in rats and humans (Kobayashi *et al.* 2002). To understand Se metabolism in an integrated manner, the fact that multiple forms of Se are usually consumed simultaneously has been taken into consideration in an attempt to develop mathematical models to effectively describe the absorption, distribution, and retention of total Se(Patterson *et al.* 1989; Wastney *et al.* 2011). These predictions take advantage of the available stable isotopes of Se and the oral administration of both organic and inorganic Se such as ^{74}Se as selenomethionine and

^{76}Se as sodium selenite, followed by the assessment of the consumed amount and the amounts in the blood, urinary and fecal samples through analyses of these Se tracers.

Glutathione peroxidase-3 (GPX3) and SELENOP are the two extracellular selenoproteins. SELENOP accounts for 76% and GPX3 21% accounts for the total Se in plasma (Olson *et al.* 2010). The minimum dietary Se that is needed to saturate liver Se concentration and *Selenop* mRNA are 0.11 μg and 0.01 μg Se/g, respectively (Sunde *et al.* 2016). These results indicate that Se in the liver is prioritized to SELENOP, which corroborates its essential role in supplying Se to other tissues through circulation (Hill *et al.* 2012). GPX3 does not seem to play an important role in Se delivery based on the results from *Selenop*$^{-/-}$*Gpx3*$^{-/-}$ mice that were fed a moderately high Se diet (Olson *et al.* 2010). In Se deficiency, Se retention is prioritized via tissue-specific SELENOP receptors. These include delivery to the kidney through Megalin and to a greater extent, to the brain and testis through the apolipoprotein E receptor-2 (Burk *et al.* 2007; Olson *et al.* 2008; Hill *et al.* 2012). We have recently shown that there are sex differences in SELENOP expression, as there is 1.4-fold greater plasma SELENOP decline by Se deficiency in females than males. Such sex differences might help to explain the greater number of downregulated selenoprotein mRNAs by dietary Se deficiency in the kidney in females when compared to males (16 vs. 4) but not in the heart (5 vs. 4) (Cao *et al.* 2017). The heart expresses very little Megalin or apolipoprotein E receptor-2 for Se import and is allocated with only 0.7% of the total Se in Se(+) rats (Behne & Wolters 1983; Burk & Hill 2015). Liver *Selenop* mRNA levels are significantly decreased in females on a Se-deficient diet containing 0.03 μg Se/g, a moderately deficient level known to saturate *Selenop* expression in growing mice (Sunde *et al.* 2016). Furthermore,

there is a 50% decrease in the dietary Se requirement to saturate the liver Se in 1-yr-old rats when compared to growing female rats (Sunde & Thompson 2009). Altogether, it is clear that Se delivery differs due to age and sex. It is also plausible to speculate that SELENOP hierarchy descends as female mice age.

1.2 Selenoproteins

1.2.1 Incorporation of selenium into selenoproteins

In the early 1970s, Se-containing proteins were located in mammals and bacteria. In 1972, it was found that a tissue fraction isolated from rats injected with ^{75}Se contained both this stable isotope and GPX activity, suggesting that Se is a prosthetic group of this enzyme (Flohe *et al.* 1973; Rotruck *et al.* 1973). In addition, two Se-containing proteins, "protein A" in the glycine reductase system and formate dehydrogenase, were identified in *Clostridium Thermoaceticum* (Andreesen & Ljungdahl 1973; Turner & Stadtman 1973). From the studies in *C. Thermoaceticum*, selenocysteine was later identified in protein A (Cone *et al.* 1976). Selenocysteine incorporation into proteins was co-translational through an otherwise stop codon, UGA (Chambers *et al.* 1986). This prompted question of how translation of selenoprotein mRNAs avoided the use of the in-frame UGA as a stop codon. This is further elucidated in prokaryotes. Selenocysteine insertion into bacterial selenoproteins and its biosynthesis are mediated by gene the products of *selA, selB, selC,* and *selD* that encode selenocysteine synthase, a specialized translation factor, selenocysteine tRNA, and selenophosphate synthetase, respectively (Böck 2001). It was later determined that, despite the increased complexity and incomplete understanding, mammalian biosynthesis of selenocysteine largely follows a

similar pattern to that of bacteria (Labunskyy *et al.* 2014). Three unique and essential *cis*- and *trans*-acting factors exist for translation of in-frame UGA in selenoprotein mRNAs as selenocysteine. They are 1) the selenocysteine tRNA (encoded by *TRSP* with additional modifications, elaborated below) that decodes UGA (Lee *et al.* 1989; Berry *et al.* 1991a); 2) the selenocysteine insertion sequence (SECIS) in the 3'-untranslated region of all selenoprotein mRNAs (Lee *et al.* 1989; Berry *et al.* 1991a); 3) a SECIS-binding protein 2 (SBP2, encoded by *SECISBP2*) that stabilizes SECIS and brings about selenocysteine tRNA. It is a complicated process to synthesize mature selenocysteine tRNA from the gene product of *TRSP.* This requires the sequential enzymatic reactions of seryl-tRNA synthetase, phosphoseryl-$tRNA^{[Ser]Sec}$ kinase, and selenocysteine synthase (encoded by *SEPSECS*) on the *TRSP* gene product. Interestingly, *TRSP* encodes a precursor of both selenocysteine and cysteine tRNAs. Although these two tRNAs are catalyzed by selenocysteine synthase, the synthesis of selenocysteine or cysteine tRNA depends on whether monoselenophosphate ($H_2SePO_3^-$) or thiophosphate ($H_2SPO_3^-$) is incorporated into the serine moiety on $tRNA^{[Ser]Sec}$. As such, misincorporation of cysteine at the selenocysteine residue may occur, and this is stimulated by Se deficiency (Labunskyy *et al.* 2014). Because $Trsp^{-/-}$ mice are embryonically lethal (Bosl *et al.* 1997), this suggests that at least some selenoproteins are also embryonic lethal. Interestingly, a couple of human mutations in genes that were necessary for selenoprotein synthesis are identified in patients. These include *TRSP* (Schoenmakers *et al.* 2016), *SECISBP2* (Schoenmakers *et al.* 2010), and *SEPSECS* (Agamy *et al.* 2010; Anttonen *et al.* 2015) in humans. Defective Se metabolism and phenotypes of these mutations are summarized in **Table 1.1**. Similar to deficiency in selenocysteine tRNA, mutations in these genes essential for

translation of selenoprotein mRNA impact all selenoproteins. This is exemplified by the observations significant decrease in plasma selenium concentrations and certain selenoprotein expression in tissues of patients with these mutations.

1.2.2 Selenoprotein functions

There are 24 and 25 selenoproteins identified in rodents and humans, respectively, by a search for SECIS appearance in whole genomes (Kryukov et al. 2003). Selenocysteine is located in active sites to participate in redox reactions in all known selenoenzymes. Considering their structures and functions, selenoproteins are categorized into glutathione peroxidases, thioredoxin reductases, and iodothyronine deiodinases, the thioredoxin-like, endoplasmic reticulum proteins (Sep15 and selenoprotein M), and other proteins with functions related to selenium transport and storage. Overexpression or knockout of a couple of selenoprotein genes in mice has enabled research on their physiological function of the selenoproteins.

1.2.2.1 Glutathione peroxidases

While the presence of Se in GPX and its importance for the peroxidase activity were confirmed 1972 (Flohe et al. 1973; Rotruck et al. 1973), the enzymatic reaction of GPX was discovered in erythrocytes in 1957 (Mills 1957). Because the GPX1 enzyme that isolated from bovine erythrocyte exhibits “ping-pong” kinetics without saturation with glutathione (the substrate for GPX), it has an infinite extrapolated V_{max} and no true K_M (Flohé et al. 1972; Günzler et al. 1972). While GPX4 is a monomer, GPX1-3 and GPX6 are homotetramers. Mammalian GPX5 or rodent GPX6 is not a selenoprotein. The peroxide substrate preference for GPX1-3 and GPX4 is H_2O_2 and organic

hydroperoxides, respectively (Brigelius-Flohe & Maiorino 2013). It is interesting that only GPX4 can catalyze the reduction of phospholipid hydroperoxides. Gene expression and protein production of the GPX family are tissue- and organelle-specific (Brigelius-Flohe & Maiorino 2013). GPX1 and GPX2 resides mainly in cytosol. While GPX1 is known to be expressed in all types of cells in all tissues, GPX2 is found almost exclusively in intestines but to a minor extent in the mammary gland and liver (Chu et al. 1993). Although GPX1 expression is ubiquitous, the highest abundance is found in the liver, kidney, erythrocyte, and placenta. Previously and commonly known as plasma GPX, extracellular GPX3 is mainly expressed in and secreted from the kidney and epididymis (Burk et al. 2011). Different from GPX1-3, Phospholipid hydroperoxide GPX (GPX4) is a monomer that is expressed highly in the testis, and is found to have three isoforms in cytosol, mitochondria and the nucleus (Pushpa-Rekha et al. 1995; Maiorino et al. 2003; Brigelius-Flohe & Maiorino 2013). The cellular localization of GPX6 is unknown, although human GPX6 is highly expressed in the embryos and the olfactory epithelium (Dear et al. 1991; Kryukov et al. 2003).

Through the use of *Gpx1*$^{-/-}$ mice 20 years ago, it was concluded that GPX1 accounts for 60% of total liver Se (Cheng *et al.* 1998a; Cheng *et al.* 1999; Fu *et al.* 1999). Furthermore, studies that employed *Gpx1* knockout mice enabled the discovery of the first known physiological function of this selenoprotein that protects against acute oxidative stress that is induced by paraquat and diquat through the redox protection of lipids and proteins in mice (Cheng *et al.* 1998b; Cheng *et al.* 1999; Fu *et al.* 1999). While *Gpx1*$^{-/-}$ mice develop normally, using this line of mice later resulted in the identification of functional roles of GPX1 in cardiovascular disease, neurodegeneration, and

autoimmune disorders under stressed or diseased conditions (Lei *et al.* 2007). Surprisingly, mice develop a type-2 diabetes-like phenotype when GPX1 is overexpressed (McClung *et al.* 2004). Although such an extreme scenario of GPX1 overexpression is unlikely to spontaneously occur in nature, it is speculated that this paradoxical role of GPX1 is ascribed to over-quenching oxygen free radicals and over-depletion of intracellular H_2O_2 that hampers insulin signaling. Consistent with this observation, while insulin resistance is produced by the consumption of a high-fat diet, such a pathophysiological response is attenuated in *Gpx1*$^{-/-}$ mice (Loh *et al.* 2009). On the other hand, under a more physiological setting, it is known that β-cell specific overexpression of GPX1 in the leptin receptor was defective *db*/*db* in obese mice, but prevented diabetes and rescues the intrinsic β-cell dysfunction at 20 weeks of age (Harmon *et al.* 2009; Guo *et al.* 2013). Despite these seeming inconsistencies, it is prudent to conclude that GPX1 differentially regulates glucose homeostasis in response to distinctive physiological or pathophysiological circumstances.

Although the GPX1 expression is up-regulated in the colon and ileum of *Gpx2*$^{-/-}$ mice (Florian *et al.* 2010), there is no phenotype in *Gpx2*$^{-/-}$ mice under unstressed conditions. This is similar to *Gpx1*$^{-/-}$ mice. In the double knockout model, *Gpx1*$^{-/-}$*Gpx2*$^{-/-}$ mice show increased lipid peroxidation and develop intestinal tumors (Esworthy *et al.* 2001). Considering the same substrate preference, results from these studies suggest that GPX1 and GPX2 interact to protect against oxidative stress in the intestines. Consistent with the antioxidative role of GPX1 and GPX2, the cerebral infarction symptom in *Gpx3*$^{-/-}$ mice can be relieved by antioxidant treatments (Jin *et al.* 2011). While the knockout of *Gpx1*, *Gpx2*, or *Gpx3* in mice do not yield the apparent

phenotype, GPX4 is an essential selenoprotein as *Gpx4*$^{-/-}$ mice are embryonically lethal (Yant *et al.* 2003). To circumvent this limitation so that the physiological functions of GPX4 can be studied, various lines of conditional or inducible knockouts of GPX4 have been generated in mice. Results demonstrated GPX4 protect against the defective development of photoreceptor cells (Ueta *et al.* 2012b), male infertility (Imai *et al.* 2009; Schneider *et al.* 2009), and symptoms of neurodegeneration (Seiler *et al.* 2008).

1.2.2.2 Thioredoxin reductases

There are three thioredoxin (TXN) reductases (TXNRD) in mammals including cytosolic TXNRD1 (Tamura & Stadtman 1996), mitochondrial TXNRD2 (Miranda-Vizuete *et al.* 1999), and the spermatid-specific TXNRD3 (also known as thioredoxin glutathione reductase) (Su *et al.* 2005). These three selenoproteins recycle oxidized TXN at the expense of NADPH and belong to a family of pyridine nucleotide-disulfide oxidoreductases. TXNRD1 and TXNRD2 are essential proteins because *Txnrd1*$^{-/-}$ and *Txnrd2*$^{-/-}$ mice display embryonic lethality (Conrad *et al.* 2004; Jakupoglu *et al.* 2005; Bondareva *et al.* 2007). To understand their physiological functions, many conditional knockouts of *Txnrd1* and *Txnrd2* have been generated in mice for functional studies of these two selenoproteins in relation to cancer and neurodegeneration (Jakupoglu *et al.* 2005; Soerensen *et al.* 2008; Carlson *et al.* 2012).

1.2.2.3 Iodothyronine deiodinases

Iodothyronine deiodinases (DIOs) catalyze the transformations between thyroxine (T_4), 3,5,3'-triiodothyronine (T_3) and reverse triiodothyronine (rT_3) (Arthur *et al.* 1990; Berry *et al.* 1991b). DIO1 or DIO2 remove one iodine from the less active T_4 to produce

the more active T_3, followed by secretion from the thyroid gland into circulation. However, *Dio1*$^{-/-}$ or *Dio2*$^{-/-}$ mice do not display abnormal serum T_3 levels (Galton *et al.* 2009), suggesting a redundant role as a deiodinase or a compensatory increase in T_4 levels. Indeed, T_4 levels in the serum of *Dio2*$^{-/-}$ mice are increased (St Germain *et al.* 2009). In addition to the enzymatic role in thyroid hormone maturation, other physiological functions of DIOs have been shown. First, *Dio2*$^{-/-}$ mice display hearing loss, impaired thermogenesis and cognition (St Germain *et al.* 2009), and increased susceptibility to ventilator-induced lung injury (Barca-Mayo *et al.* 2011). Second, *Dio3*$^{-/-}$ mice show defective cerebellar development and restrictive cardiomyopathy (Ueta *et al.* 2012a; Peeters *et al.* 2013). Third, both DIO2 and DIO3 are involved in glucose metabolism since *Dio2*$^{-/-}$ or *Dio3*$^{-/-}$ mice exhibit glucose intolerance, insulin resistance, and/or impaired glucose-stimulated insulin secretion (Castillo *et al.* 2011; Marsili *et al.* 2011; Medina *et al.* 2011). Forth, DIO1-3 are all implicated in carcinogenesis because thyroid hormones regulate the signaling events of differentiation, proliferation, and apoptosis (Piekielko-Witkowska & Nauman 2011; Casula & Bianco 2012).

1.2.2.4 Selenoproteins responsible for protein quality control

By structural analyses, selenoprotein F (SELENOF, also known as 15-kDa selenoprotein or Sep15) and selenoprotein M (SELENOM) are categorized as members of the TXN1-like protein family that possess thiol-disulfide oxidoreductase activity and control the quality of protein folding in the endoplasmic reticulum (Ferguson *et al.* 2006). Furthermore, SELENOF is abundant in the liver, kidney, testis, and prostate of mice and regulates protein folding through interactions with UDP-glucose:glycoprotein glucosyltransferase, a chaperon protein (Korotkov *et al.* 2001; Davis *et al.* 2012).

Interestingly, results of *Selenof*$^{-/-}$ mice suggest an unexpected role of SELENOF in the promotion and metastasis of colon cancer (Irons *et al.* 2010). Knockout of *Selonom*$^{-/-}$ has developed to express the obesity phenotype. While SELENOM is highly expressed in the brain and can sequester zinc in the Alzheimer's brain (Du *et al.* 2013), *Selonom*$^{-/-}$ mice have normal motor and cognitive functions (Pitts *et al.* 2013). Methionine-*R*-sulfoxide reductase 1 (MsrB1), also known as selenoprotein R or X, is another TXN-dependent protein that reduces the oxidized form of methionine-*R*-sulfoxide on proteins in the cytosol and nucleus. *MsrB1*$^{-/-}$ mice have been developed, and express increased malondialdehyde, protein carbonyls, methionine sulfoxide, and oxidized glutathione in the liver and kidney, but not the heart, testis and brain (Fomenko *et al.* 2009). Studies of *MsrB1*$^{-/-}$ mice revealed that MSRB1 is involved in the conservation of reduced methionine, which supports innate immunity through macrophages (Lee *et al.* 2013).

1.2.2.5 Other selenoproteins

SELENOP is the major extracellular selenoprotein for Se delivery. Such a primed role in Se homeostasis is consistent with the unique feature of this selenoprotein, that contains 10 selenocysteine residues. In fact, SELENOP is the only mammalian selenoprotein known to have more than one selenocysteine residue. SELENOP is mainly synthesized in the liver and then secreted to the whole-body via circulation to maintain Se homeostasis (Burk & Hill 1994; Himeno *et al.* 1996). In addition to the role in Se delivery, results from *Selenop*$^{-/-}$ mice implicate SELENOP in spermatogenesis and the prevention of brain degeneration (Burk & Hill 2009). SELENOP is also known to bind zinc and prevent amyloid-β peptide aggregation in the brain (Du *et al.* 2013), suggesting a role in Alzheimer's disease. However, SELENOP may not always accurately

incorporate selenocysteine in response to UGA because this could be a wobble codon for either decoding selenocysteine or translation termination. This is evidenced by the identification of the three shortened SELENOP isoforms that are generated by alternative termination at the second, third, and seventh UGAs for selenocysteine residues as stop signals (Burk & Hill 2005). Moreover, selenoprotein W (SELENOW) is mainly expressed in the muscle, heart, spleen and brain of mammals and is suggested to play important roles in immune responses and TXN-dependent pathways (Whanger 2009). Selenoprotein K (SELENOK) (Fredericks *et al.* 2014) and selenoprotein N (SELENON) (Arbogast & Ferreiro 2010; Castets *et al.* 2012) are implicated in calcium homeostasis and muscle integrity. Biological roles of selenoprotein H (SELENOH) and other nuclear selenoproteins are discussed below.

1.3 Nuclear Selenoproteins and Functions

Based on biochemical and cellular studies, five selenoproteins present in the nucleus constitutively, temporarily, or in a tissue-specific manner. These proteins include are SELENOH, MSRB1, GPX4, TXNRD1, and thioredoxin glutathione reductase (TGR) (Sun *et al.* 2001; Kim & Gladyshev 2004; Borchert *et al.* 2006; Novoselov *et al.* 2007; Go & Jones 2010). Only SELENOH is exclusively localized in the nucleus. To provide a comprehensive scheme of nuclear selenoproteins, for the nuclear localization signal (NLS) has been searched for (Zhang *et al.* 2016). As shown in **Table 1.2**, the results predicted 10 additional nuclear selenoproteins; however, experimental verification for these selenoproteins is necessary. For these predictions, the cNLS Mapper program that takes monopartite and bipartite NLS into consideration was used. This program is

believed to be more accurate than a few others (Kosugi *et al.* 2009). SELENOH is the only selenoprotein to score >10 (monopartite NLS), which denotes nucleus exclusive localization. MSRB1, SELENOT, and DIO2 are scored between 5 and 10, which denotes localizations in and the shuttle between nucleus and cytoplasm. Although GPX4, TXNRD1, and TGR have previously been empirically identified to reside in the nucleus. The predicted low scores suggest that their appearance in the nucleus is transient, possibly only under certain circumstances or only certain isoforms are nuclear. On the other hand, nuclear predictions by cNLS Mapper for the abundant extracellular GPX3 and SELENOP and cytosolic GPX1 (< 2) are consistent with the known non-nuclear localization of these selenoproteins. Illustration of the positions and types of NLS for these selenoproteins are specified in **Figure 1.1**. Based on both experimental and predicted results, five nuclear selenoproteins are discussed hereafter on the basis of molecular, cellular, and physiological perspectives. Because a prime function of nuclear proteins is to maintain genome integrity, genome maintenance is also briefly discussed.

1.3.1 Genome maintenance

Endogenous and exogenous DNA damage constantly hamper genome stability through forms such as oxidative by-products from mitochondrial respiration, errors in DNA replication, and environmental stimuli including ultraviolet radiation and pro-oxidants. Genome maintenance mitigates DNA damage through the detection, signaling and repair of DNA lesions. The fact that genome instability syndromes are often associated with cancer, developmental defects, neurodegeneration, premature aging, and other chronic diseases strongly suggests that genome maintenance is essential for optimal health and life (Jackson & Bartek 2009). It is clear that selenoproteins and Se metabolites

play important roles in genome maintenance through mechanisms such as DNA damage response and epigenetic regulation. It is noteworthy that although both DNA and RNA are subjecte to damage, it is generally conceived that RNA damage is less of a concern because transcription is continuous and damaged RNA can simply be degraded. However, this simplified or even subjective view has been challenged recently, as there is clear evidence for the existence and biological significance of RNA repair, including genome stability in the nucleolus (Tsekrekou *et al.* 2017).

Early detection of DNA damage enables timely cessation of the cell cycle from progressing into the next phase, which can prevent the replication of mutated DNA when this occurs in the S phase of the cell cycle. A key molecular signal for recruitment of DNA repair and checkpoint proteins to sites of damaged DNA is the phosphorylation of histone H2AX on Ser-137 by ATM and other kinases. In the signal cascade, sensor proteins first detect DNA damage and subsequently transmit the signal to downstream sensor kinases. Among these, ataxia-telangiectasia mutated (ATM) is a key kinase in the early response to DNA damage, chromatin conformational changes, and oxidative stress (Guo *et al.* 2010). ATM is activated by autophosphorylation on Ser-1981 in humans or Ser-1987 in mice, which in turn, activate its downstream targets for cell cycle arrest and/or DNA repair. Depending on the severity of genome instability, the cell can be fixed and back to life or become senescent and/or apoptotic cells.

Besides direct damage to nucleic acids, genome instability can also be induced by adverse changes in histone proteins or chromatin structures. These epigenetic events include cis-epigenetics that directly methylate or demethylate cytosine bases and trans-epigenetics that change chromatin accessibility (Bonasio *et al.* 2010). At CpG

dinucleotides that surround the transcriptional initiation site, the addition or removal of methyl groups dictates whether this gene is transcribed or not, respectively. For chromatin accessibility, this occurs on histone proteins that can be modulated by various forms of modifications including methylation, acetylation, ubiquitination and/or phosphorylation. Defects in optimized regulation of these epigenetic events are implicated in the pathophysiology of a growing list of chronic diseases.

1.3.2 SELENOH

Computational analyses of nuclear localization sequences and results from cellular and biochemical studies strongly implicate SELENOH as a genuine nucleolar protein in the nucleus (**Table 1.2**) (Novoselov *et al.* 2007; Panee *et al.* 2007). Through approaches of 1) cellular localization of SELENOH fused to green fluorescent protein, 2) western analyses of sub-nuclear fractions, and 3) proteomic analyses of SELENOH-associated proteins. Results strongly suggest localization of SELENOH to the nucleolus (Novoselov *et al.* 2007). As evidenced by the presence of an AT-hook motif at the extreme N-terminus, SELENOH is a member of the high-mobility group HMG family of DNA-binding proteins (Panee *et al.* 2007). Proteins in this family bind DNA minor grooves and specific regulatory DNA sequences, thus regulating various aspects of DNA metabolism such as DNA repair, replication, and transcription (Grosschedl *et al.* 1994). A role of SELENOH as a transactivator is evidenced by results from chromatin immunoprecipitation experiments that show associations between GFP-SELENOH and heat shock or stress response elements and up-regulation of genes *de novo* glutathione synthesis and phase II detoxification by SELENOH (Panee *et al.* 2007). Human SELENOH contains a high amount of basic amino acids (19.7%) (Zhang *et al.* 2016),

which is reminiscent of histone proteins and facilitates binding with negatively charged DNA. Another proposed function of SELENOH is to catalytically regulate redox status. Structural analyses suggest that SELENOH is a homologue of TXNRD that has a redox-regulatory CXXU motif. Enzymatic analyses show that SELENOH exhibits GPX-like activity as well (Novoselov *et al.* 2007).

Results from biochemical and cellular analyses of SELENOH are largely consistent with those from functional studies. In HT22 neuronal cells, overexpression of SELENOH protects superoxide formation after UVB irradiation (Ben Jilani *et al.* 2007). In mammals, there is differential expression of SELENOH in a manner that is dependent on tissues and life cycle stage. At the mRNA level, SELENOH expression is high during embryogenesis and in certain cancer cells such as colorectal HCT116 and prostate LNCaP cells. Its expression is also high in tissues from the brain, thymus, testis and uterus in mice (Novoselov *et al.* 2007). Upon exogenous stimuli, *SELENOH* mRNA is up-regulated upon cellular exposure to H_2O_2 (Wu *et al.* 2014) or binding of metal transcription factor-1 to its metal response element (Stoytcheva *et al.* 2010). Thus, SELENOH appears to be a sensor of oxidative stress in the nucleolus. Such critical roles of SELENOH in genome maintenance and redox regulation are consistent with results from our Lab using cells (Wu *et al.* 2014) and other researchers using zebrafish (Cox *et al.* 2016). Collectively, SELENOH may interact with ATM, p53, and ROS to function in replicative senescence, embryogenesis, and carcinogenesis

1.3.3 MSRB1

Methionine-*R*-sulfoxide is an oxidized product on proteins but can be catalytically reversed to methionine by MSRB1. While mammalian MSRB1 is primarily located in the

cytosol and nucleus, the cysteine-containing non-selenoproteins MSRB2 and MSRB3 are present in the mitochondria and endoplasmic reticulum (Kim 2013). Altogether, the MSRB system reduces oxidized proteins in various cellular compartments. However, MSRB1 does not seem to universally repair methionine-*R*-sulfoxide on proteins because it is known to selectively target certain proteins such as actin. In *Msrb1*$^{-/-}$ mice, innate immunity is repressed and actin polymerization is disrupted in the macrophages (Lee *et al.* 2013). This suggests that MSRB1 may target methionine-*R*-sulfoxide on actin and maintain genome stability in the nucleus, which is plausible considering the fact that nuclear actin can regulate gene expression and chromatin remodeling upon extracellular stimuli (Vartiainen *et al.* 2007).

MSRB1 was initially identified with the use of bioinformatic tools in 1999 and named selenoprotein R or selenoprotein X (Kryukov *et al.* 1999; Lescure *et al.* 1999). MSRB1 contains zinc and is expressed mainly in the liver, and to a less extent, in the kidney and prostate in mice (Novoselov *et al.* 2010). Although MSRB1 is not detectable in all parts of the brain using Western analysis, this selenoprotein is selectively expressed in the hippocampus and cerebellar cortex in mice (Zhang *et al.* 2008). Interestingly, consumption of supranutritional Se at 3-fold greater than nutritional needs results in a substantial increase in hepatic MSRB1 protein level and activity in a mouse model of hepatic carcinogenesis (Novoselov *et al.* 2005). This is atypical for selenoprotein because expression of most selenoproteins reaches a plateau at nutritionally adequate levels.

1.3.4 GPX4

As described above, GPX4 differs from GPX1-3 and GPX6 in protein structures (monomer vs. tetramer) and substrate preferences (lipid peroxides vs. H_2O_2) (Labunskyy

et al. 2014). Furthermore, one of the three isoforms of GPX4 locates to the nucleus. Alternative splicing of *GPX4* mRNA results in translation products of the mitochondrial mGPX4, the cytosolic cGPX4, and the nuclear nGPX4. Expression of these GPX4 isoforms is in a tissue-specific. Although mGPX4 and nGPX4 are found only in testis, cGPX4 is present in various somatic and embryonic tissues (Schneider *et al.* 2006a). The function of GPX4 in the nucleus is not fully understood, but it is known that chromatin in the caput epididymis of nGPX4 knockout mice is more relaxed, suggesting that GPX4 can regulate chromatin compactness (Conrad *et al.* 2005). Furthermore, nGPX4 catalytically reduces the DNA-binding protamine and increase its linkage with histone proteins through disulfide cross-linking (Pfeifer *et al.* 2001). GPX4's function of limiting chromatin accessibility seems to be attributed to its structural roles and not peroxidase activity (Ursini *et al.* 1999). Altogether, testicular nGPX4 may inhibit gene expression through epigenetic mechanisms in a manner depending on its general structural interactions with chromatin instead of the specific recognition of target DNA sequences.

To date, GPX4 is one of the three selenoproteins that are essential, based on the observations of embryonic lethality in *Gpx4*$^{-/-}$, *Txnrd1*$^{-/-}$, and *Txnrd2*$^{-/-}$ mice (Yant *et al.* 2003; Conrad *et al.* 2004; Jakupoglu *et al.* 2005). Interestingly, knockout of DIO3 renders the mice partially lethal during embryogenesis (Hernandez *et al.* 2006). To circumvent the limitation of embryonic lethality in the whole body and full *Gpx4* gene knockout, GPX4 isoform-specific and tissue-specific conditional knockout mice have been generated to understand physiological functions of these three GPX4 isoforms. It is hypothesized that not all of these three GPX4 isoforms are essential. With the use of these sophisticated mouse models, it has been shown that 1) spermatocyte-specific *Gpx4*

or *mGpx4* knockout results in male infertility (Imai *et al.* 2009; Schneider *et al.* 2009), and 2) *nGpx4* knockout mice are viable and fertile (Conrad *et al.* 2005). These results collectively suggest that cGPX4 and mGPX4 are essential for embryogenesis and fertility, respectively; however, the proposed epigenetic role of nGPX4 in the regulation of chromatin condensation may not be necessary for male fertility or survival. Mice overexpressed with *GPX4* had less liver apoptosis that was induced by *t*-butylhydroperoxide and diquat (Ran *et al.* 2004). Paradoxically, the lifespan of $Gpx4^{+/-}$ mice is slightly longer (7%, 1029 vs. 963 days, $P < 0.05$) than that of $Gpx4^{+/+}$ control mice (Ran *et al.* 2007). This unexpected role of GPX4 in lifespan is consistent with our recent results that show that long-term dietary Se deficiency increases ($P < 0.05$) longevity by 4 and 7 % in male and female mice with humanized telomeres, respectively (Wu *et al.* 2017). Nonetheless, it is of future interest to elucidate the nuclear function of GPX4 in various tissues and during the life cycle.

1.3.5 TXNRD1 and TGR

After protein disulfides are reversed by reduced TNX, oxidized TXN can only be recycled by the three TXNRN members of selenoproteins. TXNRD1, TXNRD2, and TGR are encoded by *Txnrd1*, *Txnrd2* and *Txnrd3*, respectively (Tamura & Stadtman 1996; Miranda-Vizuete *et al.* 1999; Sun *et al.* 1999). TGR is unique because it carries both glutaredoxin and TXN-fold domains (Su *et al.* 2005). Although TXNRD1 is present in mitochondrion and cytosol and TGR is mainly expressed in microsome, results from ^{75}Se-labeled proteins demonstrated that a portion of TXNRD1 and TRG is localized to the nucleus in mouse testis (Sun *et al.* 2001). Although the functional significance of TGR localization in the nucleus is unknown, genetic analyses clearly suggest that

TXNRD1 has important roles in the nucleus. Isoforms of TXNRD1 exist as a result of alternative splicing and localize to various cellular localizations. Through the approach of rapid amplification of TXNRD1 cDNA, cytosolic TXNRD1b is known to bind to the nuclear receptors, estrogen receptor-α and -β through its LXXLL motif (Rundlof *et al.* 2004), which, in turn, induces translocation of this selenoprotein to the nucleus for modulation of estrogen signaling (Damdimopoulos *et al.* 2004). Another functional implication of TXNRD1 in the nucleus is evidenced by studies with the use of embryos from *Txnrd1*$^{-/-}$ mice, in which nonfunctional oxidized ribonucleotide reductase is expressed and DNA synthesis is impaired (Jakupoglu *et al.* 2005). Although the mechanisms are unclear, this suggests TXNRD1 has critical roles in the regulation of DNA metabolism. Members of the TXNRD family also indirectly participate in genome maintenance through post-translational regulation of nuclear proteins including NF-κB, AP-1, p53 and glucocorticoid receptor (Arner 2009; Lu & Holmgren 2009). The transient and isoform-specific nature of these two selenoproteins indicates that the contribute to the regulation of genome stability. However, the mechanism by which they translocate intracellularly and how they mediate downstream targets in response to various stimuli remains to be elucidated.

1.3.6 Selenoprotein expression at supranutritional level in mice and supplemental Se in cells

Although it was previously reported that selenoprotein expression is saturated at the nutritional level, this simplified view is challenged by a strong body of recent evidence. Supranutritional Se up-regulates a couple of selenoproteins, such as MSRB1 activity in TGFα/c-Myc mice with hepatic tumors (Novoselov *et al.* 2005; Novoselov *et*

al. 2010) and SELENOH protein in the liver of healthy pigs (Liu *et al.* 2012). Supranutritional selenized yeast containing Se at 3-4 fold higher than nutritional needs, with 20 Se-containing chemicals was efficacious at cancer prevention in human study (Clark *et al.* 1996). Supplementation of supranutritional or toxic levels of a single Se species such as selenite induced diabetes in animals (Zhou *et al.* 2013). Clearly, the pathogenesis of cancer and diabetes differ, but Se speciation is also critical for health outcomes and this may also be explained from the perspective of Se regulation of epigenetics (Cheng *et al.* 2014). Previous studies on Se nutrition mainly employed animal models. Cell cultures were considered inappropriate in this regard because fetal bovine serum, an essential component for cell culture medium, may contain sufficient Se to saturate selenoprotein expression. In addition to selenoproteins, supplemental Se clearly regulates other proteins. In HCT116 colon and LNCaP prostate cancer cells that were supplemented with Se compounds at above the nutritional level, DNA methyltransferase (DNMT) activity and DNMT-1 protein expression were reduced (Fiala *et al.* 1998; Xiang *et al.* 2008). Similarly, supranutritional Se in rats suppresses global DNA methylation (Zeng *et al.* 2011). Epigenetic regulation of supplemental or supplemental Se impacts not only DNA methylation but also histone modifications. Se compounds are known to activate histone H3 acetylation in a rat model of colorectal carcinogenesis and histone H2AX phosphorylation in colorectal cancer cells, but inhibits histone deacetylase activity in B-cell lymphoma (Qi *et al.* 2010; Kassam *et al.* 2012; Hu *et al.* 2013). In addition to the modulation of histone proteins, we have previously demonstrated that Se compounds at sub-lethal doses ($< LD_{50}$) can activate ATM-dependent DNA damage for senescence response in non-cancerous cells but not in cancerous cells (Qi *et al.* 2010; Wu *et al.*

2010). Since a senescence response is a hallmark of early tumorigenesis barrier, this provides a clue as to how supranutritional Se can inhibit cancer growth in some clinical studies (Clark *et al.* 1996; Wu *et al.* 2010). It is intuitive to speculate that nuclear Se or selenoproteins confer such roles of Se in genome maintenance.

1.4 Figures and Tables

Table 1.1 Human diseases linked to inborn gene mutations in association with selenoprotein synthesis

Gene Mutations		Phenotypes	Selenium/Selenoprotein deficiency	Reference
SECISBP2 R540Q/R540Q	Missense	Abnormal thyroid function tests (TFT), short stature, delayed bone age, normal mental development	Low plasma Se, low plasma SEPP1, low GPX3, low DIO2 activity in fibroblasts	(Dumitrescu *et al.* 2005)
SECISBP2 p.M515fsX563/ p.Q79X	Nonsense-mediated mRNA decay/Premature termination	Mild mental retardation, pervasive development disorders, hypoplastic thyroid gland	Extremely low levels of plasma Se, GPX and SELENOP	(Hamajima *et al.* 2012)
SECISBP2 P1:fs255X P2:C691R	P1:Frameshift premature stop mutation. P2:Missense	Abnormal TFT, azoospermia, muscular dystrophy, photosensitivity, abnormal cytokine secretion, and telomere shortening and replication stress in T lymphocytes	Low plasma Se, SELENOP and GPX3; low mGPX4, TXNRD3 and SELENOV in seminal plasma; low SELENON, MSRB1, and GPX1 protein, and SELENOH, SELENOW, and SELENOT mRNAs in fibroblasts.	(Schoenmakers *et al.* 2010)
SEPSECS Y429X/T325S	Missense, with residual activity, truncation	Cortical laminar necrosis, loss of myelin and neurons, and astrogliosis	Low GPX1, GPX4 TXNRD1 in brain	(Anttonen *et al.* 2015)
SEPSECS Y443C/Y443C Y443C/A239T	Missense	PCH2D, PCCA, microcephaly, spasticity, seizures. Autosomal recessive symptoms of progressive cerebellocerebral atrophy	Heterologous complementation assay	(Agamy *et al.* 2010)
SEPSECS D489V/D489V *SEPSECS*		Intellectual disability, developmental delay		(Makrythanasis *et al.* 2014)
TRU-TCA1-1 C65G/C65G	Reduced mutant transcript levels	Abdominal pain, fatigue, muscle weakness	Low plasma Se. Low SELENOP, GPX3 in plasma. GPX1 in fibroblasts. SELENOW mRNA in fibroblasts.	(Schoenmakers *et al.* 2016)

Mutations in *SECISBP2*, *SEPSECS* and *TRU-TCA1-1* distinctly results in an array of phenotypes and selenoprotein deficiency. Of note, they are not selenoprotein genes but they encode proteins necessary for selenoprotein synthesis.

Table 1.2 Hierarchy human nuclear selenoproteins predicted by cNLS Mapper

Selenoproteins	Gene symbol	Protein ID	Gene ID	NLS type	Predicted NLS	Score
Selenoprotein H[b]	*SELENOH*	NP_734467	280636	Monopartite Bipartite	3 PRGRKRKAEA 73 KPRRGSFEVTLLRPDGSSAELWTGIKKGPP	13 3.7
Iodothyronine deiodinase 2	*DIO2*	NP_054644	1734	Monopartite	264 KRUKKTRLA	5.5
Selenoprotein T	*SELENOT*	NP_057359	51714	Monopartite	24 GGVPSKRLKMQY	5.5
methionine sulfoxide reductase B1[b]	*MSRB1*	NP_057416	51734	Bipartite Bipartite	34 RSKYAHSSPWPAFTETIHADSVAKRPEH 63 RSEALKVSCGKCGNGLGHEFLNDGPKPGQSRF	5.4 3.4
Selenoprotein K	*SELENOK*	NP_067060	58515	Monopartite	42 LQQDVKKRRSY	4.5
Selenoprotein N	*SELENON*	NP_996809	57190	Bipartite	23 PPRRRARSLALLGALLAAAAAAAVRVCARH	4.3
Selenoprotein S	*SELENOS*	NP_060915	55829	Bipartite	151 RKSDRKPLRGGGYNPLSGEGGGACSWRPGRRGP	3.4
Selenoprotein I	*SELENOI*	NP_277040	85465	Bipartite	14 GFDKYKYSAVDTNPLSLYVMHPFWNTIVKV	3.2
Thioredoxin reductase 1[b]	*TXNRD1*	NP_877419	7296	Bipartite Bipartite	29 KEAAQYGKKVMVLDFVTPTPLGTRWGL 462 KKQLDSTIGIHPVCAEVFTTLSVTKRSG	2.2 3.1
Selenoprotein W	*SELENOW*	NP_003000	6415	Bipartite Bipartite	21 QLKKKLEDEFPGRLDICGEGTPQATGFFE 59 SKKKGDGYVDTESKFLKLVAAIKAALA	3 2.8
Glutathione peroxidase 2	*GPX2*	NP_002074	2877	Bipartite Bipartite	4 IAKSFYDLSAISLDGEKVDFNTFRGRAVLI 142 WSPVRRSDVAWNFEKFLIGPEGEPFRRYSRT	2.8 2
Glutathione peroxidase 4[b]	*GPX4*	NP_002076	2879	Bipartite Bipartite	5 RLCRLLKPALLCGALAAPGLAGTMCASRDDWRC 151 PKGKGILGNAIKWNFTKFLIDKNGCVVKRY	2.4 2.6
Thioredoxin/glutathione reductase[b]	*TXNRD3*	NP_443115	114112	Bipartite	10 GPGKAGDAPNRRSGHVRGARVLSPPGRRAR	2.6
Glutathione peroxidase 6	*GPX6*	NP_874360	257202	Bipartite	171 WEPMKVHDIRWNFEKFLVGPDGVPVMHWFH	2.4
Iodothyronine deiodinase 1	*DIO1*	NP_000783	1733	Bipartite	25 VGKVLLILFPDRVKRNILAMGEKTGMTRNP	2.1

[a] In accordance with the input format of cNLS Mapper (36), selenocysteine (U) is substituted by cysteine (C) for amino acid input. Two types of NLS, monopartite and bipartite, are searched against the 25 selenoproteins. Monopartite is considered more accurate than bipartite (90% vs. 80%) in predicting NLS (36). Selenocysteine residues are not located in NLS except for Iodothyronine deiodinase type II. The scores are denoted as:>10, nucleus only; 8–10, mainly nucleus; 2–8, partial nucleus;<2, non-nucleus.

[b] Nuclear presence being verified by experimental evidence.

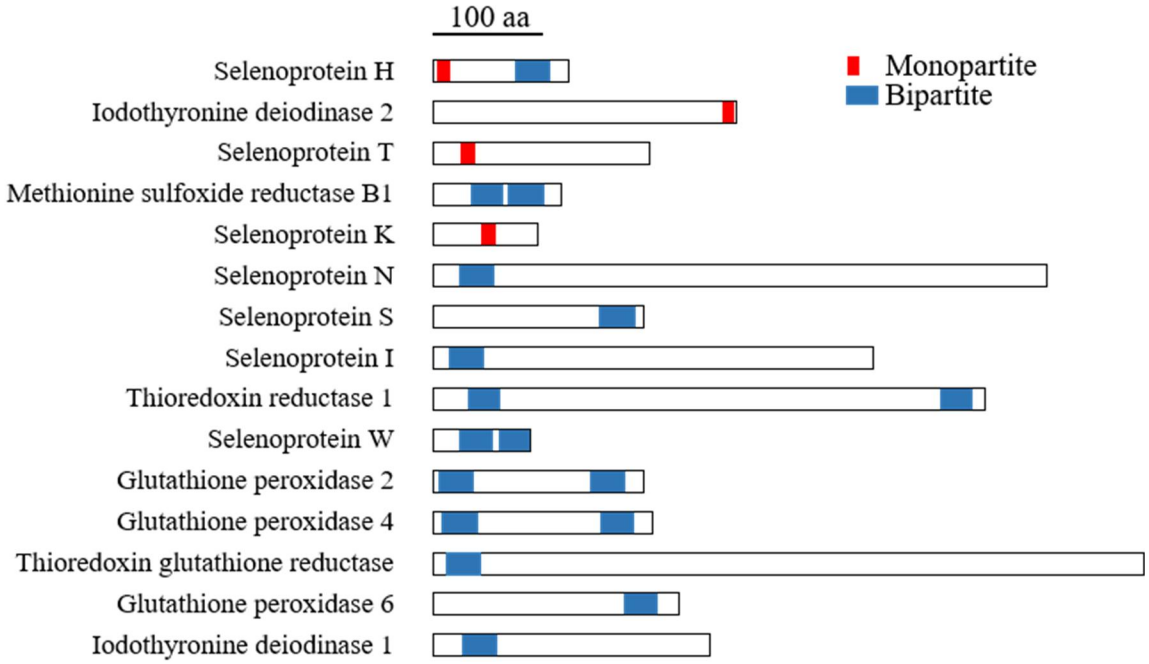

Figure 1.1 Locations and types of NLS (monopartite and/or bipartite) on the nuclear selenoproteins as predicted by cNLS Mapper. Selenoproteins are listed in descending order of the likelihood to appear in the nucleus (see Table 1.2 for details).

CHAPTER II

SELENOPROTEIN H MAINTAINS GENOME STABILITY IN THE NUCLEOLUS BY REGULATING REDOX HOMEOSTASIS AND SUPPRESSING DNA DAMAGE

2.1 Abstract

Selenoprotein H (SELENOH) is a nucleolar oxidoreductase with DNA binding properties whose function is not well understood. To determine the role of SELENOH in genome maintenance, a knockout of *SELENOH* was generated in cell lines using CRISPR/Cas9-mediated genomic deletion. Based on the sequenced genome, results of deduced protein sequences indicated various forms of mutants in the CRISPR/Cas9-mediated knockout including a frame-shift by aberrant splicing and truncated SELENOH by early termination of translation. Loss of SELENOH in HeLa cells induced slow cell proliferation, the formation of giant multinucleated cells, accumulation of unrepaired DNA damage and oxidative stress, and cellular senescence. The nuclei within *SELENOH* cells were enlarged and possessed a single large nucleolus. Atomic force microscopy results indicated increased stiffness in the nucleoli of *SELENOH* knockout cells, suggesting that SELENOH maintains the flexible structure of the nucleolus. Furthermore, SELENOH knockout led to a large-scale reorganization of nucleolar architecture with the movement of nucleolar protein into nucleolar cap regions in response to oxidative stress.

This nucleolar reorganization is dependent on ATM signaling. Altogether, these results suggest that SELENOH appears to be a sensor for oxidative stress and contribute to redox regulation and genome maintenance in the nucleolus.

2.2 Introduction

Se exerts many of its physiological functions through selenoproteins. In 2003, it was concluded that the human genome harbors 25 selenoprotein genes (Kryukov *et al.* 2003). Selenoproteins contain the 21st amino acid, selenocysteine (Sec), with the use of a specialized mechanism to recode the otherwise stop codon UGA. The single letter abbreviation of Sec is U. Since 2003, many of selenoproteins have been studied, but the functional and physiological roles of selenoprotein H (SELENOH) has not yet been elucidated.

SELENOH was initially identified in the *Drosophila melanogaster* genome, which encodes the BthD protein (Martin-Romero *et al.* 2001), and subsequently, its homologs were found in the human and mouse genomes (Kryukov *et al.* 2003; Morozova *et al.* 2003). SELENOH expression is high in the brain, during embryogenesis, and in the nucleolus. The human *SELENOH* gene is found in open reading frame 31 on chromosome 11. The *SELENOH* gene contains 3 exons and 3 introns, totaling 2305 base pairs (bp). Based on the NCBI database, there are two transcript variants for *SELENOH*: transcript variant 1 (1448 bp, NM_170746) and transcript variant 2 (1428 bp, NM_001321335) (**Figure 2.2**). Since the length difference is located to the 3`-untranslated region, both variants encode the same SELENOH with 122 amino acids. Sec is located at position 44 and within the CXXU (CTSU) motif of this 14-kDa

selenoprotein. SELENOH also has a conserved nuclear targeting RKRK motif in the N-terminal sequence. SELENOH has a unique subcellular localization pattern that is specific to the nucleoli (Novoselov *et al.* 2007). Expression of SELENOH is relatively low in adult mouse tissues but is high during embryonic development and in certain cancer cell lines. SELENOH is one of the few selenoproteins whose expression is sensitive to dietary Se fluctuations (Howard *et al.* 2013). SELENOH contains an AT-hook motif, and may potentially serve as a redox sensor that functions in conjunction with some of the redox-responsive transcription factors (Panee *et al.* 2007). Overexpression of *SELENOH* protects HT22 mouse hippocampal neuronal cells from UVB irradiation-induced death through the reduction of superoxide formation, mitochondrial depolarization, and cell survival (Ben Jilani *et al.* 2007; Mendelev *et al.* 2009). Furthermore, overexpression of SELENOH in HT22 cells promotes mitochondrial biogenesis and improves mitochondrial functional performance (Mendelev *et al.* 2011). Furthermore, a recent study indicates that SELENOH as an essential regulator of redox homeostasis that also interacts with p53 in development and tumorigenesis (Cox *et al.* 2016). SELENOH also contributes to the suppression of senescence and DNA damage responses to oxidative stress in the presence of ATM kinase and p53 (Wu *et al.* 2014), which suggested that this nucleolar selenoprotein as a gatekeeper protein for genomic integrity.

Our preliminary studies have demonstrated that depletion of *SELENOH* leads to a mitotic defect that results in slow proliferation and multinucleation in HeLa cells. Such failure in proper mitotic progression is associated with disruption of genomic integrity. These observations suggest that SELENOH may play an important role in response to the

DNA damage in mitosis. Furthermore, loss of SELENOH results in significant changes in nucleolar morphology and nucleolar organization. In order to address this hypothesis, SELENOH knockout models were produced in cells in order to study the functions of SELENOH in cell cycling control and genome stability within the nucleolus. *SELENOH* knockout cell lines were constructed by the CRISPR/Cas9 technology. Biallelic mutants were selected by single colony screening and genomic DNA sequencing.

2.3 Materials and Methods

2.3.1 Cell culture and chemicals

The HeLa human cervix carcinoma cells and HEK 293T human embryonic kidney cells were cultured in Dulbecco's modified Eagle's medium (DMEM, Gibco, Thermo Fisher Scientific, Karlsruhe, Germany) with high glucose that was supplemented with 10% fetal calf serum (FCS, Gibco), 100 U/mL penicillin and 100 g/mL streptomycin (Sigma-Aldrich, Taufkirchen, Germany) at 37 ºC with 5% CO_2.

2.3.2 Generation of *SELENOH* knockout transfer constructs by CRISPR/Cas9 system

To knock out *SELENOH* using the CRISPR/Cas9 technology, two single guide RNA (sgRNA) oligonucleotides, SELENOH-CR1 and SELENOH-CR2 (**Figure 2.2**), were chosen to target the *SELENOH* gene with the use of publicly available on-line tools (Cong & Zhang 2015) to reduce the likelihood of off-target cleavage. CRISPR/Cas9 constructs for the *SELENOH* knockout were generated as described previously in the Zhang laboratory (Sanjana *et al.* 2014). Briefly, lentiCRISPRv2 plasmid (5 µg, Addgene plasmid #52961, Cambridge, MA) was digested and dephosphorylated with Fermentas

FastDigest BsmBI (3 units) and FastAP thermosensitive alkaline phosphatase (3 units, Thermo Fisher Scientific) at 37 ºC for 30 min in a 60 µL reaction mixture that contained 1X FastDigest Buffer and 1 mM DTT. The digested plasmid was gel purified with the use of a DNA Gel Extraction Kit (Thermo Fisher Scientific). To introduce BsmBI cloning site, the CACC and AAAC sequences were added at 5′ end to the sense and anti-sense sgRNA-specifying oligo sequences, respectively (sense sequence: *SELENOH*-CR1, CACCGCACTAGCTGACGCGTCTAT; *SELENOH*-CR2, CACCGTCGTCGGGTTCACCTTTAC; anti-sense sequence: *SELENOH*-CR1, AAACGATAGACGCGTCAGCTAGTG; *SELENOH*-CR2, AAACGTAAAG GTGAACCCGA CGAC). Next, the two complementary guiding nucleotides (10 µM) were phosphorylated and annealed in a 10 µL mixture that contained 1X T4 DNA Ligase Reaction Buffer (New England Biolabs, Ipswich, MA), ddH_2O (6.5 µL), and T4 polynucleotide kinase (0.5 µL, New England Biolabs) at 37 ºC for 30 min, 95 ºC for 5 min, and then ramping down to 25 ºC at 5 ºC /min. Next, annealed duplex DNA (0.5 µM) was cloned into linearized lentiCRISPRv2 plasmid (50 ng) in a mixture containing 1X Quick Ligase Buffer (New England Biolabs), Quick Ligase (1 µL, New England Biolabs), and ddH_2O (to a total of 11 µL). After incubation at room temperature for 10 min, the ligated lentiCRISPRv2 constructs were transformed into GCI-L3 competent cell (GeneCopoeia, Rockville, MD). Selected colonies were analyzed by plasmid isolation and sequencing. The lentiCRISPRv2 construct was ligated with a non-target guiding RNA duplexes as a negative control (5′-CGCGATAGCGCGAATATATT-3′) (Perez *et al.* 2015).

2.3.3 Packaging of lentiviruses

To prepare lentiviruses for *SELENOH* knockout, the lentiCRISPRv2 SELENOH-CR1 and SELENOH-CR2 transfer constructs were co-transfected with the packaging plasmids pCMV-VSV-G and psPAX2 (Addgene plasmids #8454 and #12260). 293FT cells (Thermo Fisher Scientific) at 70-80% confluency in 6-well plates were transfected with the transfer construct (0.75 μg) and the pCMV-VSV-G (0.56 μg) and psPAX2 (1.69 μg) packing plasmids in lentivirus packaging medium (Opti-MEM with GlutaMAX that was supplemented with 5% FBS and 1mM sodium pyruvate, Invitrogen) in the presence of Lipofectamine 3000 Transfection Reagent (7 μL) and P3000 Enhancer Reagent (6 μL). Cell culture medium was replaced by pre-warmed lentivirus packaging medium at 6h post-transfection. At 24 h post-transfection, the cell medium was centrifuged at 2,000 × *g* for 10 min at room temperature and filtered with the use of a 45 μm polyethersulfone low protein binding membrane (Millipore) to remove cell debris. Next, 1 volume of Lenti-X concentrator (Clontech, Mountain View, CA) was mixed with 3 volumes of the filtered supernatant by gentle inversion, followed by incubation at 4 ºC for 30 min and centrifugation at 1,500 × *g* and 4 ºC for 45 min. After the supernatants were removed, the pellets were re-suspended in complete DMEM to 1/10 of the original volume and stored at -80 ºC in single-use aliquots.

2.3.4 Generation of *SELENOH* knockout cells

HeLa and HEK293T cells were plated in a 24-well plate (2×10^4 cells per well) for 24 h prior to infection of lentiviruses carrying the lentiCRISPRv2 *SELENOH* knockout constructs in the presence of polybrene (6 μg/mL, Millipore, Billerica, MA) for

12 h at 37 ºC with 5% CO_2. Two days after recovery from the infection, sgRNA/Cas9 positive cells were screened with the use of puromycin (2 μg/mL, Goldbio, Olivette, MO). Two weeks later, the cells were expanded to three 35-mm dishes. *SELENOH* knockdown efficiency was assessed with the use of quantitative real-time polymerase chain reaction (RT-qPCR).

2.3.5 RT-qPCR analysis

Total RNA was isolated with the use of RNeasy Mini Kits (Qiagen, Hilden, Germany). DNA was removed by on-column DNase digestion using RNase-free DNaseI (Invitrogen, Rockville, MD). One μg of DNaseI-treated RNA was (5 μg of RNA/unit DNaseI) reversely transcribed to cDNA by using the High Capacity cDNA synthesis kit (Thermo Fisher Scientific). All PCR reactions were performed in 10 μL with the use of an SYBR Green Super Mix (Bio-Rad, Hercules, CA). Reactions were performed in an ABI Prism 7500 Fast Sequence Detection System (Thermo Fisher Scientific) with the following conditions: 95 °C for 30 sec, 40 cycles at 95 °C for 15 sec, and then 60 °C for 30 sec. A dissociation curve was run for each plate to confirm the production of single products. SDS software was used to quantitate data by using the ΔΔCt method and β-actin mRNA (*ACTB*) as an internal control. The following gene-specific primers were used for RT-qPCR reactions in this study:

sense sequence: HSH_CR1_F, CATTGCACTAGCTGACGCGTCTATG;

HSH_CR2_F, GTAGCCGAGAAGCGAGAGAAGCTGG;

Actin_F, CACTCTTCCAGCCTTCCTTCCTGG;

anti-sense sequence: HSH_CR1_R, CTTCTTAATCCCAGTCCAGAGCTCC;

HSH_CR2_R, GGCTTCGTCGGGTTCACCTTTACTGG;

Actin_R, TCCTTCTGCATCCTGTCGGCAATGC.

The HSH_CR1_R and HSH_CR1_F primers for CR1 were targeted *SELENOH* exon 3 and the junction of *SELENOH* exons 1 and 2, respectively (**Figure 2.1**). The HSH_CR2_F and HSH_CR2_R primers for CR2 targeted *SELENOH* exon 1 and exon 2, respectively (**Figure 2.1**). Such designs excluded the possibility to detect genomic DNA (Hsu *et al.* 2011). The specificity of each primer pair was verified by PCR with the use of recombinant plasmid DNA that contained *SELENOH*.

2.3.6 Cell growth assay

To assess the impact of *SELENOH* knockout on cell proliferation, cells infected with *SELENOH*-CR1 and *SELENOH*-CR2 knockout and non-targeting constructs were grown in 6-well plates and counted daily with the use of a hemocytometer until they reached ~ 2×10^6 cells/mL or no longer grew logarithmically.

2.3.7 Clonal selection

Cells were counted and seeded into 96 well plates through serial dilution starting from 4,000 cells/well to about one cell/well. After 7-10 days of expansion, wells that contained only a single colony were marked. These colonies were transferred into 24-well plates and cultured with fresh media. Genomic DNA was extracted by re-suspension of the cells in an extraction buffer (10 mM Tris-HCl, pH 8.0, 1 mM EDTA, 0.2 mg/mL protease K, 20 μg/mL RNaseA), incubation at 55 °C for 30 min, and purification by the phenol-chloroform method. RNA isolation and cDNA synthesis were performed with the use of RNeasy Mini Kits (Qiagen) and the High Capacity cDNA synthesis kit (Thermo Fisher Scientific), respectively. *SELENOH* genomic DNA and cDNA were separately

amplified by Phusion Hot Start II DNA Polymerase (Thermo Fisher Scientific). Fifty μL PCR reactions were carried out in 1 μL Phusion Hot Start II DNA Polymerase, 5X Phusion HF buffer, 200 μM dNTPs each, and 0.2 μM HSH_CDS_F and HSH_CDS_R primers (**Figure 2.1**)

(HSH_CDS_F, CTTCCTTTGAGAGAGGTTTCCGCTG,

HSH_CDS_R, TACAATGCCTTACTAGAGGGTTGCCTC), with cycling conditions of 98 °C for 3 min, 35 cycles of 98 °C for 10 s, 72 °C for 45 s, and a final extension of 72 °C for 5 min. Amplicons were sliced out from a 1% (w/v) agarose gel, purified with a DNA Gel Extraction Kit (Thermo Fisher Scientific), the PCR products were A-tailed and then cloned into a pGEM-T easy vector (Promega). At least 10 clones for each colony were picked and cultured in LB medium that contained 50 μg/mL ampicillin and was agitated at 200 rpm and 37°C overnight. Plasmid DNA was isolated using a Plasmid Miniprep Kit (Thermo Fisher Scientific) and subjected to Sanger sequencing with M13F and M13R sequencing primers from Eurofins Genomics (Louisville, KY). Sequences were analyzed by Blast (NCBI, Bethesda, MD) with the use of *SELENOH* genomic NC_000011.10 (region: 57741250-57743554) and transcript NM_170746.3 as references. The ExPasy tool "Translate" was used to predict the consequences of the observed nucleotide changes (Kapahnke *et al.* 2016).

2.3.8 Scoring cell, nuclei, and nucleolar size/number

HeLa cells were seeded onto coverslips and fixed in pre-chilled 100% methanol at -20°C for 10 min. Coverslips were incubated with the cell-permeable SYTO RNASelect Green Fluorescence Cell Stain (500 nM, Thermo Scientific Scientific) for 20 min at 37°C, washed and mounted onto glass slides by using ProLong Gold antifade mountant

with DAPI (Thermo Scientific Scientific). The area of an individual cell or clustered cells were traced and scored with the use of freehand measurement tools of ImageJ software (NIH). Areas cross-sectioned with nuclei and nucleoli were measured. Nucleoli were counted by SYTO RNASelect staining. A contrast threshold was applied to micrographs to allow for the semi-automated, unbiased measurement of nucleolar area and number by using the wand (tracing) tool of ImageJ software.

2.3.9 Cell cycle analysis

Control or *SELENOH* knockout HeLa cells were subjected to cell cycle analysis. Briefly, 3×10^6 cells were fixed with cold ethanol (70%) for 1 hr, centrifuged, resuspended and incubated in PBS containing RNase A (0.2 mg/mL, Thermo Fisher Scientific) and Propidium Iodide (10 µg/mL, Roche Diagnostics GmbH, Indianapolis, IN) for 20 min, and analyzed immediately by flow cytometry. The channel FL2 was used to analyze 50,000 events per condition. Gated cells were manually categorized into cell cycle stages. Cell cycle analysis was performed using Flowjo V10 software (Treestar, Inc.).

2.3.10 Cellular glutathione peroxidase (GPX) activity

Cells were harvested by rubber policemen, washed twice with cold PBS, collected cells by centrifugation (1,000 × *g* for 10 min at 4 °C), homogenized in 200 µL ice-cold buffer (50 mM Tris-HCl, pH 7.5, 5 mM EDTA, and 1 mM DTT), and centrifuged (20,000 × *g* for 10 min at 4°C) twice. The supernatant was stored on ice for immediate measurement of GPX activity according to the manufacturer's protocol (Cayman Chemical, Ann Arbor, MI, USA). Cumene hydroperoxide was used as a GPX substrate in

the presence of glutathione (GSH) to generate oxidized GSH (GSSG). The rate of NADPH consumption by glutathione reductase in the subsequent reduction of GSSG was determined spectrophotometrically by a Synergy HTX plate reader (BioTek Instruments, VT) and used to calculate GPX activity. GPX activity was expressed as units per mg protein determined by the Pierce BCA protein assay (Thermo Scientific Scientific).

2.3.11 Thioredoxin reductase (TXNRD) activity

TXNRD activity was quantified using a thioredoxin reductase assay kit (Cayman Chemical, Ann Arbor) based on the measurement of gold-inhibited NADPH dependent DTNB reduction by a Synergy HTX plate reader (BioTek Instruments, VT). Cells were harvested by rubber policemen and homogenized in a potassium phosphate buffer (50 mM) that contained 1 mM EDTA (pH 7.4). TXNRD activity per minute was estimated as the difference between the reducing activity of the sample in the absence and presence of gold thioglucose, followed by normalization against total protein concentration as determined by the Pierce BCA protein assay (Thermo Scientific Scientific). TXNRD activity was analyzed in duplicates for each sample in four independent experiments.

2.3.12 Protein oxidation

Protein carbonyl content was measured using a protein carbonyl assay kit (Cayman Chemical, Ann Arbor) that was based upon a DNPH reaction. Cells were harvested by rubber policemen and homogenized in an MES buffer (50 mM) that contained 1 mM EDTA (pH 6.7). The supernatant was clarified by centrifugation at 10,000 × *g* for 15 min and 4 °C. Followed by incubation at 25°C for 15 min with streptomycin sulfate (1% v/v). After centrifugation at 6,000 × *g* for 10 min and 4°C,

protein carbonyl content was measured with the use of a Synergy HTX plate reader (BioTek Instruments, VT). Calculation of the carbonyl content was performed by using a molar absorption coefficient of 22 mmol/L per cm.

2.3.13 Identification of senescence cells

Cells were plated at 0.3×10^6 cells per well in 6-well plates overnight, washed twice in PBS, fixed at 25°C with 3% formaldehyde for 5 min, and washed twice with PBS. Senescent cells were assessed with the use of a senescence-associated β-galactosidase kit (BioVision, Milpitas, CA) according to the manufacturer's protocol. Cells were then visualized at 40× magnification under an inverted microscope (Wilovert A, Hund, Wetzlar, Germany) with bright field illumination. Senescent cells that stained blue were counted in a blinded-manner using 15 different microscopic fields for each sample.

2.3.14 Western blotting analysis

The soluble fraction was prepared by lysing the cells in ice-cold RIPA buffer that contained protease inhibitors cocktail and sodium orthovanadate (Santa Cruz Biotech, Santa Cruz, CA) for 30 min, centrifuging at 10,000 × *g* for 30 min at 4 °C, separating proteins using 12% SDS-PAGE, and transferring to PVDF membranes (Bio-Rad Lab., CA). The membranes were blocked with a solution containing 5% bovine serum albumin for 1 h and then incubated separately overnight at 4 °C with primary antibodies (pATM Ser1981, 1:5000, 2152-1, Epitomics, Burlingame, CA), γH2AX (phosphor-H2AX on Ser-139, 1:2000, 05-636, Upstate, Charlottesville, VA), ATM (1:2000, sc-23931, Santa Cruz Biotech.), UBF (1:2000, sc-13125, Santa Cruz Biotech.), C23 (1:2000, sc-8031,

Santa Cruz Biotech.) and β-actin (1:2000, sc-8432, Santa Cruz Biotech.) at 4 °C. This was followed by incubation with HRP-conjugated secondary antibodies (Santa Cruz Biotech.) for 1 h at 25°C. An enhanced chemiluminescence detection kit (Bio-Rad Lab., CA) was used for signal acquisition by Chemidoc XRS+ Imaging System (Bio-Rad Lab., CA). The quantification of the bands was conducted using Image Lab (Bio-Rad Lab., CA).

2.3.15 Measurement of nucleolar stiffness by atomic force microscopy (AFM)

Cells were treated with or without H_2O_2 (1 mM) for 15 min. Nucleoli were fractioned from HeLa cells as previously described (Hacot *et al.* 2010). Isolated nucleoli were seeded on a 0.01% poly-L-lysine-coated slide for 30 min in sucrose buffer (0.25 M) and measured at room temperature with the use of a Bruker Catalyst AFM (Bruker AXS, Santa Barbara, CA) that was mounted on an inverted optical microscope (Observer Z1, Carl Zeiss Microscopy, Jena, Germany). This allowed simultaneous optical visualization and force measurement. The cantilevers with triangular-shaped tips (SNL-C, Bruker, f0:40-75 kHz, k: 0.32 N/m) have been used previously (Preta *et al.* 2016; Ruiz-Rincon *et al.* 2017). Sensitivity of the cantilevers were calibrated in dry conditions on a clean glass surface to measure the spring constant using the thermal method (Stark *et al.* 2001). The sensitivity was calibrated again in liquid. Nucleoli were randomly selected to measure stiffness. The Young's modulus was calculated using the Derjaguin–Mueller–Toporov model.

$$F_{tip} = \frac{4}{3} E^* \sqrt{Rd^3} + F_{adh}$$

Where E* is the reduced Young's modulus, F_{tip} is the force on the tip, F_{adh} is the adhesion force, R is the tip end radius and d is the tip-sample separation.

Young's moduli in control and H_2O_2-treated or *SELENOH* knockout nucleoli were averaged per experiment. Each set of experiments was repeated at least three times, averaged and illustrated as histograms with SEM.

2.3.16 Immunofluorescence

Immunofluorescence was performed on control and *SELENOH* knockout HeLa cells that were grown on circular coverslips in 12-well plates to 50% to 70% confluence. Cells were incubated in the presence or absence of 4 μM NU7441, an inhibitor of DNA-dependent protein kinase (Leahy *et al.* 2004), and/or 2 μM KU60019, an inhibitor of ATM (Harding *et al.* 2015), for 1 hour prior to addition of H_2O_2 (1 mM) for 15 min. Followed by extensive washing (three times on ice in drug-free medium) and incubation at 37 °C for up to 4 h in medium with or without inhibitors. Actinomycin D (0.2 μg/mL, Sigma) was added to the culture media for 2 h. All drugs were added to cells such that the final concentration of DMSO was 0.1% and the results were compared with controls that were incubated with 0.1% DMSO alone. Coverslips were washed in PBS and fixed in 4% formaldehyde at 25°C for 30 min. Following 0.3% Triton X-100 permeabilization, cells were blocked for 1 h at 25°C in PBS+0.02% Tween 20 (PBST)/5% BSA. Primary antibodies were diluted in blocking buffer, added to coverslips, and incubated overnight at 4 °C. After washing with PBST, goat anti-rabbit or donkey anti-mouse secondary antibodies that were conjugated to AlexaFluor 488 or 568 (Invitrogen) were diluted (1:500) in PBST and incubated at 25°C for 1 h. After washing with PBST, coverslips were mounted in ProLong Gold Antifade Mountant that contained DAPI (Thermo

Scientific Scientific). Images were captured with a Zeiss LSM 510 confocal microscope and a 63 × oil objective (Carl Zeiss Microscopy, Jena, Germany). Images were prepared for publication using ImageJ software (NIH), and all panels of a given image were only adjusted for brightness and contrast. Primary antibodies and dilutions were: 53BP1, 1:1000 (NB100-904, Novus) and UBF, 1:100 (F-9, Santa Cruz).

2.3.17 Statistical analysis

Data were represented as mean ± SEM. The one-way analysis of variance (ANOVA) was conducted to determine the effect of the *SELENOH* gene knockout on cell performance. Differences among groups were determined by least square difference tests. All analysis was conducted using SAS (SAS 9.4, Cary, NC) at a significance level of $P < 0.05$.

2.4 Results

2.4.1 Generation of *SELENOH* knockout cells

In order to understand the functional roles of SELENOH, *SELENOH* knockout cells were generated with the use of the CRISPR/Cas9 system. *SELENOH* contained three exons. Because there was another ATG codon at the end of exon 1 (93 bp), a shortened *SELENOH* may be expressed by beginning from this alternative start codon if CRISPR is edited upstream of the exon 1. A truncated *SELENOH* that contained exons 1 and 2 was likely to be expressed if the CRISPR targeted *SELENOH* exon 3. Thus, two sgRNAs that targeted exon 2 of *SELENOH* gene, *SELENOH*-CR1 and *SELENOH*-CR2, were cloned into a Cas9-expressing lentiviral transfer vector lentiCRISPRv2. While

SELENOH-CR1 covered the selenocysteine codon (TGA) and targeted the beginning of the exon 2, *SELENOH*-CR2 matched the middle part of exon 2 (**Figure 2.2**).

HEK 293T and HeLa cells were transduced with the lentiCRISPRv2 construct, followed by maintenance in complete DMEM medium that contained puromycin to select for resistant cells. Seven days later, cells were grown in the puromycin-deprived medium for an additional 16 d. Results from RT-qPCR analysis demonstrated that *SELENOH* mRNA levels were reduced ($P < 0.05$) in HEK 293T and HeLa cells that were transduced with *SELENOH*-CR1 and *SELENOH*-CR2 lentiCRISPRv2 knockout constructs (**Figure 2.3**). *SELENOH* mRNA levels were reduced by 83% in *SELENOH*-CR2-transfected HeLa cells and more than 90% reduction in *SELENOH*-CR1-transfected HeLa cells and *SELENOH*-CR1- or *SELENOH*-CR2- transfected HEK 293Tcells. *SELENOH* mRNA levels did not differ ($P > 0.05$) in knockout cells that were generated by *SELENOH*-CR1 and *SELENOH*-CR2 knockout constructs.

2.4.2 Cell growth

Cell numbers were reduced ($P < 0.05$) in HEK 293T (44 and 55%) and HeLa (43 and 48%) cells 6 days after transfection with *SELENOH*-CR1 and *SELENOH*-CR2 lentiCRISPRv2 knockout constructs ($P > 0.05$) (**Figure 2.4**). The impact of *SELENOH* knockout on proliferation showed no difference between these two constructs. Furthermore, *SELENOH* knockout HeLa cells showed morphological changes and were multinucleated (**Figure 2.9**).

2.4.3 Single-cell derived clones and sequence analysis

Because the multinucleated phenotypes were observed in HeLa but not in non-cancerous 293T cells, *SELENOH* loci were sequenced in single-cell-derived clones of HeLa cells with *SELENOH*-CR1 lentiCRISPRv2 constructs. As expected, 90% of cells contained mutations at the proximity of Cas9 excision site. Among the 31 cell lines that were generated by clonal expansion, 3 were wild-type, and 28 were deletion mutations. (**Figure 2.5**). Except the homozygous B6 clone, all other clones had heterozygous mutations in the two alleles. These mutations were predicted to result in frameshifted, prematurely terminated, and deleted SELENOH. Interestingly, one allele of clone A11 (A11-a) was wild-type. Although 16 of them were mixed clones based on sequencing results, the remaining 12 *SELENOH* mutant cell lines (1 monoallelic and 11 biallelic mutations) were originated from single clones (**Figures 2.5** and **2.6**). Results from RNA sequencing demonstrated that cDNA sequences were present in all of these mutations in *SELENOH*, which suggests that both *SELENOH* gene alleles were expressed.

To study the effects of *SELENOH* knockout at the mRNA level, cDNA was prepared from the total RNA of NTC and knockout HeLa cells B6, D3, D4 and D9 and PCR amplified using primers that were specific for the coding region of *SELENOH*. The resulting fragments were cloned into a plasmid. The mRNA sequences obtained from the NTC HeLa cells were identical to the *SELENOH* reference sequence and contained 122 amino acids. The mRNA sequences of the homozygous clone B6 and one allele of clone D3 (D3-a) contained the deletion of 36 bp and 42 bp within exon 2 and resulted in 12 and 14 amino acid deletions, respectively (**Figures 2.7** and **2.8**).

For the other allele of clone D3, its gDNA sequence showed deletions of 144 bp in exon 2, 162 bp for intron 2, 101 bp for exon 3 and 75 bp of gDNA. Its mRNA sequences altered the splicing at the right exon-intron borders, which resulted in the deletion of whole exons 2 and 3 and an insertion of 30 bp of gDNA. The deduced amino acid sequences of D3-b showed a frame-shift mutation and an early stop contained 50 aa residues from the N-terminus (**Figures 2.7** and **2.8**).

The mRNA sequences of the two alleles of clone D4 corresponded to their gDNA sequences, which contained the deletion of 1 bp and 31 bp within exon 2 and resulted in a frame-shift and an early stop that was contained 66 (D4-a) and 56 (D4-b) residues from the N-terminus (**Figures 2.7** and **2.8**).

The mRNA sequences of D9-b altered the correct splicing site. Its gDNA sequence showed a deletion of 31 bp from intron 1 and 38 bp from exon2, but its mRNA sequence indicated that the whole exon 2 (146 bp) spliced off and resulted in a frame-shift and an early stop that contained only 48 residues (**Figures 2.7** and **2.8**).

For D9-a, its gDNA sequence showed that 76 bp were deleted from intron 1, 146 bp from exon 2 and 53 bp from intron 2, and its mRNA sequence showed that exon 2 and 3 were spliced off and contained insertions of 15 bp in intron 1 and 28 bp in intron 3 sequences, which resulted in a frame-shift and an early stop that contained 54 aa residues.

Clone B6 and D3-a produced a truncated protein product in which 12 and 14 residues were missing. D3-b and clones D4 and D9-b showed aberrant splicing with a frame-shift in generating an early stop with a severely truncated protein. These changes may produce dysfunctional proteins, and that can be expected to be knockouts.

2.4.4 *SELENOH* knockout hampers mitosis and the number and size of nucleoli in HeLa cells

Microscopic examination *SELENOH* knockout HeLa cells revealed a multinucleated phenotype (**Figure 2.9 A**). Although 2.9% of the non-targeting control HeLa cells were multinucleated, such a phenotype accounted for 7.4-21.1% in 7 clones (B6, D3, D4, D9, A10, A11, and C4) of *SELENOH* knockout cells (**Figure 2.9 B**). Among these *SELENOH* knockout cell lines, the multinucleated phenotype was the most prominent (21.1%) in cells derived from the D3 clone. The multinucleated cells that were derived from the D3 clone were up to 22 times larger than control cells and contained up to 18 nuclei (**Figure 2.9 C**). DAPI staining revealed that multinucleated *SELENOH* knockout cells had an abnormal organization of nuclei (**Figure 2.9 C**), which may impede normal mitosis and result in incomplete karyokinesis without cytokinesis. Four *SELENOH* knockout cell lines (B6, D3, D4 and D9) had the highest percentage of multinucleated phenotype and were therefore selected for further analyses.

In these four *SELENOH* knockout cells, the number of nuclei per multinucleated cell ranged from 2 to 18 (**Figure 2.9 C**). In contrast, the 3% multinuclear NTC cells had two nuclei per cell and most likely represented mitotic cells. Not only was the number of nuclei changed when the *SELENOH* genes were deleted, but also the total nuclear area was changed as shown in **Figure 2.10 C**. When compared to the nuclear area of NTC cells (204.7 μm^2), B6, D3, D4 and D9 nuclei had greater nuclear areas ($P < 0.05$), which were 272.0, 398.3, 286.5 and 259.3 μm^2, respectively.

Like many other functional domains in the nucleus, the nucleolus is not bound by a membrane. The nucleolus is also one of the most highly dynamic organelles in terms of number, size and shape, which vary significantly by cell type, cell-cycle stage and culture

conditions (Thiry & Lafontaine 2005). *SELENOH* is known to be the only nucleolar selenoprotein that is known by sequence analysis (Zhang *et al.* 2016) and expressed in the nucleoli when tagged to green fluorescence protein (Novoselov *et al.* 2007). We hypothesized that depletion of *SELENOH* disrupts nucleolar stability. To address this hypothesis, control and *SELENOH* knockout HeLa cells were simultaneously stained with DAPI and SYTO RNASelect as indicators of the nuclei and nucleoli, and observed under confocal microscopy (**Figure 2.10 A**).

Ribosomal gene clusters form the nucleolus organizer regions (NORs) are located on chromosomes 13, 14, 15, 21, and 22 in humans and express 5.8S, 18S, and 28S ribosomal RNAs. Human cells could, in theory, have 10 nucleoli. However, this is rarely observed likely due to the natural clustering of NORs and the failure of all NORs to become activated (Booth *et al.* 2014). In our HeLa NTC cells, most cells contained more than one nucleolus, and the average number of nucleoli per nucleus is 2.13. In the multinucleated *SELENOH* knockout HeLa cells, there were two phenotypes. First, as shown in **Figure 2.10 A-a**, the nuclei contained a clear nuclear envelope that is predominantly carried by a single large nucleolus. Second, as shown in **Figure 2.10 A-b**, the nuclear envelope was broken down, the nucleoli were disassembled, and their components were dispersed. It is noteworthy that, in higher eukaryotes, nucleoli undergo a cycle of disassembly and reassembly during mitosis (Thiry & Lafontaine 2005). When cells exit mitosis, nucleolar components reassemble around the individual NORs, which can later coalesce to form either one or multiple functional nucleoli (Leung *et al.* 2004). The knockout of *SELENOH* resulted in a decreased ($P < 0.05$) number of countable nucleoli (**Figure 2.10 A-a**) per nucleus from 2.13 in NTC cells to 1.63, 1.54, 1.71 and

1.81 in B6, D3, D4, and D9 cells, respectively (**Figure 2.10 B**). Results of the calculation of nucleolar areas showed that nucleoli were aggregated in *SELENOH* knockout multinucleated cells. When compared to the nucleolar area in NTC HeLa cells (32.6 μm^2), that in D3, D4 and D9 *SELENOH* knockout cells had greater ($P < 0.05$; 57.4, 46.5, and 40.2 μm^2, respectively) nucleolar areas. However, the nucleolar area (38.4 μm^2) in B6 *SELENOH* knockout cells was not different ($P > 0.05$) from the NTC cells (**Figure 2.10 C**). When compared to NTC cells, the relative nucleolar area divided by nuclear area was decreased ($P < 0.05$) by 10% in B6 knockout cells and 12.2% in D3 knockout cells; however, a nucleolar area divided by nuclear area remained unchanged in the D9 and D4 knockout cells (**Figure 2.10 E**).

2.4.5 Cell cycle analyses in *SELENOH* knockout cells

The phenotype of incomplete mitosis with multinucleated cells (**Figure 2.9**) is consistent with reduced proliferation in *SELENOH* knockout HeLa cells (**Figure 2.4**), which was likely the cause of cell death. Results of flow cytometric analyses indicated that the percent sub-G1 and S phase cell populations did not differ ($P > 0.05$) between the control and the four *SELENOH* knockout HeLa cells (**Figure 2.11**). The percent G1 phase cells were decreased ($P < 0.05$) in the four *SELENOH* knockout cells when compared to NTC. In contrast, G2/M content was increased in the D3 knockout clone (up to 22%, $P < 0.05$), but not in B6, D4 or D9 knockout clones. The polyploid DNA content was increased (B6, 1.8-fold; D3, 2.3-fold; D4, 1.2-fold; D9, 2.1-fold; $P < 0.05$) in the four SELENOH knockout when compared to the control HeLa cells.

These results suggest that apoptosis is not associated with reduced proliferation in *SELENOH* knockout HeLa cells; rather, these cells did not complete mitosis, resulting in

the multinucleated feature and reduced G1 cell population. Analyses of DAPI and SYTO stained cells displayed near complete cell segregation, since there was re-appearance of nucleoli and chromatin formation, with the exception of two daughter cells. These results suggest a role of *SELENOH* in cytokinesis.

2.4.6 Activities of two antioxidant enzymes and protein oxidation in *SELENOH* knockout HeLa cells

Since SELENOH is known as a thioredoxin-like protein and carries glutathione peroxidase activity (Novoselov *et al.* 2007), the impact of *SELENOH* knockout on GPX and TXNRD activities was determined. The thioredoxin system is one of the critical cellular redox regulators, and TXNRD is the only group of enzymes known to catalyze the reduction of thioredoxin (Kim *et al.* 2004). The D3 clone of *SELENOH* knockout cells has higher ($P < 0.05$) GPX (2.9-fold) and TXNRD (50%) activities than the NTC control HeLa cells (**Figure 2.12 A-B**). GPX and TXNRD activities were not different ($P > 0.05$) between the NTC control and the B6, D4, or D9 *SELENOH* knockout HeLa cells. Protein carbonyl contents were comparable between the NTC control and the four *SELENOH* knockout HeLa cells (**Figure 2.12 C**).

2.4.7 Knockout of *SELENOH* induces cellular senescence in the multinucleated cells

Senescent cells often exhibit an increase in the number of multinucleated cells (Matsumura 1980). The observation of multinucleation in *SELENOH* knockout cells prompted the investigation of cellular senescence in these cells. Senescence-associated β-galactosidase (SA-β-gal) is a lysosomal enzyme that is overexpressed and accumulates in senescent cells (Yuan *et al.* 2008). As shown in **Figure 2.13**, SA-β-gal expression was

11- to 31-fold higher ($P < 0.05$) in the four *SELENOH* knockout cells than the NTC cells. In particular, almost all adherent multinucleated cells were SA-β-gal positive.

2.4.8 *SELENOH* knockout cells display sustained DNA damage response before and after treated with H_2O_2

Senescence in human cells is associated with oxidative stress and DNA damage (Chen *et al.* 1995; Campisi & d'Adda di Fagagna 2007), both of which can result in ATM pathway activation (Wu *et al.* 2014). ɣ-H2AX and ATM phosphorylation on Ser-1981 (pATM) are well-defined markers for DNA breaks and ATM pathway activation (Bakkenist & Kastan 2003; Lobrich *et al.* 2010). Thus, ɣ-H2AX and pATM levels were evaluated in *SELENOH* knockout and NTC Hela cells.

Results of Western analyses showed that *SELENOH* knockout rendered HeLa cells induced ($P < 0.05$) ATM activation in the absence of H_2O_2, 60 min after treatment with 0.01-0.1 mM H_2O_2 (**Figure 2.14 A**), and 0-240 min after treatment with 1 mM H_2O_2 (**Figure 2.14 B**). The level of pATM displayed a time-dependent increase (0-4 h) in NTC cells in response to H_2O_2 treatment (1 mM), ATM activation by 1 mM H_2O_2 treatment reached a plateau at 15 min (**Figure 2.14 B**). Level of pATM did not differ ($P > 0.05$) between NTC and *SELENOH* knockout HeLa cells when they were treated with H_2O_2 at 0.5 or 1.0 mM for 60 min. Level of ɣ-H2AX was comparably induced by H_2O_2 treatment at 0.5 or 1 mM for 60 min in NTC and SELENOH knockout HeLa cells (**Figure 2.14 A**). However, there was a time-dependent (0-240 min) increase ($P < 0.05$) in ɣ-H2AX level after treatment with 1 Mm H_2O_2, the extent of which was greater in *SELENOH* knockout than in NTC HeLa cells (**Figure 2.14 B**). UBF and C23 protein levels did not differ ($P > 0.05$) after H_2O_2 treatment or between NTC and *SELENOH* knockout HeLa cells.

2.4.9 Nucleolar stiffness measurement

The nucleolus, a nuclear body with flexible structures, is best known for its functions in ribosome biogenesis. It has been demonstrated that SELENOH locates to the nucleoli. The impact of *SELENOH* knockout on stiffness and structure of the nucleoli was determined by immunofluorescence and AFM. Nucleoli were isolated from the control and *SELENOH* knockout HeLa cells with or without H_2O_2 treatment. Force was applied to the center of a nucleolus with the use of a pyramidal-shaped tip of the cantilever. Considering the heterogeneous nature of nucleoli, Young's moduli of biological samples are not absolute values and expressed as related to control (Radmacher 1997; Yokokawa *et al.* 2008). Analyses of nucleolar stiffness by AFM showed that Young's moduli were greater (D3, 1.8-fold, and D9, 1.6-fold, $P < 0.05$; B6, 1.4-fold and D4, 1.4-fold, $P > 0.05$) in *SELENOH* knockout cells than control HeLa cells (**Figure 2.15**). However, Young's moduli did not differ ($P > 0.05$) between H_2O_2 treatment in *SELENOH* knockout or control HeLa cells. These results are consistent with our unpublished results of RNA-Seq, which indicates that *SELENOH* knockout in HeLa cells downregulated ribosome biogenesis. The downregulated ribosome biogenesis may lead to the accumulation of unprocessed rRNA within the nucleolus that increased stiffness. The nucleolar stiffness of the RPS6 and RPL11 knockdown proteins was increased in a previous study (Louvet *et al.* 2014). The morphological changes in *SELENOH* knockout HeLa cells may also contribute to the stiffness in the nucleoli.

2.4.10 *SELENOH* knockout induces nucleolar reorganization

Tumor suppressor p53-binding protein 1 (53BP1) is recruited to DNA break sites and is a marker for this form of DNA damage (Panier & Boulton 2014; Zimmermann &

de Lange 2014). The number of 53BP1 foci were greater ($P < 0.05$) in the D3 *SELENOH* knockout cells when compared to control HeLa cells for both non-treated and H_2O_2 treated groups (**Figure 2.16 A-B**). H_2O_2 treatment of D3 *SELENOH* knockout and control HeLa cells induced 53BP1 focus formation in a comparable manner. As a positive control for nucleolar caps, actinomycin D treatment induced 53BP1 focus formation in D3 *SELENOH* knockout and control HeLa cells at a similar level ($P > 0.05$). Pretreatment with the ATM kinase inhibitor KU60019, but not the DNA-PK kinase inhibitor NU7441, attenuated the H_2O_2-induced 53BP1 focus formation in a SELENOH-independent manner (**Figure 2.16 A** and **C**). The positive control, actinomycin D treatment induced UBF cap formation in D3 *SELENOH* knockout and control HeLa cells in a similar manner ($P > 0.05$). Altogether, results suggest that SELENOH prevents the formation of H_2O_2-induced DNA breaks and nucleolar cap formation in an ATM-dependent manner.

2.5 Discussion

Despite substantial advances characterizing the molecular and biochemical features of SELENOH (Ben Jilani *et al.* 2007; Novoselov *et al.* 2007; Stoytcheva *et al.* 2010; Wu *et al.* 2014), functional and physiological understanding of this selenoprotein is lacking. Genetic knockouts of individual selenoprotein genes have been applied in cells to elucidate their physiological functions. Through CRISPR/Cas9-mediated genome-editing, SELENOH was knocked out in HeLa and 293T cells. Results from the RT-qPCR analysis showed that *SELENOH* mRNA levels were reduced ($P < 0.05$), but still detectable. This is because Cas9 cleaves the gene of interest and creates a double-stranded break (DSB) in the DNA, which can be repaired by non-homologous end joining

(NHEJ) (Sander & Joung 2014). As NHEJ is an error-prone DNA repair process, insertions and deletions (indels) are often introduced into the gene, resulting in frameshifts and mutations that potentially lead to loss-of-function. Thus, it is necessary to determine indels in both alleles and to clarify whether the mutant is monoallelic or biallelic. Consequently, monoallelic mutations or, in rare occasions, wildtype cells may exist in the knockout population. To achieve a functional gene knockout, it is necessary to perform single colony screening to confirm and select clones with biallelic mutations. Analysis at the genomic level revealed expected insertion/deletion (indel) alterations in exon 2 which was targeted within the *SELENOH* gene where the functional motif CXXU locates. Based on the sequenced genome, protein sequences indicated various forms of mutants including frame-shift by aberrant splicing and truncated SELENOH by early termination of translation. Although CRISPR/Cas9 edited *SELENOH* mRNAs are expressed, they are expected to be translated as dysfunctional SELENOH that are subject to degradation.

SELENOH knockout cell lines expressed a reduced growth rate ($P < 0.05$) when compared with control cells. This is likely attributed to the following: 1) cell death is more frequent in *SELENOH* knockout cells; 2) the cell cycle is blocked. Cell cycle analysis indicated that the control and *SELENOH* knockout cells had a similar, low proportion of apoptotic cells. These results suggest that increased apoptosis is not associated with reduced proliferation in *SELENOH* knockout cells. Instead, the decreased G1 cell population and increased G2/M population and polyploid DNA content in *SELENOH* knockout cells indicated that this selenoprotein has a critical role in the G2/M phase of the cell cycle.

Knockout of *SELENOH* leads to a mitotic defect and accumulation of multinucleated cells. Analyses of DAPI- and SYTO-stained cells display near complete mitosis as evidenced by the re-appearance of nucleoli and chromatin formation without separation of two daughter cells. These results suggest that *SELENOH* has a role in cytokinesis. Multinucleation can arise from defects in DNA replication, cell proliferation, or mitosis and from the aberrant expression of proteins that regulate these critical cellular events (Faye *et al.* 2013).

Accumulation of multinucleated cells has been reported in HeLa cells that are deficient in the NF45 nuclear factor (Guan *et al.* 2008; Shamanna *et al.* 2011). Time-lapse microscopy results indicate that the multinucleated NF45-deficient cells originated from the incomplete cytokinesis of daughter cells, followed by the fusion of several binucleated cells (Shamanna *et al.* 2011). Thus, NF45 may be required for the proper progression of mitosis. In addition, the NF90-NF45 complex regulates the repair of DNA double-strand breaks by non-homologous end-joining that requires DNA-activated protein kinase (DNA-PK). These results suggest that the multinucleated phenotype may be attributed to defective DNA double-strand break repair (Shamanna *et al.* 2011). Furthermore, the multinucleated phenotype has been observed in X-ray-irradiated HeLa cells (Huang *et al.* 2008; Shang *et al.* 2010) and cells that are deficient in DNA-PKcs or Ku80 with defective DNA double-strand break repair (Difilippantonio *et al.* 2000; Shamanna *et al.* 2011).

Experiments on the down-regulation of ILF2 in 1q21-amplified MM cells indicate the expression of multinucleated phenotypes and abnormal nuclear morphologies, including nucleoplasmic bridges, nuclear buds, and micronuclei (Marchesini *et al.* 2017).

These observations suggest genomic instability in replicating cells. Other proteins that are essential to mitosis and whose aberrant expression has been linked to multinucleation include survivin (Colnaghi *et al.* 2006), aurora (Yan *et al.* 2005), and ORC6 (Prasanth *et al.* 2002). Altogether, observations from the current study on the multinucleated phenotype are consistent with these reports and suggest a defective DNA damage response, cell cycle progression, and cytokinesis in *SELENOH*-deficient cells.

Because SELENOH is reported to carry GPX activity and a TXN-like domain (Novoselov *et al.* 2007), it was determined whether or not the knockout of *SELENOH* impacted GPX and TXNRD activities. *SELENOH* knockout cells increased ($P < 0.05$) GPX activity. GPX enzymatically decomposes oxidized peroxides, H_2O_2, and lipid peroxides and can be stimulated by oxidative stress (Lee *et al.* 1990; Avissar *et al.* 1996). Altogether, these enzymes can neutralize oxidants at the expense of GSH, which is replenished through GSSG reduction. An increase in GPX activity and expression usually occurs as an adaptive response to increased oxidative stress (Velsor *et al.* 2001). Upregulation of this enzyme system in *SELENOH* knockout cells suggests increased oxidative stress in the cell.

SELENOH contains an AT-hook motif and is a member of the high-mobility group (HMG) family of DNA-binding proteins (Panee *et al.* 2007). Proteins in this family bind DNA minor grooves and specific DNA sequences, thus regulating various aspects of DNA metabolism such as DNA repair, replication, and transcription (Grosschedl *et al.* 1994). *SELENOH* shRNA knockdown in MRC-5 human primary cells induced genomic instability and cellular senescence (Wu *et al.* 2014). In the current study, the knockout of *SELENOH* in HeLa cells resulted in increased ($P < 0.05$) pATM on Ser-1981 and γ-

H2AX as evidenced by Western analyses and increased 53BP1 foci by immunofluorescence. However, H_2O_2-induced 53BP1 focus formation was exacerbated and inhibited by DNA-PK and ATM inhibitors. These results suggest that ATM has an essential role in the DNA damage response. These results are consistent with previous research that, under ambient O_2 level (20%), *SELENOH* shRNA MRC-5 cells display ATM pathway activation and intrinsic DNA breaks (Wu *et al.* 2014). These data suggest that *SELENOH* has a critical and general role in the maintenance of genomic stability against chronic oxidative stress.

Knockdown of *SELENOH* by shRNA results in replicative senescence in MRC-5 human normal diploid fibroblasts, but not in cancerous HeLa cells (Wu *et al.* 2014). Knockout of *SELENOH* by CRISPR/Cas9 genomic editing renders human cancerous HeLa cells susceptible to premature cellular senescence. Based on *SELENOH* mRNA levels, the 20% residual *SELENOH* mRNA may confer the shRNA HeLa cells from senescence responses (Wu *et al.* 2014). However, the depletion of this selenoprotein by CRISPR/Cas9 induces senescence in the same cancer cells. This suggests a need of minimal SELENOH (~ 20%) in the protection of HeLa cancerous cells from senescence induction. Thus, SELENOH is essential for the protection against cellular senescence in both non-cancerous and cancerous cells, although the former is more susceptible than the latter to the defect. Increased cellular senescence in *SELENOH* knockout HeLa cells may be attributed to the accumulation of unrepaired DNA damage and chronic oxidative stress.

Furthermore, the knockout of *SELENOH* results in the accumulation of multinucleated cells, and almost all adherent multinucleated cells were SA-β-gal positive.

Consistent with these results, a recent study indicated that NF45 knockdown HeLa cells exhibit a striking senescence-like morphology and multinucleated phenotype, which suggests a cell fusion event or a defect in cytokinesis in these cells (Faye *et al.* 2013).

More recently, it was reported that knockdown of coilin expression accelerates premature cellular senescence and increased chemo-sensitivity in HeLa cells (Song *et al.* 2017). Coilin is a hallmark protein of the Cajal body, which is a distinct nuclear area that is physically and functionally associated with the nucleolus (Shaw *et al.* 2014). This suggests that modulation of *SELENOH* expression could be considered as a potential anti-tumor strategy. It is of future interest to determine whether chemosensitivity can be increased through accelerated senescence in *SELENOH* knockout cells.

Cellular and biochemical studies and computational analyses of nuclear localization sequences indicated that SELENOH is a genuine nucleolar protein in the nucleus (Zhang *et al.* 2016). Furthermore, the structural integrity of the nucleoli may be necessary for cellular stress responses (Leung *et al.* 2004). Therefore, it was determined whether or not the knockout of *SELENOH* impacted nucleolar size, number, mechanical property and nucleolar component localization.

The nucleolus is a dynamic nuclear structure that assembles and disassembles during each round of mitotic cell division (Leung & Lamond 2003). Nucleoli in Xenopus laevisoocytes are liquid-like droplets of RNA and protein (Brangwynne *et al.* 2011). The number, size, and shape of nucleoli vary significantly by cell type, cell-cycle stage and cell culture conditions (Thiry & Lafontaine 2005).

In the current study, nucleoli were stained with SYTO RNASelect, and cell nuclei were counterstained with DAPI. SYTO RNASelect stain is a cell-permeable proprietary

cyanine dye with preferential staining of the nucleoli (Pickard & Bierbach 2013; Luciani *et al.* 2017). *SELENOH* knockout HeLa cells had larger nuclei than control cells and possessed one single large nucleolus. The phenotype of single large nucleoli could be attributed to the cell fusion event or a defect in cytokinesis. By a study of the nucleolar cycle in embryonic ovarian and kidney cells (Anastassova-Kristeva 1977), it was found that during prophase, large G2 nucleoli disassemble into small nucleoli nucleate and grow on the NORs upon completion of cytokinesis. These nucleoli increase in size as components continue assembling; moreover, the size appears to increase while their number decreases, probably due to fusion events. Ki-67 is one of the earliest proteins to bind the perichromosomal layer in mitosis. Loss of Ki-67 in HeLa cells renders small nuclei that are accompanied by a large nucleolus (Booth *et al.* 2014). This may occur because chromosomes that lack a perichromosomal layer might associate with one another more closely than normal, thus promoting NOR fusion during reactivation. Another possibility is that, upon Ki-67 depletion, the efficiency of NOR reactivation is reduced during mitotic exit. Nonetheless, the mechanism of the single nucleolus phenotype in *SELENOH* knockout cells is presently unknown. It is of future interest to determine whether or not SELENOH impacts mitotic chromosome periphery.

To investigate the mechanical properties of nucleoli in *SELENOH* knockout cells, AFM was used to assess nucleolar stiffness. The observation of increased stiffness in the nucleoli of *SELENOH* knockout cells suggests that SELENOH maintains the flexibility of the nucleolus structure. Furthermore, our unpublished results of RNA sequencing show that *SELENOH* knockout downregulates ribosome biogenesis in HeLa cells, which may accumulate unprocessed rRNA and consequently lead to increased stiffness in the

nucleolus. Consistent with this notion, it is known that knockdown of the ribosomal proteins RPS6 and RPL11 caused increased nucleolar stiffness in HeLa cells (Louvet *et al.* 2014). It is also possible that the morphological changes may have an influence on the measurement of stiffness in the nucleoli.

Cellular response to DSBs is required to cope with ongoing defects in normal DNA metabolism such as transcription in the nucleus. Similarly, nucleolar DSBs can result in a transient block in rRNA synthesis by silencing RNA polymerase I (Pol I) transcription (Kruhlak *et al.* 2007). The transcriptional silencing caused by DSBs can segregate the nucleolar structure into nucleolar caps (Shav-Tal *et al.* 2005). Nucleolar caps are known to be induced in response to various forms of DNA damage such as DSBs (Larsen & Stucki 2016). The formation of the caps has some advantages. First, by presenting the damaged rDNA at the nucleolar periphery, it is accessible to recruiting repair factors from the nucleoplasm. Second, the caps concentrate high levels of homologous sequences in close proximity to each other, which could promote repair by homologous recombination (van Sluis & McStay 2017).

As described above, *SELENOH* knockout cells display increased cellular stress and DSBs, which may lead to reorganization of the nucleolar architecture. To determine how *SELENOH* knockout influences the nucleolar structure, the localization of nucleolar proteins upstream binding factor (UBF) before and after H_2O_2 treatment was examined. *SELENOH* knockout cells induced ($P < 0.05$) the redistribution of UBF into caps that were localized in close proximity to DAPI-sparse nucleoli. Interestingly, the nucleolar cap formation in H_2O_2-treated HeLa cells was dependent on ATM signaling, which is consistent with the known functional interactions between SELENOH and ATM in

senescence (Wu *et al.* 2014). Such a role of SELENOH in the maintenance of genomic stability in the nucleoli may be critical for embryogenesis and protection against carcinogenesis in mice (Chapter 3) and zebrafish (Cox *et al.* 2016).

The nucleolus has been proposed to serve as a stress sensor (Boulon *et al.* 2010). There are a few types of stress that can lead to marked changes in the nucleolar organization. Nucleolar DSBs can be generated by ionizing radiation or UV microbeams that induce ATM-dependent silencing of Pol I transcription (Kruhlak *et al.* 2007). Cells irradiated with 10 Gy of γ-irradiation also display UBF segregation and re-distribution to nucleolar caps, a hallmark of transcriptionally inactive cells (Shav-Tal *et al.* 2005; Kruhlak *et al.* 2007). Induction of DSBs within the rDNA repeats by I-PpoI expression confirms the inhibition of nucleolar transcription upon the induction of DSBs in rDNA and segregation of nucleolar structure into nucleolar caps (Harding *et al.* 2015; van Sluis & McStay 2015). Thus, it is of future interest to elucidate the mechanism by which SELENOH regulates rDNA transcription and nucleolar cap formation.

2.6 Figures and Tables

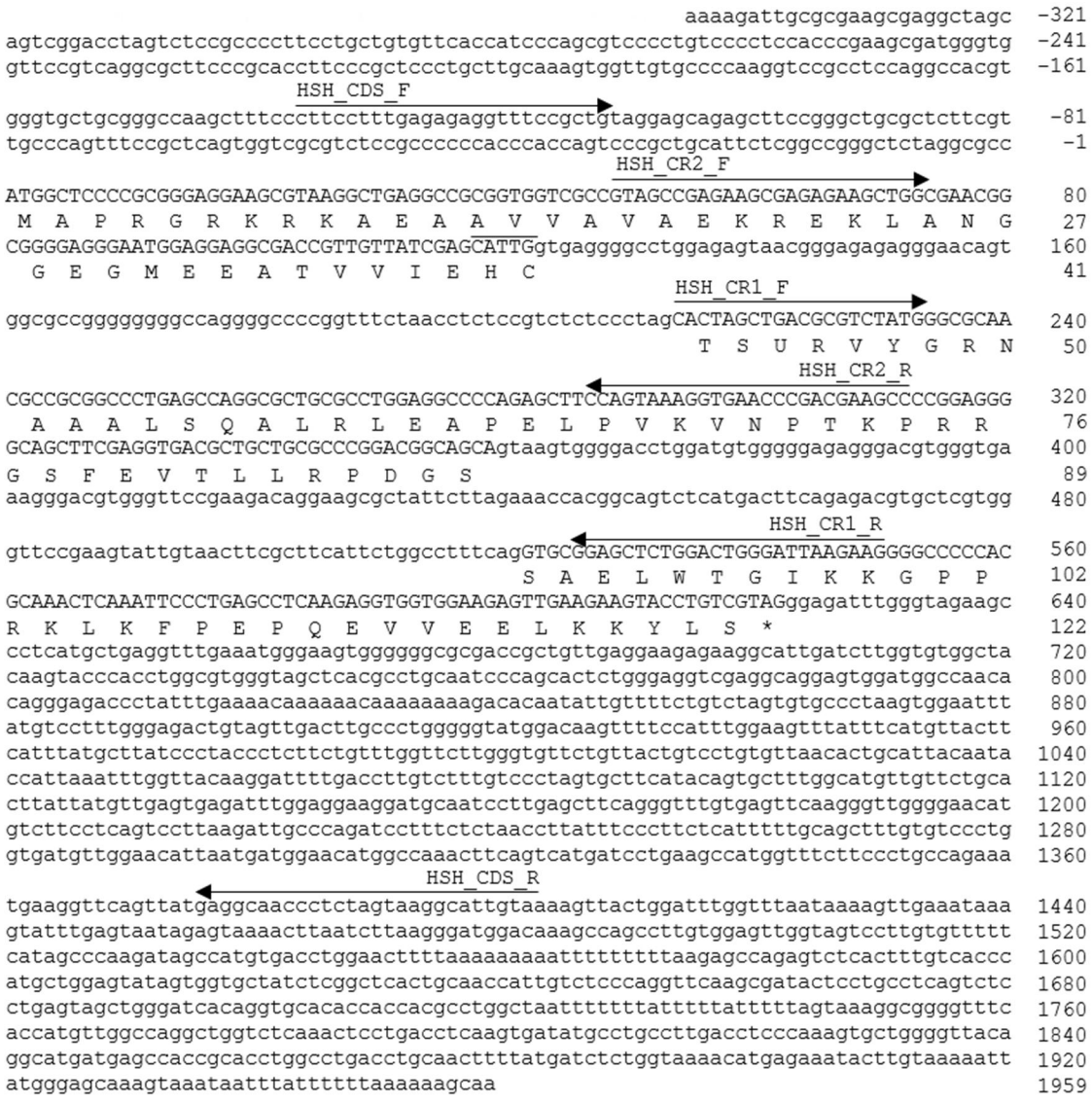

Figure 2.1 Nucleotide and derived amino acid sequences of *SELENOH* gene and six primers for PCR amplification.

The sequences of three introns are presented in lowercase letters. The translational stop codon is marked with an asterisk. The first nt (A) of translation start codon (ATG) is assigned as position 1 in the nt sequence, and the nt positions upstream of position 1 are presented with minus numbers. The sequence and direction of each primer are denoted by a long arrow. Primers HSH_CDS_F and HSH_CDS_R are used for mutation analysis. Primers HSH_CR1_F and HSH_CR1_R, HSH_CR2_F and HSH_CR2_R are used for RT-qPCR assays targeted to *SELENOH*_CR1 and *SELENOH*_CR2 mutated cells, respectively.

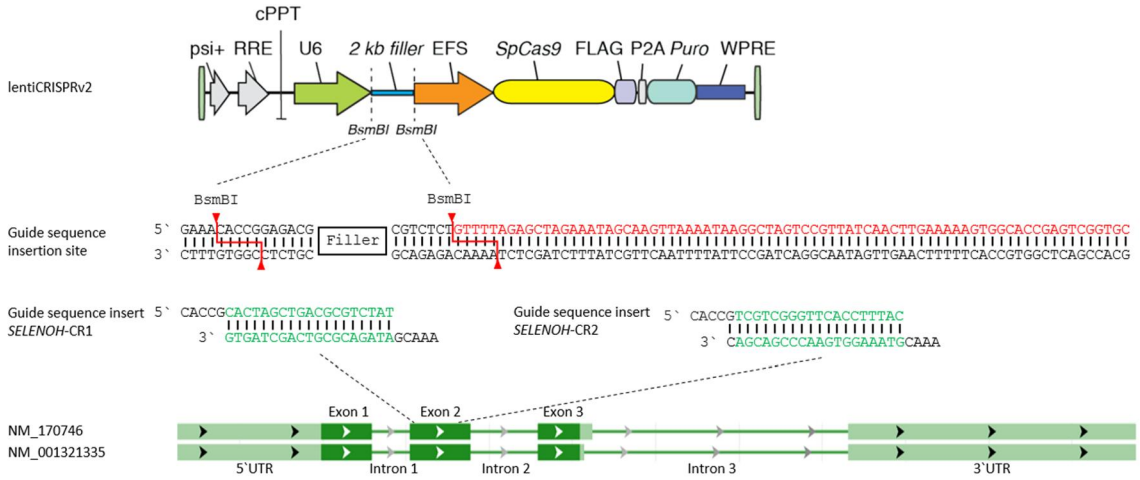

Figure 2.2 Schematic illustration of the *SELENOH* sgRNA/Cas9-expressing lentiCRISPRv2 constructs for *SELENOH* knockout.

SELENOH-CR1 and *SELENOH*-CR2 are the sgRNA-targeting sites and located in the sense and anti-sense strands of the exon 2, respectively. tracrRNA and sgRNA-targeting sites are shown in red and green, respectively. psi+, Psi packaging signal; RRE, Rev-responsive element; cPPT, central polypurine tract; U6, Pol III promoter; EFS, human elongation factor 1α promoter; SpCase9, Streptococcus pyogenes Cas9 gene; P2A, porcine teschovirus-1 self-cleaving peptide fragment; *Puro*, puromycin-resistant gene; WPRE, woodchuck hepatitis virus posttranscriptional regulatory element.

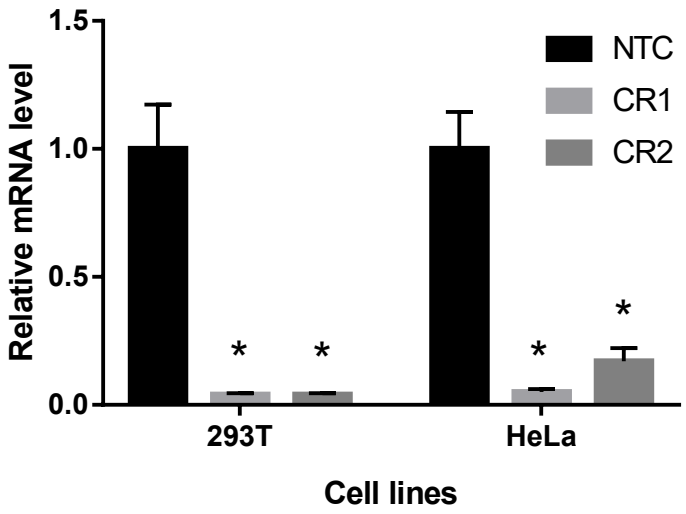

Figure 2.3 *SELENOH* mRNA levels in 293T and HeLa cells transfected with non-targeting control (NTC), *SELENOH*-CR1 (CR1) and *SELENOH*-CR2 (CR2) lentiCRISPRv2 constructs.

Values are mean ± SEM (n = 3). *, $P < 0.05$, compared to NTC. Data were normalized to *Actb* (β-actin) mRNA and calculated related to the NTC cells.

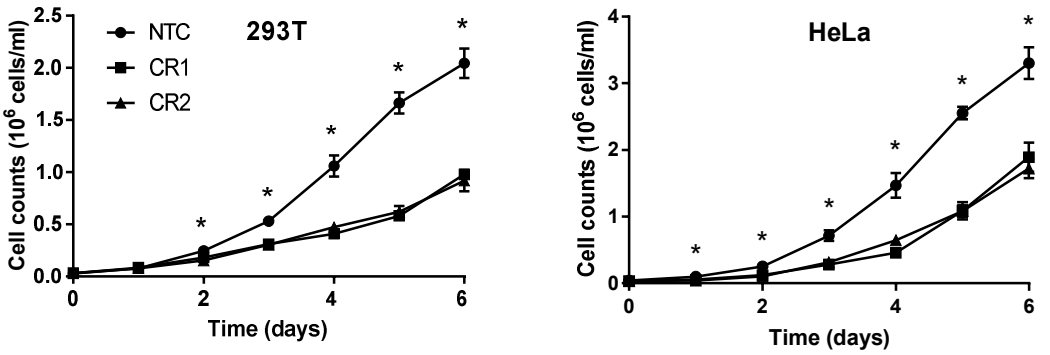

Figure 2.4 Effects of *SELENOH* gene knockout on proliferation in 293T and HeLa cells transfected with non-targeting control (NTC), *SELENOH*-CR1 (CR1) and *SELENOH*-CR2 (CR2) lentiCRISPRv2 constructs.

Cell numbers were determined by a hemocytometer daily. Values are mean ± SEM (n = 3). *, $P < 0.05$, compared to NTC.

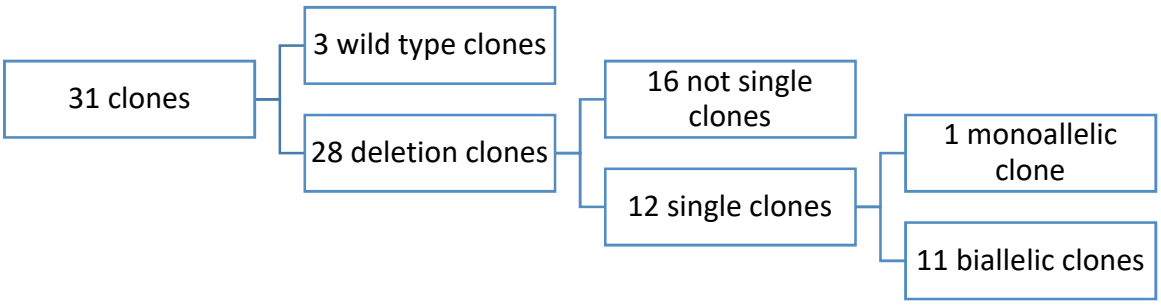

Figure 2.5 Details of the 31 *SELENOH* knockout HeLa cells derived from clonal expansion.

```
WT    5′ GGCCCCGGTTTCTAACCTCTCCGTCTCTCCCTAGCACTAGCTGACGCGTCTATGGGCGC.AACGCCGCGGCCCTGAGCCAGGCGCTGCGCCTGGAGGCCCCAGAGCTTCCAGTAAAG  3′
B6      GGCCCCGGTTTCTAACCTCTCCGTCTCTCCCTAGCACTAGC----------.----------CAGGCGCTGCGCCTGGAGGCCCCAGAGCTTCCAGTAAAG
A10-a   GGCCCCGGTTTCTAACCTCTCCGTCTCTCCCTAGCACTAGCTGACGCGT----------.----------CTGCGCCTGGAGGCCCCAGAGCTTCCAGTAAAG
A10-b   GGCCCCGGTTTCTAACCTCTCCGTCTCTCCCTAGCACTAGC----------.----------TGAGCCAGGCGCTGCGCCTGGAGGCCCCAGAGCTTCCAGTAAAG
A11-a   GGCCCCGGTTTCTAACCTCTCCGTCTCTCCCTAGCACTAGCTGACGCGTCTATGGGCGC.AACGCCGCGGCCCTGAGCCAGGCGCTGCGCCTGGAGGCCCCAGAGCTTCCAGTAAAG
A11-b   GGCCCCGGTTTCTAACCTCTCCGTCTCTCCCTAGCACTAGCTGACGCACTAGCTGA---.----------CCTGAGCCAGGCGCTGCGCCTGGAGGCCCCAGAGCTTCCAGTAAAG
C4-a    GGCCCCGGTTTCTAACCTCTCCGTCTCTCCCTAGCACTAGC----------.----------CTGAGCCAGGCGCTGCGCCTGGAGGCCCCAGAGCTTCCAGTAAAG
C4-b    GGCCCCGGTTTCTAACCTCTCCGTCTCTCCCTAGCACTAGC----------.----------TGAGCCAGGCGCTGCGCCTGGAGGCCCCAGAGCTTCCAGTAAAG
D3-a    GGCCCCGGTTTCTAACCTCTCCGTCTCTCCCTAGCACTAGCTGACGC---.----------CTGGAGGCCCCAGAGCTTCCAGTAAAG
D3-b    GGCCCCGGTTTCTAACCTCTCCGTCTCTCCCTAGCA----------.----------418 BP DELETION
D4-a    GGCCCCGGTTTCTAACCTCTCCGTCTCTCCCTAGCACTAGCTGACGCGTC-ATGGGCGC.AACGCCGCGGCCCTGAGCCAGGCGCTGCGCCTGGAGGCCCCAGAGCTTCCAGTAAAG
D4-b    GGCCCCGGTTTCTAACCTCTCCGTCTCTCCCTAGCACTAGC----------.----------TGAGCCAGGCGCTGCGCCTGGAGGCCCCAGAGCTTCCAGTAAAG
D9-a    GGC----------.----------TGAGCCAGGCGCTGCGCCTGGAGGCCCCAGAGCTTCCAGTAAAG
D9-b    56 BP DELETION----------.----------132 BP DELETION
B2-a    GGCCCCGGTTTCTAACCTCTCCGTCTCTCCCTAGCACTAGCTGACGCGTCTATGGGCGC.AACGCCGCGGCCCTGAGCCAGGCGCTGCGCCTGGAGGCCCCAGA----------G
B2-b    GGCCCCGGTTTCTAACCTCTCCGTCTCTCCCTAGCACTAGCTGACGC---.----------CTGAGCCAGGCGCTGCGCCTGGAGGCCCCAGAGCTTCCAGTAAAG
C1-a    GGCCCCGGTTTCTAACCTCTCCGTCTCTCCCTAGCACTAGCTGACGCGTCCCCGCGGC-C----------CTGAGCCAGGCGCTGCGCCTGGAGGCCCCAGAGCTTCCAGTAAAG
C1-b    GGCCCCGGTTTCTAACCTCTCCGTCTCTCCCTAGCACTAGCTGACGCGTCATATGGGCGCAACGCCGCGGCCCTGAGCCAGGCGCTGCGCCTGGAGGCCCCAGAGCTTCCAGTAAAG
C6-a    GGCCCCGGTTTCTAACCTCTCCGTCTCTCCCTAGCACTAGC----------.----------TGAGCCAGGCGCTGCGCCTGGAGGCCCCAGAGCTTCCAGTAAAG
C6-b    GGCCCCGGTTTCTAACCTCTCCGTCTCTCCCTAGCACTAGCTGACGCG---.----------CAGCGCCTGGAGGCCCCAGAGCTTCCAGTAAAG
D1-a    GGCCCCGGTTTCTAACCTCTCCGTCTCTCCCTAGCACTAGCTGACGC---.----------CTGGAGGCCCCAGAGCTTCCAGTAAAG
D1-b    GGCCCCGGTTTCTAACCTCTCCGTCTCTCCCTAGCACTAGC----------.----------TGAGCCAGGCGCTGCGCCTGGAGGCCCCAGAGCTTCCAGTAAAG
D8-a    GGCCCCGGTTTCTAACCTCTCCGTCTCTCCCTAGCACTAGC----------.----------TGAGCCAGGCGCTGCGCCTGGAGGCCCCAGAGCTTCCAGTAAAG
D8-b    GGCCCCGGTTTCTAACCTCTCCGTCTCTCCCTAGCAC----------.----------CAGGCGCTGCGCCTGGAGGCCCCAGAGCTTCCAGTAAAG
```

Figure 2.6 Genomic DNA Sequences of *SELENOH* loci from clones of HeLa cells infected with *SELENOH*-CR1 lentiCRISPRv2 constructs.

Top row indicates the sequence of unmodified allele *SELENOH*-CR1. sgRNA sequence was shown in green and PAM sequences in red. Deletion events are shown by an equivalent number of dash marks and insertions is highlighted in blue. Vertical lines indicate predicted cleavage site. The black box indicates selenocysteine codon.

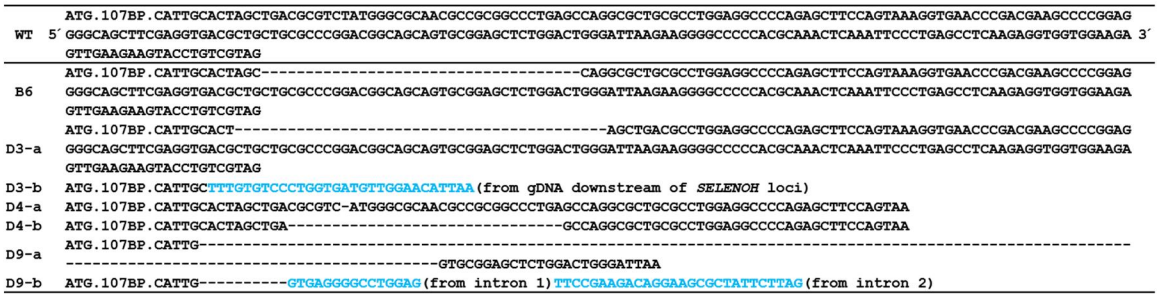

Figure 2.7 Consequences of the CRISPR/Cas9-mediated *SELENOH* knockout in HeLa cells (B6, D3, D4 and D9) at mRNA level.

Top row indicates the sequence of the unmodified allele. Deletion events are shown by an equivalent number of dash marks and insertions is highlighted in blue.

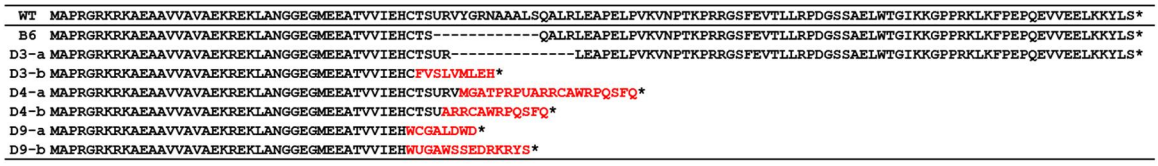

Figure 2.8 Deduced amino acid sequences of SELENOH based on mRNA sequence analysis of the open reading frame of *SELENOH* genes in *SELENOH* knockout HeLa cells.

All the deletion mutations in *SELENOH* resulted in deduced changes of SELENOH as frameshift (highlighted in red), premature termination (an asterisk), or deletion (dash line).

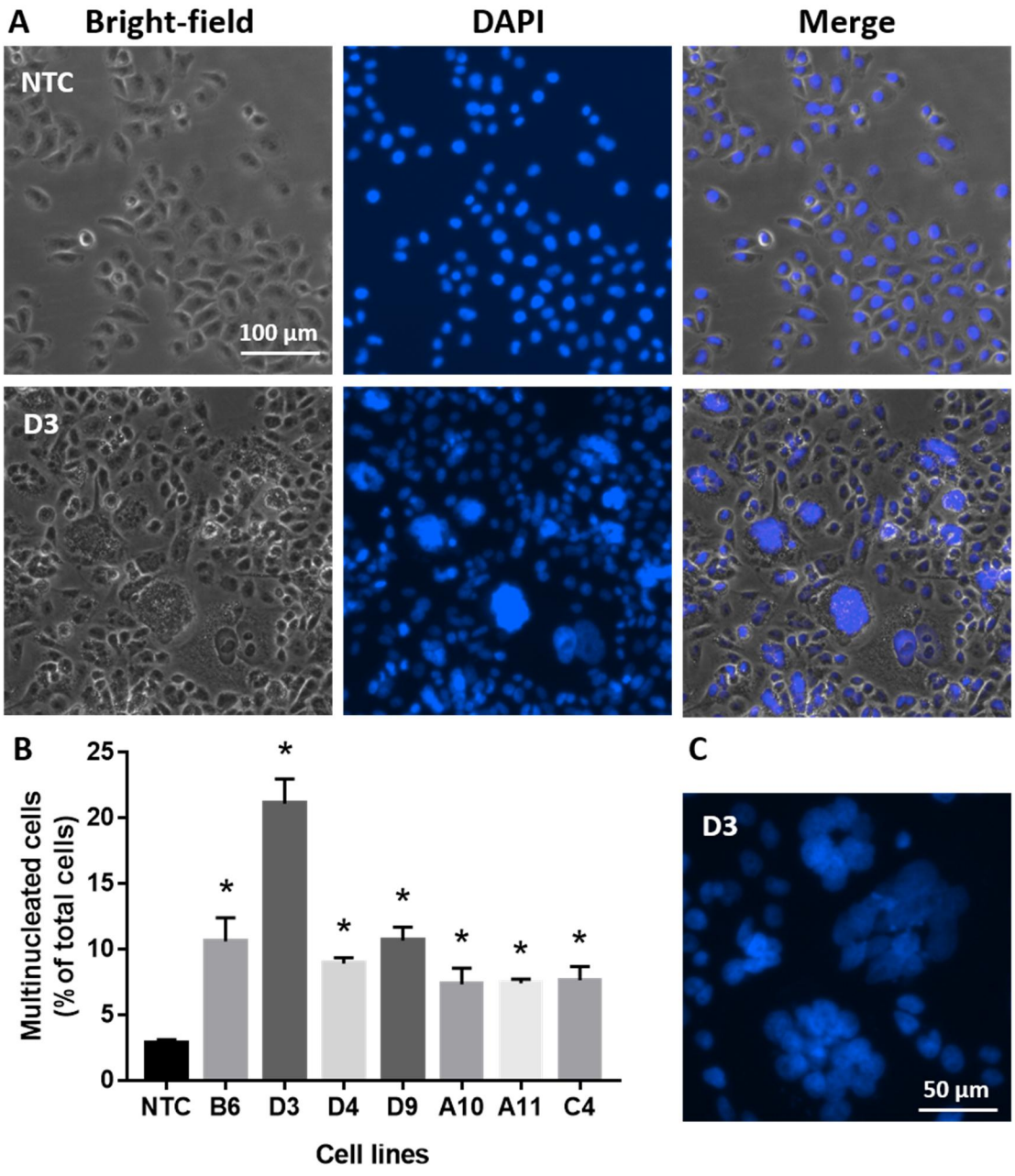

Figure 2.9 Morphological changes in *SELENOH* knockout HeLa cell lines.

(A) Bright-field and fluorescent images of control and *SELENOH* knockout D3 cell line. (B) Quantitation of multinucleated cells in NTC control and 7 *SELENOH* knockout clones. Multinucleated cells were counted in three fields of at least 100 cells each. Percent multinucleated cells were plotted for each cell line (n = 3). *, $P < 0.05$, compared to NTC. (C) Giant cells are containing interconnected nuclei. DAPI images of DNA-stained multinucleated cells with incomplete karyokinesis.

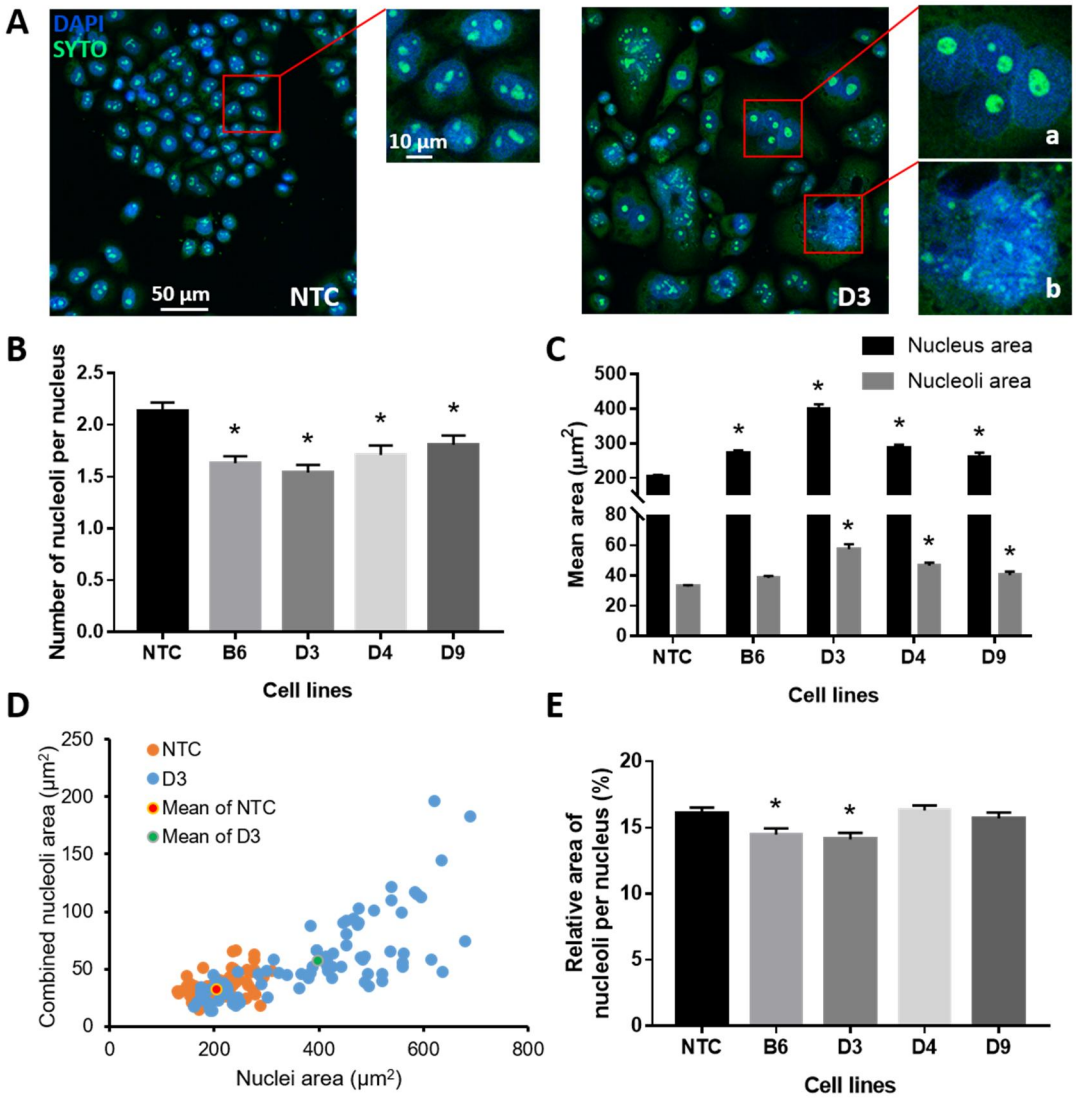

Figure 2.10 Changes in the number and size of nucleoli in *SELENOH* knockout cells.

(A) Representative fields of *SELENOH* knockout (D3) and non-targeting control (NTC) HeLa cells and images enlarged nuclei and nucleoli. DAPI and SYTO are markers of nuclei and nucleoli, respectively. (B) Quantification of the nucleolar number in 100 control and *SELENOH* knockout cells. Values are mean ± SEM. *, $P < 0.05$, compared to NTC. (C) Quantification of the nuclear area and the nucleolar area in 100 control and *SELENOH* knockout cells. Values are mean ± SEM. *, $P < 0.05$, compared to NTC cells. (D) A 2D scatter plot showing combined nucleolar area (per nucleus) on the Y axis, vs nuclear area on the X-axis, for control (yellow) and SELENOH knockout D3 (blue) cells. Each translucent dot represents one nucleus. The red dot represents the mean value of control cells, and the green dot represents the mean value of D3 cells. (E) Quantification of the relative area of nucleoli per nuclei. Values are mean ± SEM. *, $P < 0.05$, compared to NTC cells.

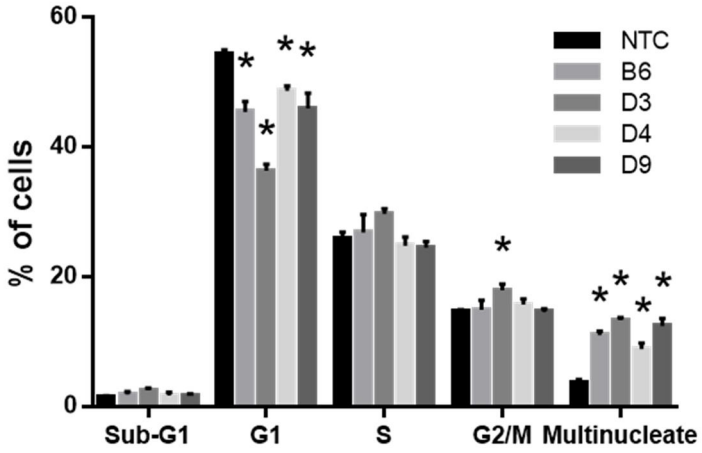

Figure 2.11 Cell cycle analyses in control (NTC) and *SELENOH* knockout (B6, D3, D4 and D9) cells.

Cells were stained with propidium iodide and analyzed with the use of a BD FACSCalibur flow cytometer. The percent sub-G1, G1, S, G2/M and polyploid cells were assessed by using FlowJo V10 software. Values are mean ± SEM, n = 3. *, $P < 0.05$, compared to NTC.

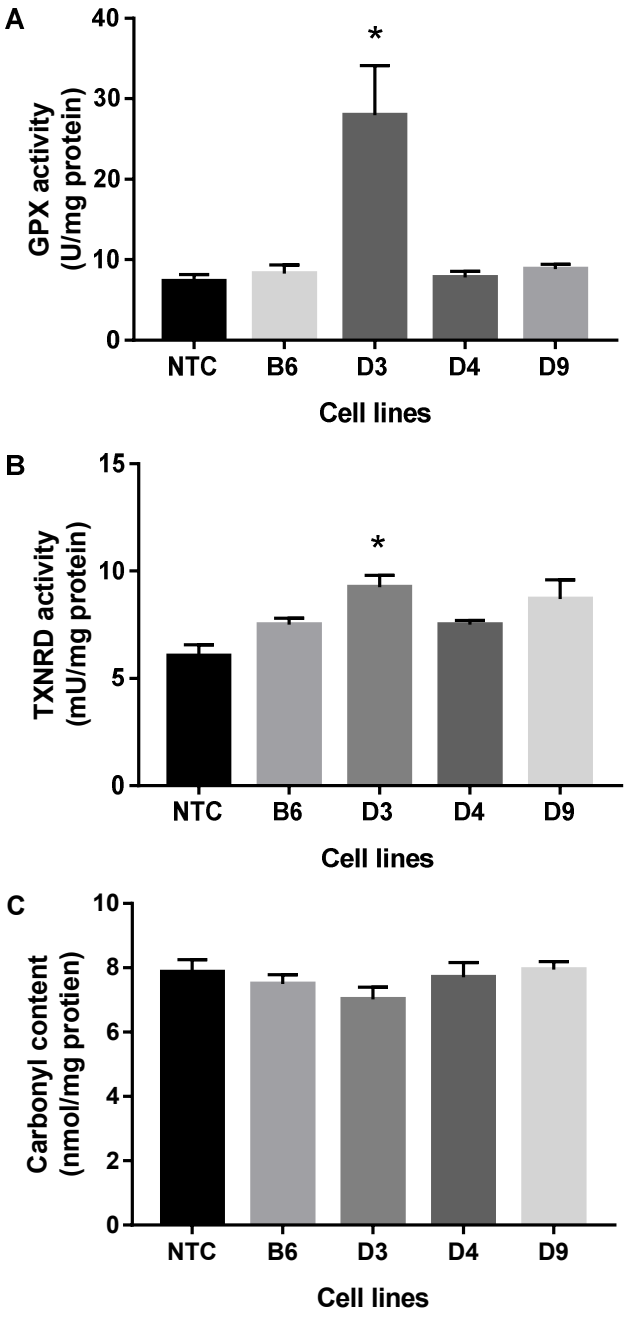

Figure 2.12 Glutathione peroxidase (**A**) and thioredoxin reductase (**B**) activities and protein carbonyl level (**C**) in control and *SELENOH* knockout HeLa cells.

Specific enzymatic activities were expressed as related to sample protein amount. Values are mean ± SEM (n = 3). *, $P < 0.05$, compared to NTC. GPX, glutathione peroxidase; TXNRD, thioredoxin reductase

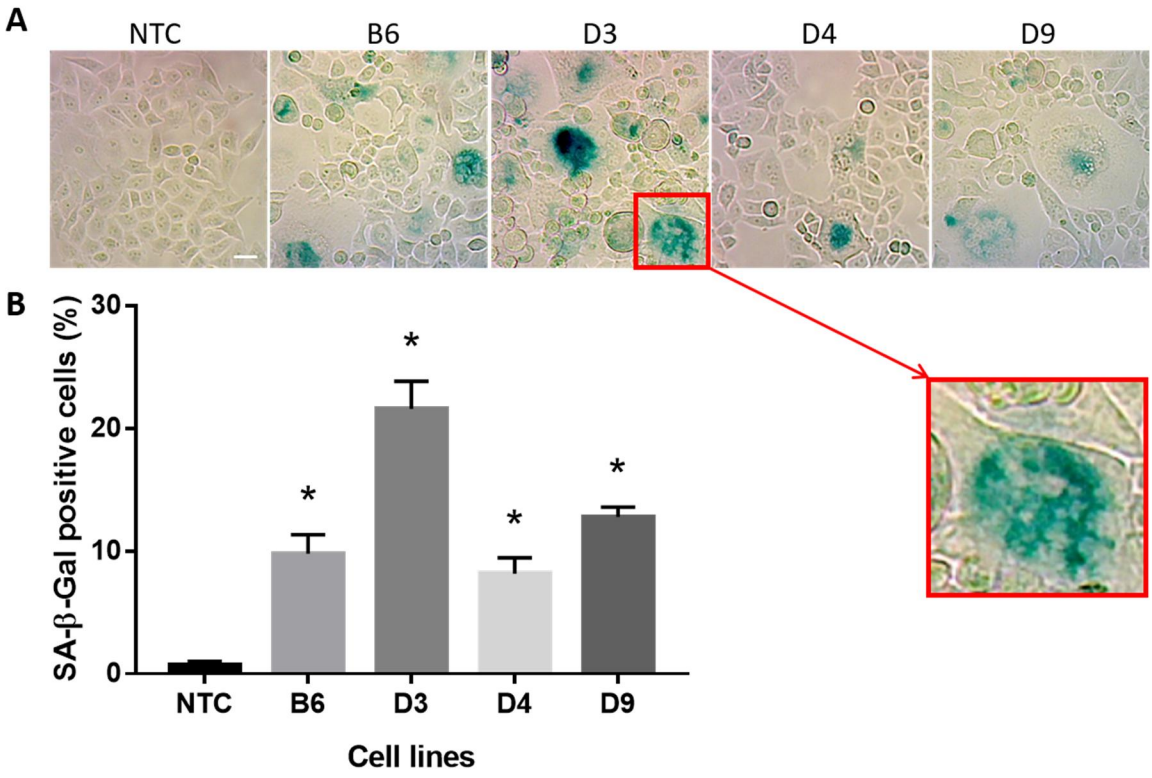

Figure 2.13 *SELENOH* knockout HeLa cells display exacerbated senescence induction.

(A) Cells were stained for the detection of senescence-associated β-galactosidase (SA-β-gal), and images were taken with a 10× objective lens. (B) Quantification of the SA-β-gal positive cells. Values are mean ± SEM (n = 3). *, $P < 0.05$, compared to NTC. NTC, non-treating control; B6, D3, D4, and D9 are *SELENOH* knockout HeLa cells.

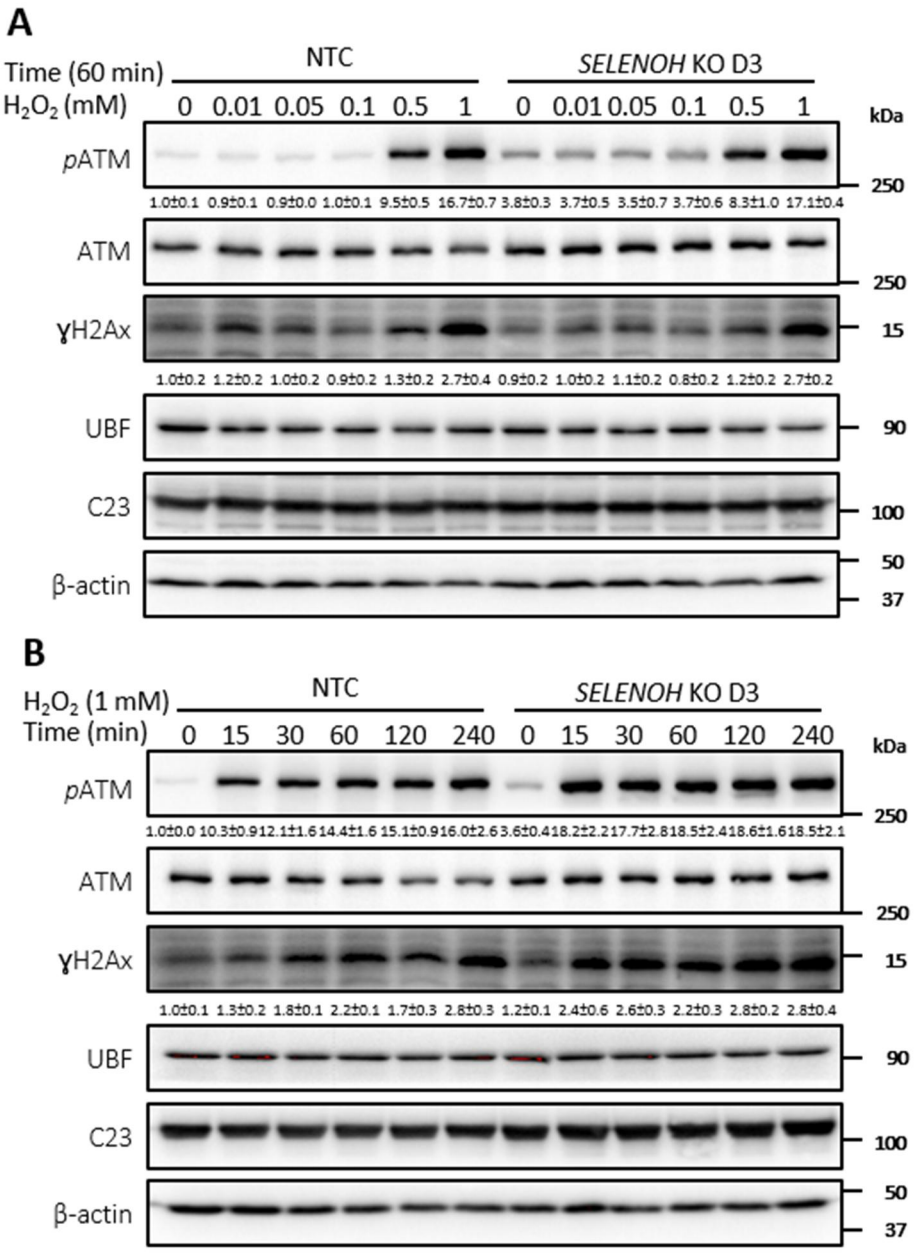

Figure 2.14 Knockout of *SELENOH* rendered HeLa cells enhanced ataxia telangiectasia kinase (ATM) activation in the absence and presence of H_2O_2 treatment.

Western analyses of the indicated proteins in non-targeting control (NTC) and the D3 clone of *SELENOH* knockout cells treated with H_2O_2 (0-1 mM) for 60 min (A) or 1 mM for 0-240 min (B). pATM and γH2AX were normalized to ATM and actin, respectively, and expressed as relative to the no H_2O_2 group. pATM, phosphorylated ATM on Ser-1981; γH2AX, phosphorylated H2AX on Ser-139; C23, nucleolin; UBF, upstream binding factor.

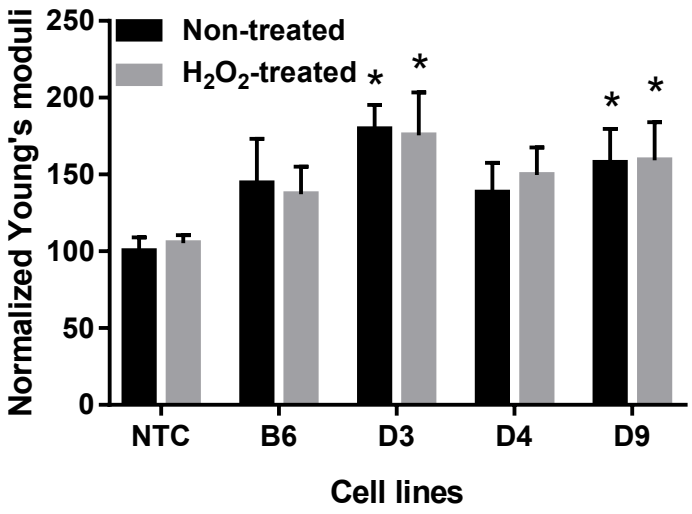

Figure 2.15 The stiffness of nucleoli in control and *SELENOH* knockout HeLa cells with or without H_2O_2 treatment.

Stiffness was directly assessed using Young's moduli with the use of atomic force microscope, as expressed as related to untreated HeLa cells. Values are presented as mean ± SEM of three independent experiments. *, $P < 0.05$, compared to control (NTC) HeLa cells. B6, D3, D4 and D9 are *SELENOH* knockout cells as detailed in Fig. 2.9.

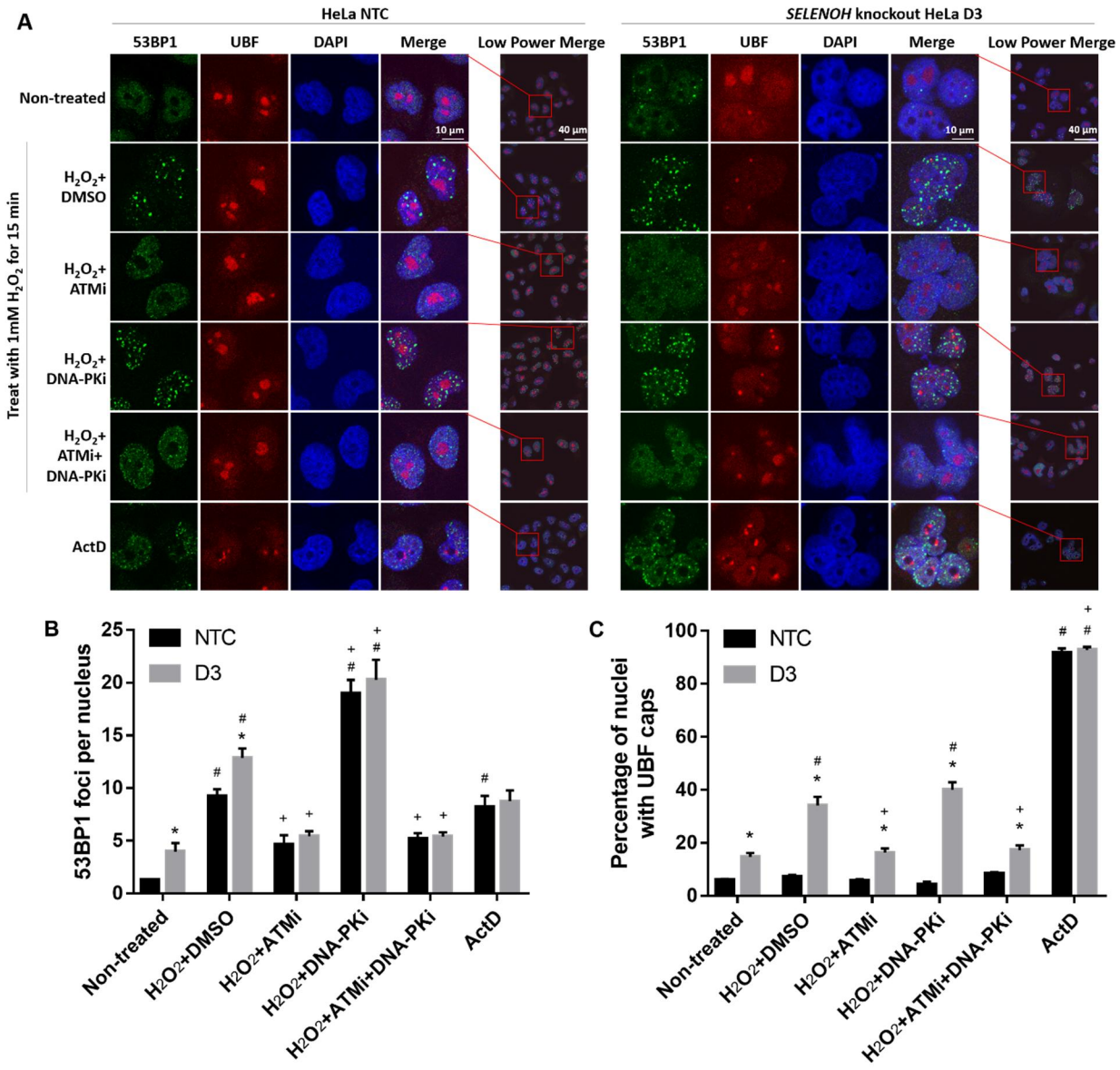

Figure 2.16 *SELENOH* knockout resulted in the large-scale reorganization of nucleolar architecture with the movement of nucleolar proteins into nucleolar cap regions in response to cellular stress and DSBs.

(A) Immunofluorescence staining of 53BP1 (green) and UBF (red). ActD treatment serves as a control for cap formation in the absence of H_2O_2 treatment. (B) Quantification of 53BP1 foci per nucleus for the experiment described in (A). (C) Quantification of the percentage of nuclei with UBF nucleolar caps for the experiment described in (A). Values are presented as mean ± SEM of three independent experiments. *, $P < 0.05$, compared to NTC. $^{\#}$, $P < 0.05$, compared to non-treated cells. $^{+}$, $P < 0.05$, compared to H_2O_2+DMSO treated cells.

CHAPTER III

SELENOPROTEIN H IS PARTIALLY ESSENTIAL FOR EMBRYOGENESIS AND PROTECTS AGAINST COLON CARCINOGENESIS

3.1 Abstract

Selenium is an essential mineral, in which there is a significant negative correlation between selenium intake and incidence of different cancers in humans. The biological properties of selenium are mediated mainly by selenoproteins at nutritional levels and selenium metabolites. Selenoprotein H (SELENOH) carries redox domains and suppresses oxidative stress to maintain genome stability *in vitro*. However, its function *in vivo* remains largely unknown. To determine the physiological role of SELENOH function *in vivo*, *Selenoh* knockout mice were generated by targeted deletion through homologous recombination. *Selenoh*$^{+/-}$ mice were fertile and phenotypically indistinguishable from wild-type littermates. Results from matings of *Selenoh*$^{+/-}$ mice showed a significantly reduced fraction of *Selenoh*$^{-/-}$ offspring on the basis of Mendelian segregation. Because some *Selenoh*$^{-/-}$ were born, this suggested that *Selenoh* is a partially essential gene in mice. Live-born *Selenoh*$^{-/-}$ mice were viable and born without apparent phenotypes. *Selenoh*$^{-/-}$ mice at 2-month of age showed increased GPX activity in the lung but not in the brain and liver. Furthermore, loss of *Selenoh* resulted in the aggravated formation of aberrant crypt foci in the colon of *Selenoh*$^{+/-}$ mice that were

injected with azoxymethane (AOM). Results indicated that SELENOH has important roles during embryogenesis and in colorectal carcinogenesis.

3.2 Introduction

Selenium is known to mitigate certain forms of age-related degeneration such as cancer, cardiovascular diseases, and neurologic disorders (Rayman 2012). The biological properties of selenium are mediated mainly by selenoproteins at nutritional levels and selenium metabolites at supranutritional levels (Qi *et al.* 2010; Labunskyy *et al.* 2014). Since most selenoproteins have antioxidant activity (Moghadaszadeh & Beggs 2006), it can be assumed that higher selenium intake would lead to the higher expression of selenoproteins within the nutritional level, hence protecting DNA against oxidative damage.

SELENOH carries redox domains and suppresses oxidative stress to maintain genome stability *in vitro*. However, its physiological functions remain largely unknown. It was recently reported that SELENOH is essential for organ development in zebrafish (Cox *et al.* 2016). In particular, larvae of SELENOH-deficient zebrafish exhibit an increased susceptibility to oxidative stress and DNA damage, and this selenoprotein interacts with p53 in adulthood to palliate gastrointestinal tumor development. These findings strongly suggest that SELENOH has a critical role in the maintenance of redox homeostasis and genome stability. Compared to cell models and the non-mammalian fish, mouse models are particularly useful to determine selenoprotein functions in humans. To date, no *Selenoh* knockout model has been reported in mice. To fill this key knowledge gap, *Selenoh*$^{+/-}$ mice were generated through homologous recombination and bred from

Selenoh$^{-/-}$ and *Selenoh* $^{+/+}$ to conduct experiments that address the physiological functions of this nucleolar selenoprotein.

With the use of knockout mice, selenoproteins that are known to be essential for embryogenesis include GPX4 (Yant *et al.* 2003), TXNRD1 (Jakupoglu *et al.* 2005) and TXNRD2 (Conrad *et al.* 2004). Interestingly, *Dio3* knockout mice exhibit impaired growth, low fertility and partial perinatal lethality (Hernandez *et al.* 2006). In contrast, mice that were deficient in SELENOP (Hill *et al.* 2003; Schomburg *et al.* 2003), GPX1 (Cheng *et al.* 1997), GPX2 (Esworthy *et al.* 2000), GPX3 (Jin *et al.* 2011), MSRB1 (Fomenko *et al.* 2009), SELENOF (SEP15) (Kasaikina *et al.* 2011), DIO1 (Schneider *et al.* 2006b), DIO2 (Schneider *et al.* 2001), SELENOK (Verma *et al.* 2011), SELENOM (Pitts *et al.* 2013) were viable. In the current study, the generation and characterization of *Selenoh* knockout mice are described. Mating of *Selenoh* heterozygous knockout mice suggests SELENOH is partially essential during embryogenesis in mice. *Selenoh*$^{-/-}$ mice exhibit increased GPX activity in the lung, but not in the brain and liver. Loss of SELENOH develops increased aberrant crypt foci in the colon of *Selenoh*$^{+/-}$ mice that were injected with azoxymethane, suggesting that SELENOH may function as a caretaker type of tumor suppressor.

3.3 Materials and Methods

3.3.1 Generation of *Selenoh* knockout mice

Selenoh$^{+/-}$ mice were made through targeted disruption (Cyagen Biosciences, Santa Clara, CA). To engineer the targeting vector, homology arms were generated by PCR using BAC clone RP23-134L7 or RP23-259I24 from the C57BL/6J library as template. Mouse genomic fragments were amplified from the BAC clone with high

fidelity Taq DNA polymerase and were assembled into a targeting vector together with recombination sites and selection markers.

Male and female *Selenoh* $^{+/-}$ mice were mated, and genotypes (*Selenoh* $^{+/+}$, *Selenoh* $^{+/-}$ or *Selenoh*$^{-/-}$) of their offspring were tested by PCR at 3-4 weeks of age. Mouse DNA was isolated by standard procedures after proteinase K digestion of tail snips. DNA was resuspended in Tris-EDTA buffer (10 mM Tris-Cl, 1 mM EDTA, pH 7.6). The PCR protocol consisted of 38 cycles that included 30 seconds at 94 °C, 35 seconds at 60 °C, and 35 seconds at 72 °C, with a final extension of 5 min. The primers used were as follows: MoSeHF, 5′-CCAAACACCTCTAGACCTCAACTTCC-3′; MoSeHwtR, 5′-CCTTCAAGCCCAACTACGCTATCA-3′; MoSeHkoR, 5′-TCCCAGCAATCTAGAGGCAGAGG-3′. The PCR products were 458 bp for the *Selenoh*$^{+/+}$ allele with the use of the MoSeHF and MoSeHwtR primers and 341 bp for the *Selenoh*$^{-/-}$ allele with the use of the MoSeHF and MoSeHkoR primers.

3.3.2 Animal husbandry

Experiments were approved by the IACUC (approval numbers are 13-133, 14-054, 16-575, 17-033) of Mississippi State University and conducted in accordance with the NIH guidelines for the care and use of laboratory animals. Mice were given free access to diets and distilled water and housed in ventilated cages (up to 4 mice/cage) in an animal room (22-23°C, 12:12 h light-dark cycle). Weanling mice were fed an AIN-93G purified diet that contained 0.15 ppm Se as sodium selenate until they were sacrificed. Mice were weighed weekly.

3.3.3 Mating of *Selenoh*$^{+/-}$ mice

Selenoh$^{+/-}$ mice were mated, and their pups were monitored as previously described (Hernandez *et al.* 2006) to determine the impact of knocking out SELENOH on reproduction and viability of the pups. This was done to determine whether or not *Selenoh* is an essential gene.

3.3.4 Sample collection and preparation of tissue homogenates

Mice were anesthetized with carbon dioxide and sacrificed by exsanguination via heart puncture using a heparinized syringe. Tissues were rinsed with PBS solution (pH 7.4) to clean out blood cells and clots, snap-frozen in liquid nitrogen, and stored at -80 °C until analyses. Tissues were powdered and homogenized under liquid nitrogen and sonicated in cold buffer. Homogenates were resuspended in cold buffer and centrifuged at 10,000 × *g* for 20 min at 4 °C. Protein concentrations were estimated using Pierce BCA protein assay (Thermo Scientific Scientific) with bovine serum albumin as a standard.

3.3.5 Glutathione peroxidase (GPX) activity

Brains, lungs and livers were homogenized by sonication in 200 µL ice-cold buffer (50 mM Tris-HCl, pH 7.5, 5 mM EDTA, and 1 mM DTT) and centrifuged (20,000 × *g* at 4 °C for 10 min). The supernatant was collected and kept on ice for immediate analysis of total GPX activity as described in 2.3.10.

3.3.6 Thioredoxin reductase (TXNRD) activity

Brains and lungs were homogenized by sonication in 200 µL ice-cold buffer (50 mM potassium phosphate, pH 7.4, 1 mM EDTA) and centrifuged (20,000 × *g* at 4 °C for

10 min). The supernatant was collected and kept on ice for immediate analysis of total TXNRD activity as described in 2.3.11.

3.3.7 Protein oxidation

Livers were homogenized by sonication in a buffer (MES, 50 mM; EDTA, 1mM; pH 6.7), followed by centrifugation at 10,000 × *g* for 15 min at 4 °C. The supernatant was incubated at room temperature for 15 min with streptomycin sulfate (1%). After centrifugation at 6,000 × *g* for 10 min at 4 °C, the protein carbonyl content in the supernatant was measured as described in 2.3.12.

3.3.8 Animals and carcinogen treatment

Since a recent study showed that SELENOH functioned as a tumor suppressor in zebrafish with carcinogen-induced tumorigenesis (Cox *et al.* 2016), the impact of *Selenoh* haploinsufficiency in old mice (15-22 months of age) with AOM-induced intestinal carcinogenesis was evaluated in the next phase of our research.

Mice received either weekly intraperitoneally (i.p.) injections of azoxymethane (AOM, an intestinal carcinogen) (Sigma) (*Selenoh*$^{+/+}$, n = 8; *Selenoh*$^{+/-}$, n = 6) at a concentration of 8 mg/kg body weight or saline carrier solution (*Selenoh*$^{+/+}$, n = 3; *Selenoh*$^{+/-}$, n = 3) for 4 weeks, followed by 15 mg/kg for one week. Body weight was recorded weekly throughout the experiments. Mice were anesthetized with carbon dioxide 13 weeks after the first AOM injection. Colons were excised from the caecum at the ileo-caecal valve and rinsed with 0.25 M sucrose/10 mM tris buffer, pH 7.4, to remove colon contents. The cecum, anus, and rectum were removed. Colons were trisected starting at the distal end into three equal lengthwise segments that were

operationally defined as descending, transverse, and ascending regions. Segments of colon tissue were prepared by laying the serosal surface down onto 75 × 25 mm 3-aminopropyltriethoxysilane-treated microscope slides (Statlab Medical Products, McKinney, TX, Cat. No. 418), fixed flat in buffered formalin for 16 h, and stained with methylene blue (0.2% (v/v) in PBS) for 30 min. By viewing the stained colons under a light microscope at a magnification of 40 ×, the number of ACF per colon was determined as described previously (Chung *et al.* 2003; Padidar *et al.* 2012).

3.3.9 Statistical analysis

The one-way analysis of variance (ANOVA) was conducted to determine the effect of the genotype on enzymatic activities of mouse organs. Differences among groups were determined by least square difference tests. All analysis was conducted using SAS (SAS 9.4, Cary, NC) at a significance level of $P < 0.05$. Survival analysis was conducted using GraphPad Prism version 7.0 (GraphPad Software, La Jolla, CA).

3.4 Results

3.4.1 Generation of mice deficient in *Selenoh*

Mouse *Selenoh* gene is located in the reverse strand of chromosome 2 and contains 4 exons. *Selenoh* knockout mice were generated with the use of the strategy of homologous recombination as detailed in **Figure 3.1 A**. The targeting vector contains homology arms, a neomycin cassette that is flanked by two loxP sites, and a DTA cassette. After completion of homologous recombination, the *Selenoh* gene was replaced with a neomycin cassette, followed by Cre-mediated excision to generate the constitutive knockout allele. C57BL/6 blastocysts were then injected with *Selenoh*$^{+/-}$ embryonic stem

cells and implanted into pseudopregnant mice. A male chimera was identified among the offspring. This male was mated with two C57BL/6 female mice, and the heterozygote progeny (*Selenoh*$^{+/-}$) from these mating events were used to establish the *Selenoh* knockout mouse colony. *Selenoh*$^{+/+}$, *Selenoh*$^{+/-}$, and *Selenoh*$^{-/-}$ alleles in these mice were verified by PCR genotyping as detailed in **Figure 3.1 B**.

3.4.2 *Selenoh* is a partially essential gene during embryogenesis

Selenoh$^{+/-}$ mice were fertile and phenotypically indistinguishable from wild-type littermates. When *Selenoh*$^{+/-}$ mice were intercrossed, a significantly reduced fraction of *Selenoh*$^{-/-}$ offspring was born on the basis of Mendelian segregation. Instead of the expected 25% by the principle of segregation, only 10.7% (8 of 75; $P < 0.005$, χ^2) were *Selenoh*$^{-/-}$ (**Table 3.1**). This suggests that more than half of the homozygous knockout mice were lost during pregnancy. Thus, *Selenoh* is a partially essential gene in mice. However, the delivered *Selenoh*$^{-/-}$ mice appeared healthy as evidenced by normal weight gains (**Figure 3.2**) and lack of apparent phenotype for up to 14 months of age at the time of death. Interestingly, an approximately equal number of *Selenoh*$^{+/+}$ and *Selenoh*$^{+/-}$ mice were born instead of the 1:2 ratio based on Mendelian segregation. This suggests that haploinsufficiency of *Selenoh* promote embryonic lethality. Similarly, *Selenoh*$^{+/-}$ mice appeared healthy up to 22 months of age at the time of sacrifice. According to Mendelian segregation, there were 48% and 76% less neonatal *Selenoh*$^{+/-}$ and *Selenoh*$^{-/-}$ mice, respectively, this is strongly indicating an essential role of *Selenoh* in embryogenesis in a manner depending on gene dosage.

3.4.3 Activity of antioxidant enzymes and carbonyl contents in tissues of *Selenoh*$^{+/+}$ and *Selenoh*$^{-/-}$ mice

Body weight gains did not differ *Selenoh*$^{+/+}$ and *Selenoh*$^{-/-}$ mice during the 8-week experiment (**Figure 3.2**). Weanling *Selenoh*$^{+/+}$ and *Selenoh*$^{-/-}$ mice were sacrificed at week 8. Because SELENOH carries GPX activity and a TXN-like domain (Novoselov *et al.* 2007), the impact of *Selenoh* knockout was evaluated for its GPX and TXNRD activities. Pulmonary GPX activity in *Selenoh*$^{-/-}$ mice was 28.5% greater ($P < 0.05$) than that in *Selenoh*$^{+/+}$ mice (**Figure 3.3 A**). Knockout of *Selenoh* in mice did not affect GPX activity in the brain or liver ($P > 0.05$) (**Figure 3.3 A**), TXNRD activity in the brain or lung (**Figure 3.3 B**), and carbonyl content in the liver (**Figure 3.3 C**).

3.4.4 AOM-induced aberrant crypt foci (ACF) in *Selenoh*$^{+/+}$ and *Selenoh*$^{+/-}$ mice

It was recently reported that *SELENOH* deficiency (heterozygous mutant) disrupts redox homeostasis, provokes an inflammatory response, activates p53 in development, and accelerates the onset of tumors in zebrafish (Cox *et al.* 2016). To determine such a role of SELENOH in mammals, *Selenoh*$^{+/+}$ and *Selenoh*$^{+/-}$ mice were intraperitoneally injected with AOM or saline weekly for 5 weeks. While there was no significant weight gain or loss in mice injected with saline during the experimental period, injection with AOM resulted in reduced ($P < 0.05$) body weights by 37% in *Selenoh*$^{+/+}$ and 34% in *Selenoh*$^{+/-}$ mice over the course of 7 weeks (**Figure 3.4 B** and **C**).

In accordance with our approved animal protocol by IACUC, the following mice were killed following AOM injection as determined by inertia, ruffled fur, and >11% weight loss in a week: 1) one *Selenoh*$^{+/+}$ mouse at week 4, 2) four *Selenoh*$^{+/+}$ and three *Selenoh*$^{+/-}$ mice at week 5, and 3) *Selenoh*$^{+/-}$ mouse each at 7 and 11 weeks (**Figure 3.4**

A). One *Selenoh*$^{+/+}$ and one *Selenoh*$^{+/-}$ mice injected with saline were sacrificed 7 weeks after the injection as determined by aging phenotypes that are different from those injected with AOM.

AOM-induced ACF in the colon of experimental mice were counted (**Table 3.2**). The *Selenoh* $^{+/-}$ mouse had more ($P < 0.05$) lesions (19.5 ± 4.5 ACF/mouse) than *Selenoh* $^{+/+}$ mice (4.3 ± 0.9 ACF/mouse). The ACF that were identified were all located in the lower part of the colon with no ACF observed in the proximal part of the colon. None of the saline injected mice developed ACF. Although the difference is substantial, further studies are needed to confirm this preliminary observation.

3.5 Discussion

The gene knockout approach has been a valuable tool in functional genomics for understanding various physiological aspects of a given gene product. Mice act as a good analog for many biological processes in humans because ~99% of their genes are overlapped (Capecchi 1994). Another advantage in using mice as the mammalian model is that they are relatively small, cost-effective, prolific, and easy to handle. Although there are more sophisticated strategies to manipulate gene expression such as conditional or tissue-specific knockout, targeted deletion is typically the initial knockout approach that is used in research.

To date, genetic manipulation of *Selenoh* has not been reported in mice. We employed targeted disruption to achieve whole body *Selenoh* knockout in mice. In this study, the physiological function of the SELENOH was investigated in mice. *Selenoh*$^{+/-}$ mice were fertile and phenotypically indistinguishable from wild-type littermates. When *Selenoh*$^{+/-}$ mice were intercrossed, a reduced fraction of *Selenoh*$^{-/-}$ offspring was born by Mendelian segregation. These results suggested that *Selenoh* is a partially essential gene

in mice. This is similar to DIO3, as *Dio3*$^{-/-}$ mice are partially lethal by a reduced proportion of *Dio3*$^{-/-}$ pups (17.5%) as compared to the 25% rate predicted by Mendelian law when *Dio3*$^{+/-}$ mice were intercrossed (Hernandez *et al.* 2006).

Similar to the essential roles of *Selenoh* and *Dio3* in embryogenesis, a mammalian-specific microRNA (miRNA) cluster *mir-290-295* is critical early in life (Medeiros *et al.* 2011). Like SELENOH, the *mir-290-295* primary transcript is specifically expressed in early embryos. When heterozygous *mir-290-295* knockout mice were intercrossed, only 7% (32 of 452, $P<0.001$, $\chi 2$) of 4-wk-old postnatal progeny were *mir-290–295*$^{-/-}$, suggesting that about three-quarters of the homozygous knockout animals were lost. Interestingly, at E18.5, just before birth, the percentage of *mir-290–295*$^{-/-}$embryos was also 7% (3 out of 46, $P<0.01$, $\chi 2$). This suggests that *mir-290*-295 is essential only during embryogenesis because ll live-born *mir-290–295*$^{-/-}$mice will likely be survived. Indeed, analysis of embryos at mid-late gestation suggest that *mir-290–295*$^{-/-}$ embryos are lost over a period between E11.5 and E18.5. It is of future interest to determine the mechanism by which embryonic lethality is expressed in *Selenoh*$^{-/-}$ mice.

Complete embryonic lethality exhibits in mice with a whole-body knockout in genes coded for certain selenoproteins or their biosynthesis factors. First, *Gpx4*$^{-/-}$ embryos die by E7.5 (Yant *et al.* 2003). Second, *Txnrd1*$^{-/-}$ embryos die between E9.5 and E10.5 (Jakupoglu *et al.* 2005). Third, *Txnrd2*$^{-/-}$ embryos die around E13.0 due to defects in hematopoiesis and heart development (Conrad *et al.* 2004). Early studies indicated that *Trsp*$^{-/-}$ embryos die shortly after implantation and are resorbed by 6.5 days post coitum (Bosl *et al.* 1997). *Trsp* codes for selenocysteine (Sec)-specific tRNA gene are necessary for the expression of all selenoproteins. As such, *Trsp*$^{-/-}$ mice are null in all 24 selenoproteins. Similarly, selenocysteine insertion sequence (SECIS)-binding protein 2 (Secisbp2) plays a central role in UGA/Sec recoding and is necessary for the expression

of all selenoproteins. As expected, intercrosses of *Secisbp2*$^{+/-}$ mice yield no live *Secisbp2*$^{-/-}$ offspring, and dissection of *Secisbp2*$^{-/-}$ embryos demonstrate developmental retardation by embryonic day 8 (E8). While *Secisbp2*$^{-/-}$ embryos are developmentally arrested at the Theiler stage 7 (TS7), control embryos reach the appropriate TS12 (Seeher *et al.* 2014). Similarly, selenocysteine tRNA 1 associated protein (*Trnau1ap*) has been characterized as a tRNA$^{[Ser]Sec}$-binding protein, and homozygous mice with constitutive deletion of exons 7 and 8 of Trnau1ap die during embryogenesis (Mahdi et al. 2015). Altogether, selenium is essential for life and it's physiological essentially is mediated by selenoproteins. To date, at least 5 selenoproteins are necessary for embryogenesis, with *Gpx4*$^{-/-}$, *Txnrd1*$^{-/-}$ and *Txnrd2*$^{-/-}$ being essential and *Dio3*$^{-/-}$ and *Selenoh*$^{-/-}$ being partially essential.

Selenoh$^{-/-}$ mice are viable and born without obvious phenotype. *Selenoh*$^{-/-}$ mice have the similar body weight gains within 8 weeks of age compare with *Selenoh*$^{+/+}$ mice. Interestingly, *Selenoh*$^{-/-}$ mice show increased GPX activity in the lung but not in the brain and liver. GPX is a H_2O_2-eliminating enzyme and can be upregulated by oxidative stress (Lee *et al.* 1990; Avissar *et al.* 1996). The upregulation of GPX activity is indicative of the presence of an increased oxidant burden in the lung of *Selenoh*$^{-/-}$ mice.

Knockout of *Selenop* in mice results in decreased GPX activities in the brain, testis and kidney, but increased activity in the liver. Hepatic accumulation of selenium in combination with drastic declines of selenium content in the plasma, brain, testis, and kidney in *Selenop*$^{-/-}$ mice implies that other tissues depend on the delivery of selenium by SELENOP from the liver.

A strong body of epidemiologic, clinical, and experimental studies collectively show that dietary selenium plays an important role in cancer prevention (Clark *et al.* 1996; Peters *et al.* 2006). Evidence suggests that selenium has cancer preventive

properties that are largely mediated through selenoproteins (Tsuji *et al.* 2012). It is reasonable to expect selenoproteins to have antitumorigenic roles because some cancers appear to be subjected to redox regulation. In this regard, glutathione peroxidases 1-4 and 6 and thioredoxin reductases 1-3 are potential regulators of carcinogenesis (Saad & Diamond 2016). In particular, *Gpx1*$^{-/-}$*Gpx2*$^{-/-}$ mice exhibit bacteria-induced inflammation (colitis) that spontaneously drives intestinal tumor formation (Esworthy *et al.* 2001). GPX2 appears to play a complicated role in colon carcinogenesis (Brigelius-Flohe & Kipp 2012) because it inhibits inflammation-driven tumorigenesis (Krehl *et al.* 2012) yet promotes the growth of xenografted tumors at different stages of carcinogenesis (Banning *et al.* 2008). Loss of *Gpx2* leads to dedifferentiation of cells to a progenitor-like state (Emmink *et al.* 2014). Conversely, overexpression of *Gpx2* leads to cell differentiation, with increased proliferation and tumor-forming potential. In addition, knockout of *Txnrd1* in the liver of mice results in increased susceptibility to chemically induced hepato-carcinogenesis (Carlson *et al.* 2012).

It has recently been reported that *SELENOH* deficiency (heterozygous mutant) disrupts redox homeostasis, provokes an inflammatory response, activates p53 in development, and accelerates gastrointestinal tumor development in adulthood zebrafish (Cox *et al.* 2016). To determine such a role of SELENOH in mammals, *Selenoh*$^{+/+}$ and *Selenoh*$^{+/-}$ mice were intraperitoneally injected with AOM and the induced aberrant crypts foci were counted. Aberrant crypt foci are putative pre-neoplastic colon lesions and are considered ideal biomarkers of colorectal carcinogenesis, as the number of pre-neoplastic lesions is statistically associated with the number of tumors that ultimately develop (Pretlow *et al.* 1992; Takayama *et al.* 1998). The *Selenoh* $^{+/-}$ mice has more lesions (19.5 ± 4.5 ACF/mouse) than *Selenoh* $^{+/+}$ mice (4.3 ± 0.9 ACF/mouse). Interesting, all the ACFs in *Selenoh* $^{+/-}$ mice are located in the lower part of the colon,

with no ACF being observed in the proximal colon. These results suggest that *Selenoh* contributes to the suppression of colon carcinogenesis.

3.6 Figures and Tables

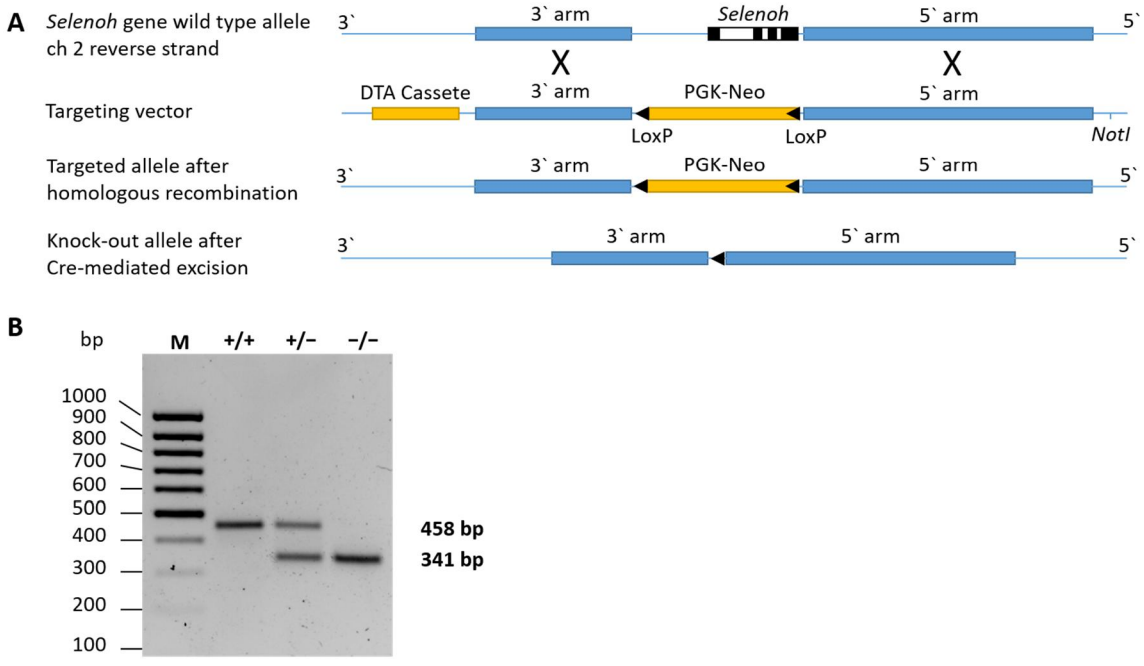

Figure 3.1 Targeted disruption of *Selenoh* in C57BL/6 mice.

(A) Genomic structure of the wildtype mouse *Selenoh* locus, the targeting vector, and the targeted locus are shown. Black boxes represent *Selenoh* exons. PGK-Neo, neomycin resistance cassette; Not I, a linearization site. (B) Representative results from PCR genotyping of wild-type ($^{+/+}$), heterozygous knockout ($^{+/-}$), and homozygous knockout ($^{-/-}$) *Selenoh* mice.

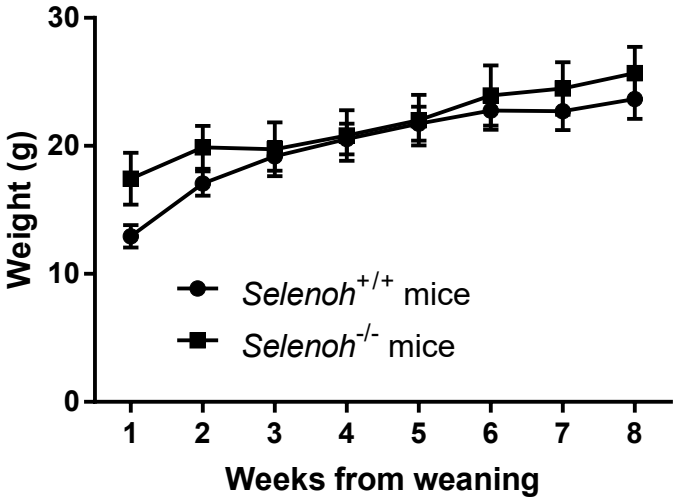

Figure 3.2 The growth of *Selenoh*$^{+/+}$ and *Selenoh*$^{-/-}$ mice fed an AIN-93G diet for 8 weeks since weaning. Numbers were mean ± SEM of measurements (n = 4-10).

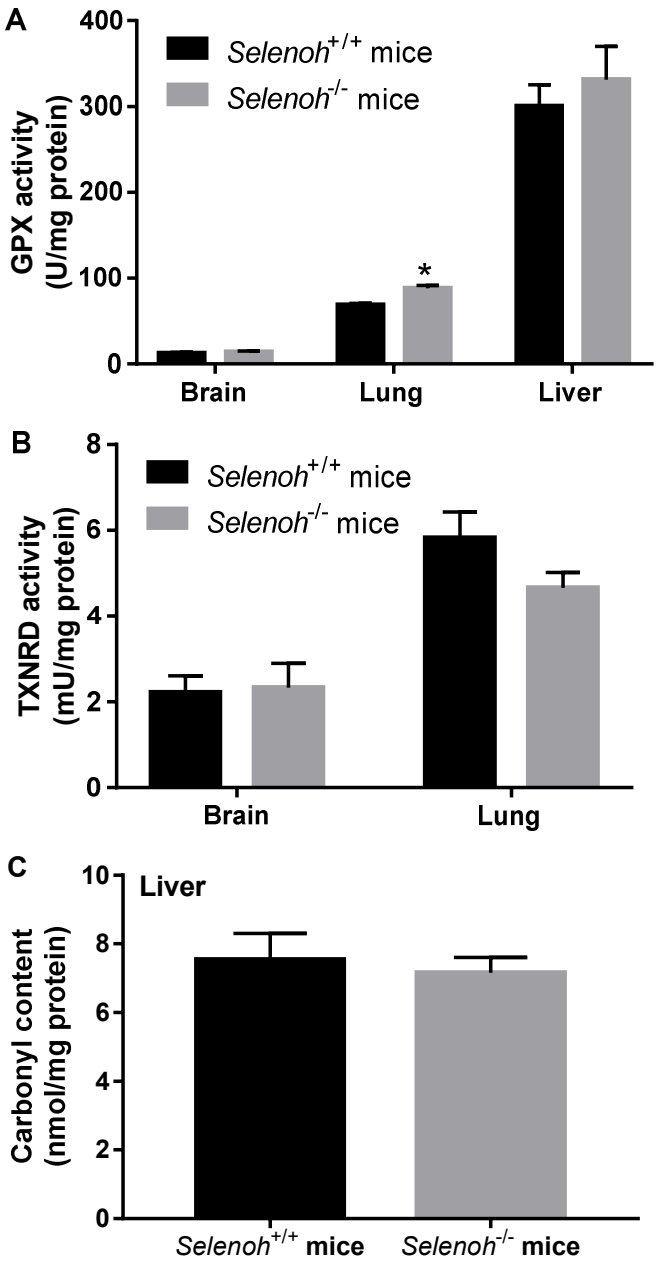

Figure 3.3 Glutathione peroxidase (**A**) and thioredoxin reductase (**B**) activities and protein carbonyl level (**C**) in tissues of *Selenoh*$^{+/+}$ and *Selenoh*$^{-/-}$ mice.

Specific enzymatic activities were expressed as related to sample protein amount. Values are mean ± SEM (n = 3). *, $P < 0.05$, compared to *Selenoh*$^{+/+}$ mice. GPX, glutathione peroxidase; TXNRD, thioredoxin reductase

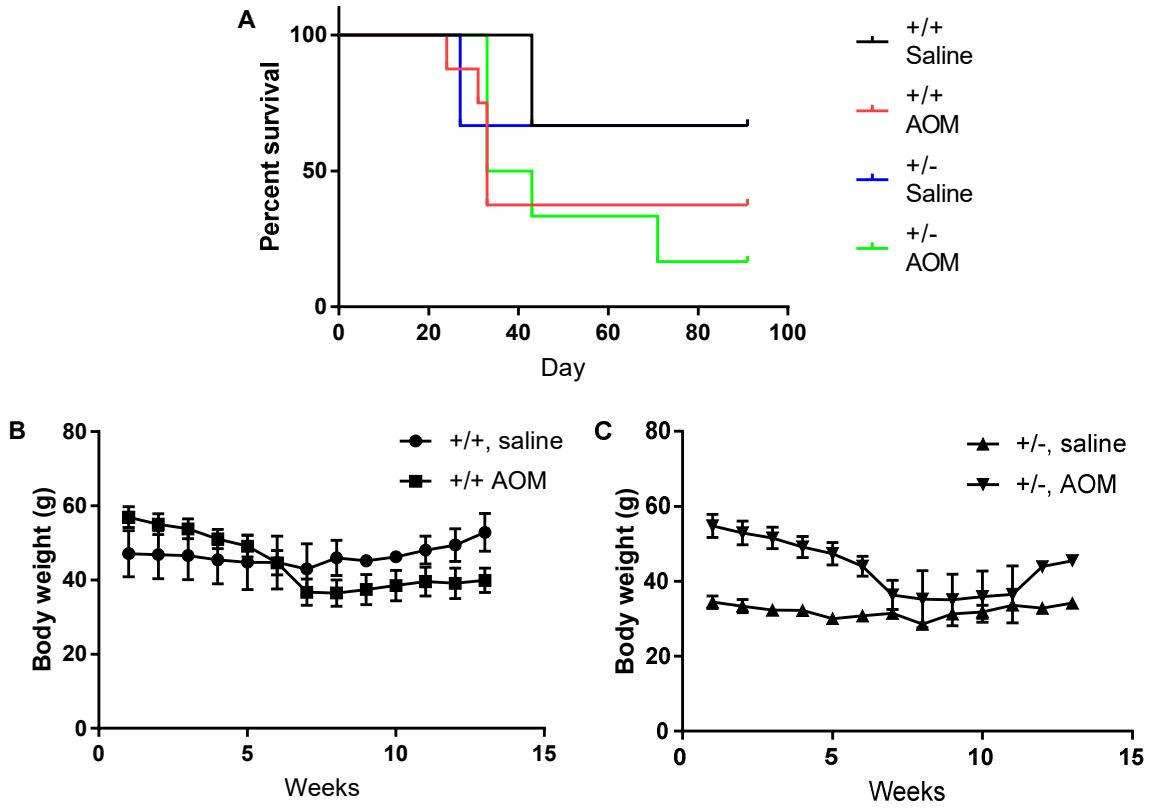

Figure 3.4 Effect of AOM injection on survival (A) and body weight in *Selenoh* $^{+/+}$ (B) and *Selenoh* $^{+/-}$ (C) mice. Values are mean ± SEM (n = 1-8).

Table 3.1 Summary of *Selenoh* heterozygous intercrosses

Mutant	Number of newborns (%)			Total
	+/+	+/–	–/–	
Selenoh$^{+/-}$	33 (44.0)	34 (45.3)	8 (10.7)	75

Table 3.2 Body weight and development of ACF

Group	Treatment group	n	Mean ACF/mouse
Selenoh $^{+/+}$	Saline	2	0
Selenoh $^{+/+}$	AOM	3	4.3 ± 0.9 b
Selenoh $^{+/-}$	Saline	2	0
Selenoh $^{+/-}$	AOM	2	19.5 ± 4.5 a

Values are expressed as mean ± SEM; lowercase letters within each column denote measurements significantly different from each other ($P < 0.05$); saline-injected mice did not develop ACF.
Abbreviations: AOM, azoxymethane; ACF, aberrant crypt foci.

CHAPTER IV

CONCLUSIONS

The overarching aim of this dissertation was to study functional and physiological roles of SELENOH through gene knockout in cells and mice. We created *SELENOH* knockout cell lines using the CRISPR/Cas9 system. Although a quality antibody is not available to detect gene expression at the protein level in SELENOH, results from RT-qPCR analyses demonstrated that *SELENOH* mRNA levels were dramatically reduced. As expected, CRISPR/cas9 system was effective at genome engineering of *SELENOH* knockout in cells. Once the site-specific DSBs were created at predicted deletion junctions at *SELENOH* exon 2, the repair of DSBs was triggered by the non-homologous end-joining pathway. This induced small insertion/deletions that resulted in frameshifts and the potential loss of function mutations. A high frequency of genomic deletions was observed. To achieve a functional gene knockout, single colony screening was performed to select clones with biallelic mutations. By the deduced protein sequences, these biallelic mutations were translated as dysfunctional SELENOH in various forms including frameshift mutation by aberrant splicing and truncated SELENOH by early termination of translation. In this study, because of the small indels at the *SELENOH* exon 2, most of the mutations still contain *SELENOH* exon 1. For a more precise genome editing such as deletion of the whole coding sequence of *SELENOH*, it is of future interest to employ an

alternative DNA repair pathway of homology-directed repair (HDR) by providing a homologous donor template.

To date, genetic manipulation of *Selenoh* has not been reported in mice. We employed the targeted disruption method to produce the whole body *Selenoh* knockout mice and investigated the physiological function of the SELENOH in mice. *Selenoh*$^{+/-}$ mice were fertile and phenotypically indistinguishable from wild-type littermates. When *Selenoh*$^{+/-}$ mice were intercrossed, a reduced fraction of *Selenoh*$^{-/-}$ offsprings were born on the basis of Mendelian segregation. These results suggest that *Selenoh* is necessary for embryogenesis and partially essential in mice. It is of future interest to test the *Selenoh*$^{-/-}$ males and females' fertility by setting up different mating combinations between *Selenoh*$^{+/-}$ and *Selenoh*$^{-/-}$ mice.

SELENOH knockout cell lines reduced cell proliferation and accumulation of giant multinucleated cells. Cell cycle analysis demonstrated that apoptosis is not associated with the observed slow cell growth. Instead, the decreased G1 cell population and increased G2/M population and polyploid DNA content in *SELENOH* knockout cells indicate that this selenoprotein has a critical role in the G2/M phase of the cell cycle. Confocal microscopy analysis of DAPI- and SYTO-stained *SELENOH* knockout cells displayed near complete mitosis as evidenced by the re-appearance of nucleoli and chromatin formation without separation of two daughter cells. Altogether, these results suggest that *SELENOH* has a role in cytokinesis. Cytokinesis is the final step of cell division and appears to proceed as a linked set of subreactions: cleavage plane specification, furrow assembly, furrow ingression and cell separation (Glotzer 1997).

Further studies are warranted on the regulation of SELENOH in the core pathways and components essential for each stage of cytokinesis.

Knockout of *SELENOH* in HeLa cells may induce oxidative stress DNA damage as evidenced by increased GPX activity, the persistence of pATM on Ser-1981 and γ-H2AX expression and 53BP1 focus formation. These results suggest that SELENOH has both critical and general role in maintaining genomic stability against chronic oxidative stress. The knockout of *SELENOH* by CRISPR/Cas9 genomic editing renders human cancerous HeLa cells susceptible to premature cellular senescence. These results suggest that modulation of SELENOH expression could be evaluated further for its potential anti-tumor properties. It is of future interest to determine whether chemosensitivity could be increased through accelerated senescence in *SELENOH* knockout cells.

SELENOH is a nucleolar protein. The nucleolus is a dynamic nuclear structure. Knockout of *SELENOH* changes the size, number, mechanical property and nucleolar component localization in the nucleolus. We found that in *SELENOH* knockout HeLa cells have larger nuclei than control, which possess a single large nucleolus. Nonetheless, the mechanism of the single nucleolus phenotype in *SELENOH* knockout cells is presently unknown. It would be interesting to research whether or not SELENOH impacts mitotic chromosome periphery and/or cytokinesis. AFM was used to assess nucleolar stiffness. The observation of increased stiffness in the nucleoli of *SELENOH* knockout cells suggests that SELENOH maintains the flexibility of the nucleolus structure. Furthermore, our unpublished results of transcriptome analysis by RNAseq show that *SELENOH* knockout downregulates ribosome biogenesis in HeLa cells, which may lead to the accumulation of unprocessed rRNA and consequently leads to increased

stiffness in the nucleolus. Interestingly, knockout of *SELENOH* renders large-scale re-organization of nucleolar architecture in HeLa cells with the movement of nucleolar proteins into nucleolar cap regions in response to oxidative stress. The nucleolar reorganization is dependent on ATM signaling. SELENOH appears to be both a sensor of oxidative stress in the nucleolus and has critical roles in redox regulation and genome maintenance. Thus, it is of future interest to elucidate the mechanism by which SELENOH regulates rDNA transcription and nucleolar cap formation.

Selenoh$^{-/-}$ mice are viable and born without an obvious phenotype. *Selenoh*$^{-/-}$ mice have the similar body weight gains within 8 weeks of age compared with *Selenoh*$^{+/+}$ mice. *Selenoh*$^{-/-}$ mice had increased GPX activity in the lung but not in the brain and liver. The upregulation of GPX activity is indicative of the presence of an increased oxidant burden in the lung of *Selenoh*$^{-/-}$ mice. To determine whether or not SELENOH plays a role in tumor development in mammals, *Selenoh*$^{+/+}$ and *Selenoh*$^{+/-}$ mice were intraperitoneally injected with azoxymethane to induce aberrant crypts foci (ACF) at the early stage of colorectal carcinogenesis. The *Selenoh* $^{+/-}$ mice had more lesions than *Selenoh* $^{+/+}$ mice. All the ACFs in *Selenoh* $^{+/-}$ mice are located in the lower part of the colon, and no ACF is observed in the proximal colon. These results suggest that *Selenoh* plays an important role in the suppression of colon carcinogenesis.

SELENOH maintains genome stability in the nucleolus by the regulation of redox homeostasis and may suppress DNA damage during embryogenesis and carcinogenesis.

REFERENCES

Agamy O, Ben Zeev B, Lev D, Marcus B, Fine D, Su D, Narkis G, Ofir R, Hoffmann C, Leshinsky-Silver E, Flusser H, Sivan S, Soll D, Lerman-Sagie T, Birk OS (2010). Mutations disrupting selenocysteine formation cause progressive cerebello-cerebral atrophy. *Am J Hum Genet*. **87**, 538-544.

Anastassova-Kristeva M (1977). The nucleolar cycle in man. *J Cell Sci*. **25**, 103-110.

Andreesen JR, Ljungdahl LG (1973). Formate dehydrogenase of Clostridium thermoaceticum: incorporation of selenium-75, and the effects of selenite, molybdate, and tungstate on the enzyme. *J Bacteriol*. **116**, 867-873.

Anttonen AK, Hilander T, Linnankivi T, Isohanni P, French RL, Liu Y, Simonovic M, Soll D, Somer M, Muth-Pawlak D, Corthals GL, Laari A, Ylikallio E, Lahde M, Valanne L, Lonnqvist T, Pihko H, Paetau A, Lehesjoki AE, Suomalainen A, Tyynismaa H (2015). Selenoprotein biosynthesis defect causes progressive encephalopathy with elevated lactate. *Neurology*. **85**, 306-315.

Arbogast S, Ferreiro A (2010). Selenoproteins and protection against oxidative stress: selenoprotein N as a novel player at the crossroads of redox signaling and calcium homeostasis. *Antioxid Redox Signal*. **12**, 893-904.

Arner ES (2009). Focus on mammalian thioredoxin reductases-important selenoproteins with versatile functions. *Biochim Biophys Acta*. **1790**, 495-526.

Arthur JR, Nicol F, Beckett GJ (1990). Hepatic iodothyronine 5'-deiodinase. The role of selenium. *Biochem J*. **272**, 537-540.

Avissar N, Finkelstein JN, Horowitz S, Willey JC, Coy E, Frampton MW, Watkins RH, Khullar P, Xu YL, Cohen HJ (1996). Extracellular glutathione peroxidase in human lung epithelial lining fluid and in lung cells. *Am J Physiol*. **270**, L173-182.

Bakkenist CJ, Kastan MB (2003). DNA damage activates ATM through intermolecular autophosphorylation and dimer dissociation. *Nature*. **421**, 499-506.

Banning A, Kipp A, Schmitmeier S, Lowinger M, Florian S, Krehl S, Thalmann S, Thierbach R, Steinberg P, Brigelius-Flohe R (2008). Glutathione peroxidase 2 inhibits cyclooxygenase-2-mediated migration and invasion of HT-29 adenocarcinoma cells but supports their growth as tumors in nude mice. *Cancer Res*. **68**, 9746-9753.

Barca-Mayo O, Liao XH, DiCosmo C, Dumitrescu A, Moreno-Vinasco L, Wade MS, Sammani S, Mirzapoiazova T, Garcia JG, Refetoff S, Weiss RE (2011). Role of type 2 deiodinase in response to acute lung injury (ALI) in mice. *Proc Natl Acad Sci U S A*. **108**, E1321-1329.

Behne D, Hilmert H, Scheid S, Gessner H, Elger W (1988). Evidence for specific selenium target tissues and new biologically important selenoproteins. *Biochim Biophys Acta*. **966**, 12-21.

Behne D, Wolters W (1983). Distribution of selenium and glutathione peroxidase in the rat. *J Nutr*. **113**, 456-461.

Ben Jilani KE, Panee J, He Q, Berry MJ, Li PA (2007). Overexpression of selenoprotein H reduces Ht22 neuronal cell death after UVB irradiation by preventing superoxide formation. *Int J Biol Sci*. **3**, 198-204.

Berry MJ, Banu L, Chen YY, Mandel SJ, Kieffer JD, Harney JW, Larsen PR (1991a). Recognition of UGA as a selenocysteine codon in type I deiodinase requires sequences in the 3' untranslated region. *Nature*. **353**, 273-276.

Berry MJ, Banu L, Larsen PR (1991b). Type I iodothyronine deiodinase is a selenocysteine-containing enzyme. *Nature*. **349**, 438-440.

Berzelius JJ (1818). Lettre de M. Berzelius à M. Berthollet sur deux métaux nouveaux. *Annales de Chimie et de Physique*. **Série 2**, 199-202.

Böck A (2001). Selenium metabolism in bacteria. In *Selenium: Its Molecular Biology and Role in Human Health*. (DL Hatfield, ed). Dordrecht, The Netherlands: Kluwer Academic Publishers, pp. 7-22.

Bonasio R, Tu S, Reinberg D (2010). Molecular signals of epigenetic states. *Science*. **330**, 612-616.

Bondareva AA, Capecchi MR, Iverson SV, Li Y, Lopez NI, Lucas O, Merrill GF, Prigge JR, Siders AM, Wakamiya M, Wallin SL, Schmidt EE (2007). Effects of thioredoxin reductase-1 deletion on embryogenesis and transcriptome. *Free Radic Biol Med*. **43**, 911-923.

Booth DG, Takagi M, Sanchez-Pulido L, Petfalski E, Vargiu G, Samejima K, Imamoto N, Ponting CP, Tollervey D, Earnshaw WC, Vagnarelli P (2014). Ki-67 is a PP1-interacting protein that organises the mitotic chromosome periphery. *Elife*. **3**, e01641.

Borchert A, Wang CC, Ufer C, Schiebel H, Savaskan NE, Kuhn H (2006). The role of phospholipid hydroperoxide glutathione peroxidase isoforms in murine embryogenesis. *J Biol Chem*. **281**, 19655-19664.

Bosl MR, Takaku K, Oshima M, Nishimura S, Taketo MM (1997). Early embryonic lethality caused by targeted disruption of the mouse selenocysteine tRNA gene (Trsp). *Proc Natl Acad Sci U S A*. **94**, 5531-5534.

Boulon S, Westman BJ, Hutten S, Boisvert FM, Lamond AI (2010). The nucleolus under stress. *Mol Cell*. **40**, 216-227.

Brangwynne CP, Mitchison TJ, Hyman AA (2011). Active liquid-like behavior of nucleoli determines their size and shape in Xenopus laevis oocytes. *Proc Natl Acad Sci U S A*. **108**, 4334-4339.

Brigelius-Flohe R, Kipp AP (2012). Physiological functions of GPx2 and its role in inflammation-triggered carcinogenesis. *Ann N Y Acad Sci*. **1259**, 19-25.

Brigelius-Flohe R, Maiorino M (2013). Glutathione peroxidases. *Biochim Biophys Acta*. **1830**, 3289-3303.

Budiman ME, Bubenik JL, Miniard AC, Middleton LM, Gerber CA, Cash A, Driscoll DM (2009). Eukaryotic initiation factor 4a3 is a selenium-regulated RNA-binding protein that selectively inhibits selenocysteine incorporation. *Mol Cell*. **35**, 479-489.

Burk RF, Hill KE (1994). Selenoprotein P. A selenium-rich extracellular glycoprotein. *J Nutr*. **124**, 1891-1897.

Burk RF, Hill KE (2005). Selenoprotein P: an extracellular protein with unique physical characteristics and a role in selenium homeostasis. *Annu Rev Nutr*. **25**, 215-235.

Burk RF, Hill KE (2009). Selenoprotein P-expression, functions, and roles in mammals. *Biochim Biophys Acta*. **1790**, 1441-1447.

Burk RF, Hill KE (2015). Regulation of Selenium Metabolism and Transport. *Annu Rev Nutr*. **35**, 109-134.

Burk RF, Hill KE, Olson GE, Weeber EJ, Motley AK, Winfrey VP, Austin LM (2007). Deletion of apolipoprotein E receptor-2 in mice lowers brain selenium and causes severe neurological dysfunction and death when a low-selenium diet is fed. *J Neurosci*. **27**, 6207-6211.

Burk RF, Norsworthy BK, Hill KE, Motley AK, Byrne DW (2006). Effects of chemical form of selenium on plasma biomarkers in a high-dose human supplementation trial. *Cancer Epidemiol Biomarkers Prev*. **15**, 804-810.

Burk RF, Olson GE, Winfrey VP, Hill KE, Yin D (2011). Glutathione peroxidase-3 produced by the kidney binds to a population of basement membranes in the gastrointestinal tract and in other tissues. *Am J Physiol Gastrointest Liver Physiol*. **301**, G32-38.

Campisi J (2005). Senescent cells, tumor suppression, and organismal aging: good citizens, bad neighbors. *Cell*. **120**, 513-522.

Campisi J, d'Adda di Fagagna F (2007). Cellular senescence: when bad things happen to good cells. *Nat Rev Mol Cell Biol*. **8**, 729-740.

Cao L, Zhang L, Zeng H, Wu RT, Wu TL, Cheng WH (2017). Analyses of selenotranscriptomes and selenium concentrations in response to dietary selenium deficiency and age reveal common and distinct patterns by tissue and sex in telomere-dysfunctional mice. *J Nutr*. **147**, 1858-1866.

Capecchi MR (1994). Targeted gene replacement. *Sci Am*. **270**, 52-59.

Carlson BA, Yoo MH, Tobe R, Mueller C, Naranjo-Suarez S, Hoffmann VJ, Gladyshev VN, Hatfield DL (2012). Thioredoxin reductase 1 protects against chemically induced hepatocarcinogenesis via control of cellular redox homeostasis. *Carcinogenesis*. **33**, 1806-1813.

Castets P, Lescure A, Guicheney P, Allamand V (2012). Selenoprotein N in skeletal muscle: from diseases to function. *J Mol Med (Berl)*. **90**, 1095-1107.

Castillo M, Hall JA, Correa-Medina M, Ueta C, Kang HW, Cohen DE, Bianco AC (2011). Disruption of thyroid hormone activation in type 2 deiodinase knockout mice causes obesity with glucose intolerance and liver steatosis only at thermoneutrality. *Diabetes*. **60**, 1082-1089.

Casula S, Bianco AC (2012). Thyroid hormone deiodinases and cancer. *Front Endocrinol (Lausanne)*. **3**, 74.

Chambers I, Frampton J, Goldfarb P, Affara N, McBain W, Harrison PR (1986). The structure of the mouse glutathione peroxidase gene: the selenocysteine in the active site is encoded by the 'termination' codon, TGA. *EMBO J*. **5**, 1221-1227.

Chen Q, Fischer A, Reagan JD, Yan LJ, Ames BN (1995). Oxidative DNA damage and senescence of human diploid fibroblast cells. *Proc Natl Acad Sci U S A*. **92**, 4337-4341.

Cheng WH, Combs GF, Jr., Lei XG (1998a). Knockout of cellular glutathione peroxidase affects selenium-dependent parameters similarly in mice fed adequate and excessive dietary selenium. *Biofactors*. **7**, 311-321.

Cheng WH, Ho YS, Ross DA, Valentine BA, Combs GF, Lei XG (1997). Cellular glutathione peroxidase knockout mice express normal levels of selenium-dependent plasma and phospholipid hydroperoxide glutathione peroxidases in various tissues. *J Nutr*. **127**, 1445-1450.

Cheng WH, Ho YS, Valentine BA, Ross DA, Combs GF, Jr., Lei XG (1998b). Cellular glutathione peroxidase is the mediator of body selenium to protect against paraquat lethality in transgenic mice. *J Nutr*. **128**, 1070-1076.

Cheng WH, Muftuoglu M, Wu RT (2014). Selenium and epigenetic effects on histone marks and DNA methylation. In *Nutrition and Epigenetics*. (E Ho , F Domann, eds). Boca Raton, FL: CRC Press, pp. 273-298.

Cheng WH, Valentine BA, Lei XG (1999). High levels of dietary vitamin E do not replace cellular glutathione peroxidase in protecting mice from acute oxidative stress. *J Nutr*. **129**, 1951-1957.

Chu FF, Doroshow JH, Esworthy RS (1993). Expression, characterization, and tissue distribution of a new cellular selenium-dependent glutathione peroxidase, GSHPx-GI. *J Biol Chem*. **268**, 2571-2576.

Chung H, Wu D, Han SN, Gay R, Goldin B, Bronson RE, Mason JB, Smith DE, Meydani SN (2003). Vitamin E supplementation does not alter azoxymethane-induced colonic aberrant crypt foci formation in young or old mice. *J Nutr*. **133**, 528-532.

Clark LC, Combs GF, Jr., Turnbull BW, Slate EH, Chalker DK, Chow J, Davis LS, Glover RA, Graham GF, Gross EG, Krongrad A, Lesher JL, Jr., Park HK, Sanders BB, Jr., Smith CL, Taylor JR (1996). Effects of selenium supplementation for cancer prevention in patients with carcinoma of the skin. A randomized controlled trial. Nutritional Prevention of Cancer Study Group. *JAMA*. **276**, 1957-1963.

Colnaghi R, Connell CM, Barrett RM, Wheatley SP (2006). Separating the anti-apoptotic and mitotic roles of survivin. *J Biol Chem*. **281**, 33450-33456.

Cone JE, Del Rio RM, Davis JN, Stadtman TC (1976). Chemical characterization of the selenoprotein component of clostridial glycine reductase: identification of selenocysteine as the organoselenium moiety. *Proc Natl Acad Sci U S A*. **73**, 2659-2663.

Cong L, Zhang F (2015). Genome engineering using CRISPR-Cas9 system. *Methods Mol Biol*. **1239**, 197-217.

Conrad M, Jakupoglu C, Moreno SG, Lippl S, Banjac A, Schneider M, Beck H, Hatzopoulos AK, Just U, Sinowatz F, Schmahl W, Chien KR, Wurst W, Bornkamm GW, Brielmeier M (2004). Essential role for mitochondrial thioredoxin reductase in hematopoiesis, heart development, and heart function. *Mol Cell Biol*. **24**, 9414-9423.

Conrad M, Moreno SG, Sinowatz F, Ursini F, Kolle S, Roveri A, Brielmeier M, Wurst W, Maiorino M, Bornkamm GW (2005). The nuclear form of phospholipid hydroperoxide glutathione peroxidase is a protein thiol peroxidase contributing to sperm chromatin stability. *Mol Cell Biol*. **25**, 7637-7644.

Cox AG, Tsomides A, Kim AJ, Saunders D, Hwang KL, Evason KJ, Heidel J, Brown KK, Yuan M, Lien EC, Lee BC, Nissim S, Dickinson B, Chhangawala S, Chang CJ, Asara JM, Houvras Y, Gladyshev VN, Goessling W (2016). Selenoprotein H is an essential regulator of redox homeostasis that cooperates with p53 in development and tumorigenesis. *Proc Natl Acad Sci U S A*. **113**, E5562-5571.

Damdimopoulos AE, Miranda-Vizuete A, Treuter E, Gustafsson JA, Spyrou G (2004). An alternative splicing variant of the selenoprotein thioredoxin reductase is a modulator of estrogen signaling. *J Biol Chem*. **279**, 38721-38729.

Davis CD, Tsuji PA, Milner JA (2012). Selenoproteins and cancer prevention. *Annu Rev Nutr*. **32**, 73-95.

Dear TN, Campbell K, Rabbitts TH (1991). Molecular cloning of putative odorant-binding and odorant-metabolizing proteins. *Biochemistry*. **30**, 10376-10382.

Difilippantonio MJ, Zhu J, Chen HT, Meffre E, Nussenzweig MC, Max EE, Ried T, Nussenzweig A (2000). DNA repair protein Ku80 suppresses chromosomal aberrations and malignant transformation. *Nature*. **404**, 510-514.

Downey CM, Horton CR, Carlson BA, Parsons TE, Hatfield DL, Hallgrimsson B, Jirik FR (2009). Osteo-chondroprogenitor-specific deletion of the selenocysteine tRNA gene, Trsp, leads to chondronecrosis and abnormal skeletal development: a putative model for Kashin-Beck disease. *PLoS Genet*. **5**, e1000616.

Du X, Li H, Wang Z, Qiu S, Liu Q, Ni J (2013). Selenoprotein P and selenoprotein M block Zn^{2+}-mediated $A\beta_{42}$ aggregation and toxicity. *Metallomics*. **5**, 861-870.

Dumitrescu AM, Liao XH, Abdullah MS, Lado-Abeal J, Majed FA, Moeller LC, Boran G, Schomburg L, Weiss RE, Refetoff S (2005). Mutations in SECISBP2 result in abnormal thyroid hormone metabolism. *Nat Genet*. **37**, 1247-1252.

Emmink BL, Laoukili J, Kipp AP, Koster J, Govaert KM, Fatrai S, Verheem A, Steller EJ, Brigelius-Flohe R, Jimenez CR, Borel Rinkes IH, Kranenburg O (2014). GPx2 suppression of H_2O_2 stress links the formation of differentiated tumor mass to metastatic capacity in colorectal cancer. *Cancer Res*. **74**, 6717-6730.

Esworthy RS, Aranda R, Martin MG, Doroshow JH, Binder SW, Chu FF (2001). Mice with combined disruption of Gpx1 and Gpx2 genes have colitis. *Am J Physiol Gastrointest Liver Physiol*. **281**, G848-855.

Esworthy RS, Mann JR, Sam M, Chu FF (2000). Low glutathione peroxidase activity in Gpx1 knockout mice protects jejunum crypts from gamma-irradiation damage. *Am J Physiol Gastrointest Liver Physiol*. **279**, G426-436.

Faye MD, Graber TE, Liu P, Thakor N, Baird SD, Durie D, Holcik M (2013). Nucleotide composition of cellular internal ribosome entry sites defines dependence on NF45 and predicts a posttranscriptional mitotic regulon. *Mol Cell Biol*. **33**, 307-318.

Ferguson AD, Labunskyy VM, Fomenko DE, Arac D, Chelliah Y, Amezcua CA, Rizo J, Gladyshev VN, Deisenhofer J (2006). NMR structures of the selenoproteins Sep15 and SelM reveal redox activity of a new thioredoxin-like family. *J Biol Chem*. **281**, 3536-3543.

Fiala ES, Staretz ME, Pandya GA, El-Bayoumy K, Hamilton SR (1998). Inhibition of DNA cytosine methyltransferase by chemopreventive selenium compounds, determined by an improved assay for DNA cytosine methyltransferase and DNA cytosine methylation. *Carcinogenesis*. **19**, 597-604.

Flohe L, Gunzler WA, Schock HH (1973). Glutathione peroxidase: a selenoenzyme. *FEBS Lett*. **32**, 132-134.

Flohé L, Loschen G, Günzler WA, Eichele E (1972). Glutathione peroxidase, V. The kinetic mechanism. *Hoppe-Seyler´ s Zeitschrift für physiologische Chemie*. **353**, 987-1000.

Florian S, Krehl S, Loewinger M, Kipp A, Banning A, Esworthy S, Chu FF, Brigelius-Flohe R (2010). Loss of GPx2 increases apoptosis, mitosis, and GPx1 expression in the intestine of mice. *Free Radic Biol Med*. **49**, 1694-1702.

Fomenko DE, Novoselov SV, Natarajan SK, Lee BC, Koc A, Carlson BA, Lee TH, Kim HY, Hatfield DL, Gladyshev VN (2009). MsrB1 (methionine-R-sulfoxide reductase 1) knock-out mice: roles of MsrB1 in redox regulation and identification of a novel selenoprotein form. *J Biol Chem*. **284**, 5986-5993.

Fredericks GJ, Hoffmann FW, Rose AH, Osterheld HJ, Hess FM, Mercier F, Hoffmann PR (2014). Stable expression and function of the inositol 1,4,5-triphosphate receptor requires palmitoylation by a DHHC6/selenoprotein K complex. *Proc Natl Acad Sci U S A*. **111**, 16478-16483.

Fu Y, Cheng WH, Porres JM, Ross DA, Lei XG (1999). Knockout of cellular glutathione peroxidase gene renders mice susceptible to diquat-induced oxidative stress. *Free Radic Biol Med*. **27**, 605-611.

Galton VA, Schneider MJ, Clark AS, St Germain DL (2009). Life without thyroxine to 3,5,3'-triiodothyronine conversion: studies in mice devoid of the 5'-deiodinases. *Endocrinology*. **150**, 2957-2963.

Glotzer M (1997). Cytokinesis. *Curr Biol*. **7**, R274-276.

Go YM, Jones DP (2010). Redox control systems in the nucleus: mechanisms and functions. *Antioxid Redox Signal*. **13**, 489-509.

Grosschedl R, Giese K, Pagel J (1994). HMG domain proteins: architectural elements in the assembly of nucleoprotein structures. *Trends Genet*. **10**, 94-100.

Guan D, Altan-Bonnet N, Parrott AM, Arrigo CJ, Li Q, Khaleduzzaman M, Li H, Lee CG, Pe'ery T, Mathews MB (2008). Nuclear factor 45 (NF45) is a regulatory subunit of complexes with NF90/110 involved in mitotic control. *Mol Cell Biol*. **28**, 4629-4641.

Günzler WA, Vergin H, Müller I, Flohé L (1972). Glutathione peroxidase, VI. Die reaktion der glutathion peroxydase mit verschiedenen hydroperoxyden. *Hoppe-Seyler´s Zeitschrift für physiologische Chemie*. **353**, 1001-1004.

Guo S, Dai C, Guo M, Taylor B, Harmon JS, Sander M, Robertson RP, Powers AC, Stein R (2013). Inactivation of specific beta cell transcription factors in type 2 diabetes. *J Clin Invest*. **123**, 3305-3316.

Guo Z, Kozlov S, Lavin MF, Person MD, Paull TT (2010). ATM activation by oxidative stress. *Science*. **330**, 517-521.

Hacot S, Coute Y, Belin S, Albaret MA, Mertani HC, Sanchez JC, Rosa-Calatrava M, Diaz JJ (2010). Isolation of nucleoli. In *Curr Protoc Cell Biol*. (JS Bonifacino, JB Harford, J Lippincott-Schwartz , KM Yamada, eds).

Hamajima T, Mushimoto Y, Kobayashi H, Saito Y, Onigata K (2012). Novel compound heterozygous mutations in the SBP2 gene: characteristic clinical manifestations and the implications of GH and triiodothyronine in longitudinal bone growth and maturation. *Eur J Endocrinol*. **166**, 757-764.

Harding SM, Boiarsky JA, Greenberg RA (2015). ATM dependent silencing links nucleolar chromatin reorganization to DNA damage recognition. *Cell Rep*. **13**, 251-259.

Harmon JS, Bogdani M, Parazzoli SD, Mak SS, Oseid EA, Berghmans M, Leboeuf RC, Robertson RP (2009). β-Cell-specific overexpression of glutathione peroxidase preserves intranuclear MafA and reverses diabetes in *db/db* mice. *Endocrinology*. **150**, 4855-4862.

Hernandez A, Martinez ME, Fiering S, Galton VA, St Germain D (2006). Type 3 deiodinase is critical for the maturation and function of the thyroid axis. *J Clin Invest*. **116**, 476-484.

Hill KE, Wu S, Motley AK, Stevenson TD, Winfrey VP, Capecchi MR, Atkins JF, Burk RF (2012). Production of selenoprotein P (Sepp1) by hepatocytes is central to selenium homeostasis. *J Biol Chem*. **287**, 40414-40424.

Hill KE, Zhou J, Austin LM, Motley AK, Ham AJ, Olson GE, Atkins JF, Gesteland RF, Burk RF (2007). The selenium-rich C-terminal domain of mouse selenoprotein P is necessary for the supply of selenium to brain and testis but not for the maintenance of whole body selenium. *J Biol Chem*. **282**, 10972-10980.

Hill KE, Zhou J, McMahan WJ, Motley AK, Atkins JF, Gesteland RF, Burk RF (2003). Deletion of selenoprotein P alters distribution of selenium in the mouse. *J Biol Chem*. **278**, 13640-13646.

Himeno S, Chittum HS, Burk RF (1996). Isoforms of selenoprotein P in rat plasma. Evidence for a full-length form and another form that terminates at the second UGA in the open reading frame. *J Biol Chem*. **271**, 15769-15775.

Hogue DE (1958). Vitamin E, selenium and other factors related to nutritional muscular dystrophy in lambs. *Proc Cornell Nutr Conf*, 32-39.

Holmgren A (2000). Antioxidant function of thioredoxin and glutaredoxin systems. *Antioxid Redox Signal*. **2**, 811-820.

Howard MT, Carlson BA, Anderson CB, Hatfield DL (2013). Translational redefinition of UGA codons is regulated by selenium availability. *J Biol Chem*. **288**, 19401-19413.

Hsu CY, Adams JP, Kim H, No K, Ma C, Strauss SH, Drnevich J, Vandervelde L, Ellis JD, Rice BM, Wickett N, Gunter LE, Tuskan GA, Brunner AM, Page GP, Barakat A, Carlson JE, DePamphilis CW, Luthe DS, Yuceer C (2011). FLOWERING LOCUS T duplication coordinates reproductive and vegetative growth in perennial poplar. *Proc Natl Acad Sci U S A*. **108**, 10756-10761.

Hu Y, McIntosh GH, Le Leu RK, Nyskohus LS, Woodman RJ, Young GP (2013). Combination of selenium and green tea improves the efficacy of chemoprevention in a rat colorectal cancer model by modulating genetic and epigenetic biomarkers. *PLoS One*. **8**, e64362.

Huang H, Fletcher L, Beeharry N, Daniel R, Kao G, Yen TJ, Muschel RJ (2008). Abnormal cytokinesis after X-irradiation in tumor cells that override the G2 DNA damage checkpoint. *Cancer Res*. **68**, 3724-3732.

Imai H, Hakkaku N, Iwamoto R, Suzuki J, Suzuki T, Tajima Y, Konishi K, Minami S, Ichinose S, Ishizaka K, Shioda S, Arata S, Nishimura M, Naito S, Nakagawa Y (2009). Depletion of selenoprotein GPx4 in spermatocytes causes male infertility in mice. *J Biol Chem*. **284**, 32522-32532.

Irons R, Tsuji PA, Carlson BA, Ouyang P, Yoo MH, Xu XM, Hatfield DL, Gladyshev VN, Davis CD (2010). Deficiency in the 15-kDa selenoprotein inhibits tumorigenicity and metastasis of colon cancer cells. *Cancer Prev Res (Phila)*. **3**, 630-639.

Jackson MI, Combs GF, Jr. (2008). Selenium and anticarcinogenesis: underlying mechanisms. *Curr Opin Clin Nutr Metab Care*. **11**, 718-726.

Jackson SP, Bartek J (2009). The DNA-damage response in human biology and disease. *Nature*. **461**, 1071-1078.

Jakupoglu C, Przemeck GK, Schneider M, Moreno SG, Mayr N, Hatzopoulos AK, de Angelis MH, Wurst W, Bornkamm GW, Brielmeier M, Conrad M (2005). Cytoplasmic thioredoxin reductase is essential for embryogenesis but dispensable for cardiac development. *Mol Cell Biol*. **25**, 1980-1988.

Jin RC, Mahoney CE, Coleman Anderson L, Ottaviano F, Croce K, Leopold JA, Zhang YY, Tang SS, Handy DE, Loscalzo J (2011). Glutathione peroxidase-3 deficiency promotes platelet-dependent thrombosis in vivo. *Circulation*. **123**, 1963-1973.

Kapahnke M, Banning A, Tikkanen R (2016). Random splicing of several exons caused by a single base change in the target exon of CRISPR/Cas9 mediated gene knockout. *Cells*. **5**, 45.

Kasaikina MV, Fomenko DE, Labunskyy VM, Lachke SA, Qiu W, Moncaster JA, Zhang J, Wojnarowicz MW, Jr., Natarajan SK, Malinouski M, Schweizer U, Tsuji PA, Carlson BA, Maas RL, Lou MF, Goldstein LE, Hatfield DL, Gladyshev VN (2011). Roles of the 15-kDa selenoprotein (Sep15) in redox homeostasis and cataract development revealed by the analysis of Sep 15 knockout mice. *J Biol Chem*. **286**, 33203-33212.

Kassam S, Juliger S, Jia L, Joel SP (2012). Methylseleninic acid antagonizes the cytotoxic effect of bortezomib in mantle cell lymphoma cell lines through modulation of Bcl-2 family proteins. *Br J Haematol*. **156**, 286-289.

Kim HY (2013). The methionine sulfoxide reduction system: selenium utilization and methionine sulfoxide reductase enzymes and their functions. *Antioxid Redox Signal*. **19**, 958-969.

Kim HY, Gladyshev VN (2004). Methionine sulfoxide reduction in mammals: characterization of methionine-R-sulfoxide reductases. *Mol Biol Cell*. **15**, 1055-1064.

Kim JR, Lee SM, Cho SH, Kim JH, Kim BH, Kwon J, Choi CY, Kim YD, Lee SR (2004). Oxidation of thioredoxin reductase in HeLa cells stimulated with tumor necrosis factor-alpha. *FEBS Lett*. **567**, 189-196.

Kobayashi Y, Ogra Y, Ishiwata K, Takayama H, Aimi N, Suzuki KT (2002). Selenosugars are key and urinary metabolites for selenium excretion within the required to low-toxic range. *Proc Natl Acad Sci U S A*. **99**, 15932-15936.

Korotkov KV, Kumaraswamy E, Zhou Y, Hatfield DL, Gladyshev VN (2001). Association between the 15-kDa selenoprotein and UDP-glucose:glycoprotein glucosyltransferase in the endoplasmic reticulum of mammalian cells. *J Biol Chem*. **276**, 15330-15336.

Kosugi S, Hasebe M, Tomita M, Yanagawa H (2009). Systematic identification of cell cycle-dependent yeast nucleocytoplasmic shuttling proteins by prediction of composite motifs. *Proc Natl Acad Sci U S A*. **106**, 10171-10176.

Krehl S, Loewinger M, Florian S, Kipp AP, Banning A, Wessjohann LA, Brauer MN, Iori R, Esworthy RS, Chu FF, Brigelius-Flohe R (2012). Glutathione peroxidase-2 and selenium decreased inflammation and tumors in a mouse model of inflammation-associated carcinogenesis whereas sulforaphane effects differed with selenium supply. *Carcinogenesis*. **33**, 620-628.

Kruhlak M, Crouch EE, Orlov M, Montano C, Gorski SA, Nussenzweig A, Misteli T, Phair RD, Casellas R (2007). The ATM repair pathway inhibits RNA polymerase I transcription in response to chromosome breaks. *Nature*. **447**, 730-734.

Kryukov GV, Castellano S, Novoselov SV, Lobanov AV, Zehtab O, Guigo R, Gladyshev VN (2003). Characterization of mammalian selenoproteomes. *Science*. **300**, 1439-1443.

Kryukov GV, Kryukov VM, Gladyshev VN (1999). New mammalian selenocysteine-containing proteins identified with an algorithm that searches for selenocysteine insertion sequence elements. *J Biol Chem*. **274**, 33888-33897.

Labunskyy VM, Hatfield DL, Gladyshev VN (2014). Selenoproteins: molecular pathways and physiological roles. *Physiol Rev*. **94**, 739-777.

Larsen DH, Stucki M (2016). Nucleolar responses to DNA double-strand breaks. *Nucleic Acids Res*. **44**, 538-544.

Leahy JJ, Golding BT, Griffin RJ, Hardcastle IR, Richardson C, Rigoreau L, Smith GC (2004). Identification of a highly potent and selective DNA-dependent protein kinase (DNA-PK) inhibitor (NU7441) by screening of chromenone libraries. *Bioorg Med Chem Lett*. **14**, 6083-6087.

Lee BC, Peterfi Z, Hoffmann FW, Moore RE, Kaya A, Avanesov A, Tarrago L, Zhou Y, Weerapana E, Fomenko DE, Hoffmann PR, Gladyshev VN (2013). MsrB1 and MICALs regulate actin assembly and macrophage function via reversible stereoselective methionine oxidation. *Mol Cell*. **51**, 397-404.

Lee BJ, Worland PJ, Davis JN, Stadtman TC, Hatfield DL (1989). Identification of a selenocysteyl-tRNA(Ser) in mammalian cells that recognizes the nonsense codon, UGA. *J Biol Chem*. **264**, 9724-9727.

Lee JS, Mustafa MG, Afifi AA (1990). Effects of short-term, single and combined exposure to low-level NO2 and O3 on lung tissue enzyme activities in rats. *J Toxicol Environ Health*. **29**, 293-305.

Lei XG, Cheng WH, McClung JP (2007). Metabolic regulation and function of glutathione peroxidase-1. *Annu Rev Nutr*. **27**, 41-61.

Lei XG, Evenson JK, Thompson KM, Sunde RA (1995). Glutathione peroxidase and phospholipid hydroperoxide glutathione peroxidase are differentially regulated in rats by dietary selenium. *J Nutr*. **125**, 1438-1446.

Lei XG, Zhu JH, Cheng WH, Bao Y, Ho YS, Reddi AR, Holmgren A, Arner ES (2016). Paradoxical roles of antioxidant enzymes: basic mechanisms and health implications. *Physiol Rev*. **96**, 307-364.

Lescure A, Gautheret D, Carbon P, Krol A (1999). Novel selenoproteins identified in silico and in vivo by using a conserved RNA structural motif. *J Biol Chem*. **274**, 38147-38154.

Leung AK, Gerlich D, Miller G, Lyon C, Lam YW, Lleres D, Daigle N, Zomerdijk J, Ellenberg J, Lamond AI (2004). Quantitative kinetic analysis of nucleolar breakdown and reassembly during mitosis in live human cells. *J Cell Biol*. **166**, 787-800.

Leung AK, Lamond AI (2003). The dynamics of the nucleolus. *Crit Rev Eukaryot Gene Expr*. **13**, 39-54.

Lin HC, Ho SC, Chen YY, Khoo KH, Hsu PH, Yen HC (2015). SELENOPROTEINS. CRL2 aids elimination of truncated selenoproteins produced by failed UGA/Sec decoding. *Science*. **349**, 91-95.

Liu Y, Zhao H, Zhang Q, Tang J, Li K, Xia XJ, Wang KN, Li K, Lei XG (2012). Prolonged dietary selenium deficiency or excess does not globally affect selenoprotein gene expression and/or protein production in various tissues of pigs. *J Nutr*. **142**, 1410-1416.

Lobrich M, Shibata A, Beucher A, Fisher A, Ensminger M, Goodarzi AA, Barton O, Jeggo PA (2010). gammaH2AX foci analysis for monitoring DNA double-strand break repair: strengths, limitations and optimization. *Cell Cycle*. **9**, 662-669.

Loh K, Deng H, Fukushima A, Cai X, Boivin B, Galic S, Bruce C, Shields BJ, Skiba B, Ooms LM, Stepto N, Wu B, Mitchell CA, Tonks NK, Watt MJ, Febbraio MA, Crack PJ, Andrikopoulos S, Tiganis T (2009). Reactive oxygen species enhance insulin sensitivity. *Cell Metab*. **10**, 260-272.

Louvet E, Yoshida A, Kumeta M, Takeyasu K (2014). Probing the stiffness of isolated nucleoli by atomic force microscopy. *Histochem Cell Biol*. **141**, 365-381.

Lu J, Holmgren A (2009). Selenoproteins. *J Biol Chem*. **284**, 723-727.

Luciani MF, Song Y, Sahrane A, Kosta A, Golstein P (2017). Early nucleolar disorganization in Dictyostelium cell death. *Cell Death Dis*. **8**, e2528.

Mahdi Y, Xu XM, Carlson BA, Fradejas N, Gunter P, Braun D, Southon E, Tessarollo L, Hatfield DL, Schweizer U (2015). Expression of selenoproteins is maintained in mice carrying mutations in SECp43, the tRNA selenocysteine 1 associated protein (Trnau1ap). *PLoS One*. **10**, e0127349.

Maiorino M, Scapin M, Ursini F, Biasolo M, Bosello V, Flohe L (2003). Distinct promoters determine alternative transcription of gpx-4 into phospholipid-hydroperoxide glutathione peroxidase variants. *J Biol Chem*. **278**, 34286-34290.

Makrythanasis P, Nelis M, Santoni FA, Guipponi M, Vannier A, Bena F, Gimelli S, Stathaki E, Temtamy S, Megarbane A, Masri A, Aglan MS, Zaki MS, Bottani A, Fokstuen S, Gwanmesia L, Aliferis K, Bustamante Eduardo M, Stamoulis G, Psoni S, Kitsiou-Tzeli S, Fryssira H, Kanavakis E, Al-Allawi N, Sefiani A, Al Hait S, Elalaoui SC, Jalkh N, Al-Gazali L, Al-Jasmi F, Bouhamed HC, Abdalla E, Cooper DN, Hamamy H, Antonarakis SE (2014). Diagnostic exome sequencing to elucidate the genetic basis of likely recessive disorders in consanguineous families. *Hum Mutat*. **35**, 1203-1210.

Marchesini M, Ogoti Y, Fiorini E, Aktas Samur A, Nezi L, D'Anca M, Storti P, Samur MK, Ganan-Gomez I, Fulciniti MT, Mistry N, Jiang S, Bao N, Marchica V, Neri A, Bueso-Ramos C, Wu CJ, Zhang L, Liang H, Peng X, Giuliani N, Draetta G, Clise-Dwyer K, Kantarjian H, Munshi N, Orlowski R, Garcia-Manero G, DePinho RA, Colla S (2017). ILF2 Is a regulator of RNA splicing and DNA damage response in 1q21-amplified multiple myeloma. *Cancer Cell*. **32**, 88-100 e106.

Marsili A, Aguayo-Mazzucato C, Chen T, Kumar A, Chung M, Lunsford EP, Harney JW, Van-Tran T, Gianetti E, Ramadan W, Chou C, Bonner-Weir S, Larsen PR, Silva JE, Zavacki AM (2011). Mice with a targeted deletion of the type 2 deiodinase are insulin resistant and susceptible to diet induced obesity. *PLoS One*. **6**, e20832.

Martin-Romero FJ, Kryukov GV, Lobanov AV, Carlson BA, Lee BJ, Gladyshev VN, Hatfield DL (2001). Selenium metabolism in Drosophila: selenoproteins, selenoprotein mRNA expression, fertility, and mortality. *J Biol Chem*. **276**, 29798-29804.

Matsumura T (1980). Multinucleation and polyploidization of aging human cells in culture. *Adv Exp Med Biol*. **129**, 31-38.

McCann JC, Ames BN (2011). Adaptive dysfunction of selenoproteins from the perspective of the triage theory: why modest selenium deficiency may increase risk of diseases of aging. *FASEB J*. **25**, 1793-1814.

McClung JP, Roneker CA, Mu W, Lisk DJ, Langlais P, Liu F, Lei XG (2004). Development of insulin resistance and obesity in mice overexpressing cellular glutathione peroxidase. *Proc Natl Acad Sci U S A*. **101**, 8852-8857.

Medeiros LA, Dennis LM, Gill ME, Houbaviy H, Markoulaki S, Fu D, White AC, Kirak O, Sharp PA, Page DC, Jaenisch R (2011). Mir-290-295 deficiency in mice results in partially penetrant embryonic lethality and germ cell defects. *Proc Natl Acad Sci U S A*. **108**, 14163-14168.

Medina MC, Molina J, Gadea Y, Fachado A, Murillo M, Simovic G, Pileggi A, Hernandez A, Edlund H, Bianco AC (2011). The thyroid hormone-inactivating type III deiodinase is expressed in mouse and human beta-cells and its targeted inactivation impairs insulin secretion. *Endocrinology*. **152**, 3717-3727.

Meinhold H, Campos-Barros A, Walzog B, Kohler R, Muller F, Behne D (1993). Effects of selenium and iodine deficiency on type I, type II and type III iodothyronine deiodinases and circulating thyroid hormones in the rat. *Exp Clin Endocrinol*. **101**, 87-93.

Mendelev N, Mehta SL, Witherspoon S, He Q, Sexton JZ, Li PA (2011). Upregulation of human selenoprotein H in murine hippocampal neuronal cells promotes mitochondrial biogenesis and functional performance. *Mitochondrion*. **11**, 76-82.

Mendelev N, Witherspoon S, Li PA (2009). Overexpression of human selenoprotein H in neuronal cells ameliorates ultraviolet irradiation-induced damage by modulating cell signaling pathways. *Experimental Neurology*. **220**, 328-334.

Mills GC (1957). Hemoglobin catabolism. I. Glutathione peroxidase, an erythrocyte enzyme which protects hemoglobin from oxidative breakdown. *J Biol Chem*. **229**, 189-197.

Miniard AC, Middleton LM, Budiman ME, Gerber CA, Driscoll DM (2010). Nucleolin binds to a subset of selenoprotein mRNAs and regulates their expression. *Nucleic Acids Res*. **38**, 4807-4820.

Miranda-Vizuete A, Damdimopoulos AE, Pedrajas JR, Gustafsson JA, Spyrou G (1999). Human mitochondrial thioredoxin reductase cDNA cloning, expression and genomic organization. *Eur J Biochem*. **261**, 405-412.

Moghadaszadeh B, Beggs AH (2006). Selenoproteins and their impact on human health through diverse physiological pathways. *Physiology (Bethesda)*. **21**, 307-315.

Moreno-Reyes R, Suetens C, Mathieu F, Begaux F, Zhu D, Rivera MT, Boelaert M, Neve J, Perlmutter N, Vanderpas J (1998). Kashin-Beck osteoarthropathy in rural Tibet in relation to selenium and iodine status. *N Engl J Med*. **339**, 1112-1120.

Morozova N, Forry EP, Shahid E, Zavacki AM, Harney JW, Kraytsberg Y, Berry MJ (2003). Antioxidant function of a novel selenoprotein in Drosophila melanogaster. *Genes to Cells*. **8**, 963-971.

Moustafa ME, Carlson BA, El-Saadani MA, Kryukov GV, Sun QA, Harney JW, Hill KE, Combs GF, Feigenbaum L, Mansur DB, Burk RF, Berry MJ, Diamond AM, Lee BJ, Gladyshev VN, Hatfield DL (2001). Selective inhibition of selenocysteine tRNA maturation and selenoprotein synthesis in transgenic mice expressing isopentenyladenosine-deficient selenocysteine tRNA. *Mol Cell Biol*. **21**, 3840-3852.

Muth OH, Oldfield JE, Remmert LF, Schubert JR (1958). Effects of selenium and vitamin E on white muscle disease. *Science*. **128**, 1090.

Novoselov SV, Calvisi DF, Labunskyy VM, Factor VM, Carlson BA, Fomenko DE, Moustafa ME, Hatfield DL, Gladyshev VN (2005). Selenoprotein deficiency and high levels of selenium compounds can effectively inhibit hepatocarcinogenesis in transgenic mice. *Oncogene*. **24**, 8003-8011.

Novoselov SV, Kim HY, Hua D, Lee BC, Astle CM, Harrison DE, Friguet B, Moustafa ME, Carlson BA, Hatfield DL, Gladyshev VN (2010). Regulation of selenoproteins and methionine sulfoxide reductases A and B1 by age, calorie restriction, and dietary selenium in mice. *Antioxid Redox Signal*. **12**, 829-838.

Novoselov SV, Kryukov GV, Xu XM, Carlson BA, Hatfield DL, Gladyshev VN (2007). Selenoprotein H is a nucleolar thioredoxin-like protein with a unique expression pattern. *J Biol Chem*. **282**, 11960-11968.

Olson GE, Whitin JC, Hill KE, Winfrey VP, Motley AK, Austin LM, Deal J, Cohen HJ, Burk RF (2010). Extracellular glutathione peroxidase (Gpx3) binds specifically to basement membranes of mouse renal cortex tubule cells. *Am J Physiol Renal Physiol*. **298**, F1244-1253.

Olson GE, Winfrey VP, Hill KE, Burk RF (2008). Megalin mediates selenoprotein P uptake by kidney proximal tubule epithelial cells. *J Biol Chem*. **283**, 6854-6860.

Olson GE, Winfrey VP, Nagdas SK, Hill KE, Burk RF (2007). Apolipoprotein E receptor-2 (ApoER2) mediates selenium uptake from selenoprotein P by the mouse testis. *J Biol Chem*. **282**, 12290-12297.

Padidar S, Farquharson AJ, Williams LM, Kearney R, Arthur JR, Drew JE (2012). High-fat diet alters gene expression in the liver and colon: links to increased development of aberrant crypt foci. *Dig Dis Sci*. **57**, 1866-1874.

Panee J, Stoytcheva ZR, Liu W, Berry MJ (2007). Selenoprotein H is a redox-sensing high mobility group family DNA-binding protein that up-regulates genes involved in glutathione synthesis and phase II detoxification. *J Biol Chem*. **282**, 23759-23765.

Panier S, Boulton SJ (2014). Double-strand break repair: 53BP1 comes into focus. *Nat Rev Mol Cell Biol*. **15**, 7-18.

Patterson BH, Levander OA, Helzlsouer K, McAdam PA, Lewis SA, Taylor PR, Veillon C, Zech LA (1989). Human selenite metabolism: a kinetic model. *Am J Physiol*. **257**, R556-567.

Patterson EL, Milstrey R, Stokstad EL (1957). Effect of selenium in preventing exudative diathesis in chicks. *Proc Soc Exp Biol Med*. **95**, 617-620.

Pedrosa LF, Motley AK, Stevenson TD, Hill KE, Burk RF (2012). Fecal selenium excretion is regulated by dietary selenium intake. *Biol Trace Elem Res*. **149**, 377-381.

Peeters RP, Hernandez A, Ng L, Ma M, Sharlin DS, Pandey M, Simonds WF, St Germain DL, Forrest D (2013). Cerebellar abnormalities in mice lacking type 3 deiodinase and partial reversal of phenotype by deletion of thyroid hormone receptor alpha1. *Endocrinology*. **154**, 550-561.

Perez JM, Chirieleison SM, Abbott DW (2015). An IκB Kinase-regulated feed-forward circuit prolongs inflammation. *Cell Rep*. **12**, 537-544.

Peters U, Chatterjee N, Church TR, Mayo C, Sturup S, Foster CB, Schatzkin A, Hayes RB (2006). High serum selenium and reduced risk of advanced colorectal adenoma in a colorectal cancer early detection program. *Cancer Epidemiol Biomarkers Prev*. **15**, 315-320.

Pfeifer H, Conrad M, Roethlein D, Kyriakopoulos A, Brielmeier M, Bornkamm GW, Behne D (2001). Identification of a specific sperm nuclei selenoenzyme necessary for protamine thiol cross-linking during sperm maturation. *FASEB J*. **15**, 1236-1238.

Pickard AJ, Bierbach U (2013). The cell's nucleolus: an emerging target for chemotherapeutic intervention. *ChemMedChem*. **8**, 1441-1449.

Piekielko-Witkowska A, Nauman A (2011). Iodothyronine deiodinases and cancer. *J Endocrinol Invest*. **34**, 716-728.

Pitts MW, Kremer PM, Hashimoto AC, Torres DJ, Byrns CN, Williams CS, Berry MJ (2015). Competition between the brain and testes under selenium-compromised conditions: insight into sex differences in selenium metabolism and risk of neurodevelopmental disease. *J Neurosci*. **35**, 15326-15338.

Pitts MW, Reeves MA, Hashimoto AC, Ogawa A, Kremer P, Seale LA, Berry MJ (2013). Deletion of selenoprotein M leads to obesity without cognitive deficits. *J Biol Chem*. **288**, 26121-26134.

Prasanth SG, Prasanth KV, Stillman B (2002). Orc6 involved in DNA replication, chromosome segregation, and cytokinesis. *Science*. **297**, 1026-1031.

Preta G, Jankunec M, Heinrich F, Griffin S, Sheldon IM, Valincius G (2016). Tethered bilayer membranes as a complementary tool for functional and structural studies: The pyolysin case. *Biochim Biophys Acta*. **1858**, 2070-2080.

Pretlow TP, O'Riordan MA, Pretlow TG, Stellato TA (1992). Aberrant crypts in human colonic mucosa: putative preneoplastic lesions. *J Cell Biochem Suppl*. **16g**, 55-62.

Pushpa-Rekha TR, Burdsall AL, Oleksa LM, Chisolm GM, Driscoll DM (1995). Rat phospholipid-hydroperoxide glutathione peroxidase. cDNA cloning and identification of multiple transcription and translation start sites. *J Biol Chem*. **270**, 26993-26999.

Qi Y, Schoene NW, Lartey FM, Cheng WH (2010). Selenium compounds activate ATM-dependent DNA damage response via the mismatch repair protein hMLH1 in colorectal cancer cells. *J Biol Chem*. **285**, 33010-33017.

Radmacher M (1997). Measuring the elastic properties of biological samples with the AFM. *IEEE Eng Med Biol Mag*. **16**, 47-57.

Ran Q, Liang H, Gu M, Qi W, Walter CA, Roberts LJ, 2nd, Herman B, Richardson A, Van Remmen H (2004). Transgenic mice overexpressing glutathione peroxidase 4 are protected against oxidative stress-induced apoptosis. *J Biol Chem*. **279**, 55137-55146.

Ran Q, Liang H, Ikeno Y, Qi W, Prolla TA, Roberts LJ, 2nd, Wolf N, Van Remmen H, Richardson A (2007). Reduction in glutathione peroxidase 4 increases life span through increased sensitivity to apoptosis. *J Gerontol A Biol Sci Med Sci*. **62**, 932-942.

Rayman MP (2012). Selenium and human health. *Lancet*. **379**, 1256-1268.

Rotruck JT, Pope AL, Ganther HE, Swanson AB, Hafeman DG, Hoekstra WG (1973). Selenium: biochemical role as a component of glutathione peroxidase. *Science*. **179**, 588-590.

Ruiz-Rincon S, Gonzalez-Orive A, de la Fuente JM, Cea P (2017). Reversible monolayer-bilayer transition in supported phospholipid LB films under the presence of water: morphological and nanomechanical behavior. *Langmuir*. **33**, 7538-7547.

Rundlof AK, Janard M, Miranda-Vizuete A, Arner ES (2004). Evidence for intriguingly complex transcription of human thioredoxin reductase 1. *Free Radic Biol Med*. **36**, 641-656.

Saad R, Diamond AM (2016). Genetic Variations in the Genes for Selenoproteins Implicate the Encoded Proteins in Cancer Etiology. In *Selenium: Its Molecular Biology and Role in Human Health*. (DL Hatfield, U Schweizer, PA Tsuji , VN Gladyshev, eds). Cham: Springer International Publishing, pp. 343-352.

Sander JD, Joung JK (2014). CRISPR-Cas systems for editing, regulating and targeting genomes. *Nat Biotech*. **32**, 347-355.

Sanjana NE, Shalem O, Zhang F (2014). Improved vectors and genome-wide libraries for CRISPR screening. *Nat Methods*. **11**, 783-784.

Schneider M, Forster H, Boersma A, Seiler A, Wehnes H, Sinowatz F, Neumuller C, Deutsch MJ, Walch A, Hrabe de Angelis M, Wurst W, Ursini F, Roveri A, Maleszewski M, Maiorino M, Conrad M (2009). Mitochondrial glutathione peroxidase 4 disruption causes male infertility. *FASEB J*. **23**, 3233-3242.

Schneider M, Vogt Weisenhorn DM, Seiler A, Bornkamm GW, Brielmeier M, Conrad M (2006a). Embryonic expression profile of phospholipid hydroperoxide glutathione peroxidase. *Gene Expr Patterns*. **6**, 489-494.

Schneider MJ, Fiering SN, Pallud SE, Parlow AF, St Germain DL, Galton VA (2001). Targeted disruption of the type 2 selenodeiodinase gene (DIO2) results in a phenotype of pituitary resistance to T4. *Mol Endocrinol*. **15**, 2137-2148.

Schneider MJ, Fiering SN, Thai B, Wu SY, St Germain E, Parlow AF, St Germain DL, Galton VA (2006b). Targeted disruption of the type 1 selenodeiodinase gene (Dio1) results in marked changes in thyroid hormone economy in mice. *Endocrinology*. **147**, 580-589.

Schoenmakers E, Agostini M, Mitchell C, Schoenmakers N, Papp L, Rajanayagam O, Padidela R, Ceron-Gutierrez L, Doffinger R, Prevosto C, Luan J, Montano S, Lu J, Castanet M, Clemons N, Groeneveld M, Castets P, Karbaschi M, Aitken S, Dixon A, Williams J, Campi I, Blount M, Burton H, Muntoni F, O'Donovan D, Dean A, Warren A, Brierley C, Baguley D, Guicheney P, Fitzgerald R, Coles A, Gaston H, Todd P, Holmgren A, Khanna KK, Cooke M, Semple R, Halsall D, Wareham N, Schwabe J, Grasso L, Beck-Peccoz P, Ogunko A, Dattani M, Gurnell M, Chatterjee K (2010). Mutations in the selenocysteine insertion sequence-binding protein 2 gene lead to a multisystem selenoprotein deficiency disorder in humans. *J Clin Invest*. **120**, 4220-4235.

Schoenmakers E, Carlson B, Agostini M, Moran C, Rajanayagam O, Bochukova E, Tobe R, Peat R, Gevers E, Muntoni F, Guicheney P, Schoenmakers N, Farooqi S, Lyons G, Hatfield D, Chatterjee K (2016). Mutation in human selenocysteine transfer RNA selectively disrupts selenoprotein synthesis. *J Clin Invest*. **126**, 992-996.

Schomburg L, Schweizer U, Holtmann B, Flohe L, Sendtner M, Kohrle J (2003). Gene disruption discloses role of selenoprotein P in selenium delivery to target tissues. *Biochem J*. **370**, 397-402.

Schwarz K, Bieri JG, Briggs GM, Scott ML (1957). Prevention of exudative diathesis in chicks by factor 3 and selenium. *Proc Soc Exp Biol Med*. **95**, 621-625.

Schwarz K, Foltz CM (1957). Selenium as an integral part of factor 3 against dietary necrotic liver degeneration. *Journal of the American Chemical Society*. **79**, 3292-3293.

Seeher S, Atassi T, Mahdi Y, Carlson BA, Braun D, Wirth EK, Klein MO, Reix N, Miniard AC, Schomburg L, Hatfield DL, Driscoll DM, Schweizer U (2014). Secisbp2 is essential for embryonic development and enhances selenoprotein expression. *Antioxid Redox Signal*. **21**, 835-849.

Seiler A, Schneider M, Forster H, Roth S, Wirth EK, Culmsee C, Plesnila N, Kremmer E, Radmark O, Wurst W, Bornkamm GW, Schweizer U, Conrad M (2008). Glutathione peroxidase 4 senses and translates oxidative stress into 12/15-lipoxygenase dependent- and AIF-mediated cell death. *Cell Metab*. **8**, 237-248.

Sengupta A, Lichti UF, Carlson BA, Ryscavage AO, Gladyshev VN, Yuspa SH, Hatfield DL (2010). Selenoproteins are essential for proper keratinocyte function and skin development. *PLoS One*. **5**, e12249.

Seyedali A, Berry MJ (2014). Nonsense-mediated decay factors are involved in the regulation of selenoprotein mRNA levels during selenium deficiency. *RNA*. **20**, 1248-1256.

Shamanna RA, Hoque M, Lewis-Antes A, Azzam EI, Lagunoff D, Pe'ery T, Mathews MB (2011). The NF90/NF45 complex participates in DNA break repair via nonhomologous end joining. *Mol Cell Biol*. **31**, 4832-4843.

Shang ZF, Huang B, Xu QZ, Zhang SM, Fan R, Liu XD, Wang Y, Zhou PK (2010). Inactivation of DNA-dependent protein kinase leads to spindle disruption and mitotic catastrophe with attenuated checkpoint protein 2 Phosphorylation in response to DNA damage. *Cancer Res*. **70**, 3657-3666.

Shav-Tal Y, Blechman J, Darzacq X, Montagna C, Dye BT, Patton JG, Singer RH, Zipori D (2005). Dynamic sorting of nuclear components into distinct nucleolar caps during transcriptional inhibition. *Mol Biol Cell*. **16**, 2395-2413.

Shaw J, Love AJ, Makarova SS, Kalinina NO, Harrison BD, Taliansky ME (2014). Coilin, the signature protein of Cajal bodies, differentially modulates the interactions of plants with viruses in widely different taxa. *Nucleus*. **5**, 85-94.

Soerensen J, Jakupoglu C, Beck H, Forster H, Schmidt J, Schmahl W, Schweizer U, Conrad M, Brielmeier M (2008). The role of thioredoxin reductases in brain development. *PLoS One*. **3**, e1813.

Song Y, Niu J, Yue Z, Gao R, Zhang C, Ding W (2017). Increased chemo-sensitivity by knockdown coilin expression involved acceleration of premature cellular senescence in HeLa cells. *Biochem Biophys Res Commun*. **489**, 123-129.

Squires JE, Berry MJ (2008). Eukaryotic selenoprotein synthesis: Mechanistic insight incorporating new factors and new functions for old factors. *IUBMB Life*. **60**, 232-235.

St Germain DL, Galton VA, Hernandez A (2009). Minireview: Defining the roles of the iodothyronine deiodinases: current concepts and challenges. *Endocrinology*. **150**, 1097-1107.

Stark RW, Drobek T, Heckl WM (2001). Thermomechanical noise of a free v-shaped cantilever for atomic-force microscopy. *Ultramicroscopy*. **86**, 207-215.

Stoytcheva ZR, Vladimirov V, Douet V, Stoychev I, Berry MJ (2010). Metal transcription factor-1 regulation via MREs in the transcribed regions of selenoprotein H and other metal-responsive genes. *Biochim Biophys Acta*. **1800**, 416-424.

Su D, Novoselov SV, Sun QA, Moustafa ME, Zhou Y, Oko R, Hatfield DL, Gladyshev VN (2005). Mammalian selenoprotein thioredoxin-glutathione reductase. Roles in disulfide bond formation and sperm maturation. *J Biol Chem*. **280**, 26491-26498.

Sun QA, Kirnarsky L, Sherman S, Gladyshev VN (2001). Selenoprotein oxidoreductase with specificity for thioredoxin and glutathione systems. *Proc Natl Acad Sci U S A*. **98**, 3673-3678.

Sun QA, Wu Y, Zappacosta F, Jeang KT, Lee BJ, Hatfield DL, Gladyshev VN (1999). Redox regulation of cell signaling by selenocysteine in mammalian thioredoxin reductases. *J Biol Chem*. **274**, 24522-24530.

Sunde RA, Li JL, Taylor RM (2016). Insights for setting of nutrient requirements, gleaned by comparison of selenium status biomarkers in turkeys and chickens versus rats, mice, and lambs. *Adv Nutr*. **7**, 1129-1138.

Sunde RA, Raines AM (2011). Selenium regulation of the selenoprotein and nonselenoprotein transcriptomes in rodents. *Adv Nutr*. **2**, 138-150.

Sunde RA, Thompson KM (2009). Dietary selenium requirements based on tissue selenium concentration and glutathione peroxidase activities in old female rats. *J Trace Elem Med Biol*. **23**, 132-137.

Takayama T, Katsuki S, Takahashi Y, Ohi M, Nojiri S, Sakamaki S, Kato J, Kogawa K, Miyake H, Niitsu Y (1998). Aberrant crypt foci of the colon as precursors of adenoma and cancer. *N Engl J Med*. **339**, 1277-1284.

Tamura T, Stadtman TC (1996). A new selenoprotein from human lung adenocarcinoma cells: purification, properties, and thioredoxin reductase activity. *Proc Natl Acad Sci U S A*. **93**, 1006-1011.

Thiry C, Ruttens A, Pussemier L, Schneider YJ (2013). An in vitro investigation of species-dependent intestinal transport of selenium and the impact of this process on selenium bioavailability. *Br J Nutr*. **109**, 2126-2134.

Thiry M, Lafontaine DL (2005). Birth of a nucleolus: the evolution of nucleolar compartments. *Trends Cell Biol*. **15**, 194-199.

Tsekrekou M, Stratigi K, Chatzinikolaou G (2017). The nucleolus: in genome maintenance and repair. *Int J Mol Sci*. **18**.

Tsuji PA, Carlson BA, Naranjo-Suarez S, Yoo MH, Xu XM, Fomenko DE, Gladyshev VN, Hatfield DL, Davis CD (2012). Knockout of the 15 kDa selenoprotein protects against chemically-induced aberrant crypt formation in mice. *PLoS One*. **7**, e50574.

Turner DC, Stadtman TC (1973). Purification of protein components of the clostridial glycine reductase system and characterization of protein A as a selenoprotein. *Arch Biochem Biophys*. **154**, 366-381.

Ueta CB, Oskouei BN, Olivares EL, Pinto JR, Correa MM, Simovic G, Simonides WS, Hare JM, Bianco AC (2012a). Absence of myocardial thyroid hormone inactivating deiodinase results in restrictive cardiomyopathy in mice. *Mol Endocrinol*. **26**, 809-818.

Ueta T, Inoue T, Furukawa T, Tamaki Y, Nakagawa Y, Imai H, Yanagi Y (2012b). Glutathione peroxidase 4 is required for maturation of photoreceptor cells. *J Biol Chem*. **287**, 7675-7682.

Ursini F, Heim S, Kiess M, Maiorino M, Roveri A, Wissing J, Flohe L (1999). Dual function of the selenoprotein PHGPx during sperm maturation. *Science*. **285**, 1393-1396.

Van Dael P, Davidsson L, Ziegler EE, Fay LB, Barclay D (2002). Comparison of selenite and selenate apparent absorption and retention in infants using stable isotope methodology. *Pediatr Res*. **51**, 71-75.

van Sluis M, McStay B (2015). A localized nucleolar DNA damage response facilitates recruitment of the homology-directed repair machinery independent of cell cycle stage. *Genes Dev*. **29**, 1151-1163.

van Sluis M, McStay B (2017). Nucleolar reorganization in response to rDNA damage. *Curr Opin Cell Biol*. **46**, 81-86.

Van Vleet JF, Carlton W, Olander HJ (1970). Hepatosis dietetica and mulberry heart disease associated with selenium deficiency in Indiana swine. *J Am Vet Med Assoc*. **157**, 1208-1219.

Vanderpas JB, Contempre B, Duale NL, Goossens W, Bebe N, Thorpe R, Ntambue K, Dumont J, Thilly CH, Diplock AT (1990). Iodine and selenium deficiency associated with cretinism in northern Zaire. *Am J Clin Nutr*. **52**, 1087-1093.

Vartiainen MK, Guettler S, Larijani B, Treisman R (2007). Nuclear actin regulates dynamic subcellular localization and activity of the SRF cofactor MAL. *Science*. **316**, 1749-1752.

Velsor LW, van Heeckeren A, Day BJ (2001). Antioxidant imbalance in the lungs of cystic fibrosis transmembrane conductance regulator protein mutant mice. *Am J Physiol Lung Cell Mol Physiol*. **281**, L31-38.

Verma S, Hoffmann FW, Kumar M, Huang Z, Roe K, Nguyen-Wu E, Hashimoto AS, Hoffmann PR (2011). Selenoprotein K knockout mice exhibit deficient calcium flux in immune cells and impaired immune responses. *J Immunol*. **186**, 2127-2137.

Wastney ME, Combs GF, Jr., Canfield WK, Taylor PR, Patterson KY, Hill AD, Moler JE, Patterson BH (2011). A human model of selenium that integrates metabolism from selenite and selenomethionine. *J Nutr*. **141**, 708-717.

Whanger PD (2009). Selenoprotein expression and function-Selenoprotein W. *Biochim Biophys Acta*. **1790**, 1448-1452.

Wu M, Kang MM, Schoene NW, Cheng WH (2010). Selenium compounds activate early barriers of tumorigenesis. *J Biol Chem*. **285**, 12055-12062.

Wu RT, Cao L, Chen BP, Cheng WH (2014). Selenoprotein H suppresses cellular senescence through genome maintenance and redox regulation. *J Biol Chem*. **289**, 34378-34388.

Wu RT, Cao L, Mattson E, Witwer KW, Cao J, Zeng H, He X, Combs GF, Jr., Cheng WH (2017). Opposing impacts on healthspan and longevity by limiting dietary selenium in telomere dysfunctional mice. *Aging Cell*. **16**, 125-135.

Xia Y, Hill KE, Byrne DW, Xu J, Burk RF (2005). Effectiveness of selenium supplements in a low-selenium area of China. *Am J Clin Nutr*. **81**, 829-834.

Xiang N, Zhao R, Song G, Zhong W (2008). Selenite reactivates silenced genes by modifying DNA methylation and histones in prostate cancer cells. *Carcinogenesis*. **29**, 2175-2181.

Yan X, Cao L, Li Q, Wu Y, Zhang H, Saiyin H, Liu X, Zhang X, Shi Q, Yu L (2005). Aurora C is directly associated with Survivin and required for cytokinesis. *Genes to Cells*. **10**, 617-626.

Yang FY, Lin ZH, Li SG, Guo BQ, Yin YS (1988). Keshan disease--an endemic mitochondrial cardiomyopathy in China. *J Trace Elem Electrolytes Health Dis*. **2**, 157-163.

Yant LJ, Ran Q, Rao L, Van Remmen H, Shibatani T, Belter JG, Motta L, Richardson A, Prolla TA (2003). The selenoprotein GPX4 is essential for mouse development and protects from radiation and oxidative damage insults. *Free Radic Biol Med*. **34**, 496-502.

Yokokawa M, Takeyasu K, Yoshimura SH (2008). Mechanical properties of plasma membrane and nuclear envelope measured by scanning probe microscope. *J Microsc*. **232**, 82-90.

Yuan H, Zhang P, Qin L, Chen L, Shi S, Lu Y, Yan F, Bai C, Nan X, Liu D, Li Y, Yue W, Pei X (2008). Overexpression of SPINDLIN1 induces cellular senescence, multinucleation and apoptosis. *Gene*. **410**, 67-74.

Zeng H, Combs GF, Jr. (2008). Selenium as an anticancer nutrient: roles in cell proliferation and tumor cell invasion. *J Nutr Biochem*. **19**, 1-7.

Zeng H, Yan L, Cheng WH, Uthus EO (2011). Dietary selenomethionine increases exon-specific DNA methylation of the p53 gene in rat liver and colon mucosa. *J Nutr*. **141**, 1464-1468.

Zhang S, Rocourt C, Cheng WH (2010). Selenoproteins and the aging brain. *Mech Ageing Dev*. **131**, 253-260.

Zhang X, Zhang L, Zhu JH, Cheng WH (2016). Nuclear selenoproteins and genome maintenance. *IUBMB Life*. **68**, 5-12.

Zhang Y, Zhou Y, Schweizer U, Savaskan NE, Hua D, Kipnis J, Hatfield DL, Gladyshev VN (2008). Comparative analysis of selenocysteine machinery and selenoproteome gene expression in mouse brain identifies neurons as key functional sites of selenium in mammals. *J Biol Chem*. **283**, 2427-2438.

Zhou J, Huang K, Lei XG (2013). Selenium and diabetes-evidence from animal studies. *Free Radic Biol Med*. **65**, 1548-1556.

Zimmermann M, de Lange T (2014). 53BP1: pro choice in DNA repair. *Trends Cell Biol*. **24**, 108-117.

APPENDIX A

LIST OF ABBREVIATION

Table A.1 LIST OF ABBREVIATION

Abbreviated	Full Name
53BP1	p53-binding protein 1
ACF	Aberrant crypt foci
AFM	Atomic force microscopy
AOM	Azoxymethane
ATM	Ataxia talengiectasia kinase
Cas9	CRISPR-associated (Cas) 9 system
CRISPR	Clustered regularly interspaced short palindromic repeats
DIO	Dodothyronine deiodinases
DNA-PK	DNA-dependent protein kinase
DNA-PKcs	DNA-dependent protein kinase, catalytic subunit
DSB	Double-stranded break
GFP	Green fluorescent protein
GPX	Glutathione peroxidases
HDR	Homology-directed repair
HMG	High-mobility group
HRP	Horseradish peroxidase
Indel	Insertion and deletion
miRNA	microRNA
MSRB1	Methionine sulfoxide reductase B1, SelR, SepR, SelX
NHEJ	Nonhomologous end-joining
NLS	Nuclear localization signal
NORs	Nucleolus organizer regions
NTC	Non-targeting control
PAM	Protospacer adjacent motif
Pol I	RNA polymerase I
RNA-Seq	RNA sequencing

SA-β-gal	Senescence-associated β-galactosidase
SBP2	SECIS-binding protein 2
Se	Selenium
Sec	Selenocysteine
SECIS	Selenocysteine insertion sequence
SELENOF	Selenoprotien F, Sep15
SELENOH	Selenoprotein H
SELENOI	Selenoprotein I
SELENOK	Selenoprotein K
SELENOM	Selenoprotein M
SELENON	Selenoprotein N
SELENOP	Selenoprotein P
SELENOT	Selenoprotein T
SELENOS	Selenoprotein S
SELENOV	Selenoprotein V
SELENOW	Selenoprotein W
SEPHS2	Selenophosphate synthetase-2
SEPSECS	Selenocysteine synthase
sgRNA	Single guide RNA
shRNA	Short hairpin RNA
ROS	Reactive oxygen species
TGR	Thioredoxin glutathione reductase
TRSP	Selenocysteinyl tRNA
TXN	Thioredoxin
TXNRD	Thioredoxin reductases
UBF	Upstream binding factor